Fakulta zemědělská
a technologická
Faculty of Agriculture
and Technology

Jihočeská univerzita
v Českých Budějovicích
University of South Bohemia
in České Budějovice

TECHNOFORUM 2024

New Trends in Machinery and Technologies for Biosystems

www.fzt.jcu.cz

České Budějovice | **2024**

TECHNOFORUM 2024

New Trends in Machinery and Technologies for Biosystems

Book of Proceedings

Martin Filip et al.

TECHNOFORUM 2024

New Trends in Machines and Technologies for Biosystems

Book of Proceedings

Editor Ing. Martin Filip, Ph.D.

Graphic design Ing. Mgr. Zbyněk Havelka, Ph.D.

Approved by the dean of the Faculty of Agriculture and Technology of the USB on 25th June 2024 as a book of proceeding of peer-reviewed scientific papers.

Published by

University of South Bohemia in České Budějovice
Faculty of Agriculture and Technology
Studentská 1668, CZ-370 00 České Budějovice
www.fzt.jcu.cz

2024

ISBN 978-80-7694-077-2

TECHNOFORUM 2024
New Trends in Machinery and Technologies for Biosystems

5.–7. June 2024; Pension Kamínek, Nové Hrady, Czech Republic

The scope of the conference embodies the contemporary state of design and utilisation of machines and equipment within a broad spectrum of manufacturing industries. Attention was given to the rationalisation and effective management based on information technologies and control engineering. The discussion allowed the exchange of knowledge among specialists from university departments and institutes focused on related scientific and educational problems.

Organisation Guarantees

doc. RNDr. Petr Bartoš, Ph.D.

Ing. Martin Filip, Ph.D.

Ing. Mgr. Zbyněk Havelka, Ph.D.

Ing. Jana Skalická, Ph.D.

Ing, Mgr. Tomáš Zoubek

Ing. Mgr. Roman Bumbálek, Ph.D.

Scientific guarantees/Reviewers

doc. RNDr. Petr Bartoš, Ph.D.

Ing. Martin Filip, Ph.D.

Ing. Mgr. Zbyněk Havelka, Ph.D.

Ing. Karel Šramhauser, Ph.D.

Ing. Zdeněk Štěrba Ph.D.

doc. Ing. Jan Moudrý, Ph.D.

doc. Ing. Jan Bárta, Ph.D.

Ing. Radim Kuneš, Ph.D.

Ing. Mgr. Roman Bumbálek, Ph.D.

Ing. Mgr. Pavel Olšan, Ph.D.

prof. Ing. Miloslav Šoch, CSc., dr. h. c.

CONTENT

DESIGN AND DEVELOPMENT OF SOFTWARE TO DETECT BIRD COLLISIONS WITH GLASS OBSTACLES
ROMAN BUMBÁLEK, TOMÁŠ ZOUBEK, RADIM STEHLÍK, RADIM KUNEŠ, JEAN DE DIEU MARCEL UFITIKIREZI 6

DESIGN OF A LONG-TERM PERIODIC MEASUREMENT DEVICE FOR REMOTE LOCATIONS USING AN ARDUINO BOARD
MATĚJ KOHÚTEK, JIŘÍ MARČAN, FRANTIŠEK KUMHÁLA, JITKA KUMHÁLOVÁ 20

BIOGAS PRODUCTION FROM FOOD PRODUCTION WASTE
TOMÁŠ GIERTL, JÁN GADUŠ, MICHAL ANGELOVIČ 25

MANAGEMENT OF THE WINE FILTRATION PROCESS IN A WINERY
ZUZANA LAUKOVÁ, JÁN JOBBÁGY, KOLOMAN KRIŠTOF, MICHAL ANGELOVIČ, ZUZANA BAJUSOVÁ 32

POSSIBILITIES OF USING BIOCHAR FROM BIOMASS
ĽUBOŠ KÚDEĽA, JURAJ MAGA, JÁN JOBBÁGY, ADAM TKÁČ 40

EVALUATION OF THE PRODUCTION POTENTIAL OF BIOMASS FROM VINEYARDS
KOLOMAN KRIŠTOF, MARTIN SELICKÝ, JÁN JOBBÁGY, MICHAL ANGELOVIČ, BEÁTA NOVOTNÁ 48

ANALYSIS OF THE SELECTED LINE OF MACHINES FOR POST-HARVEST PROCESSING OF CEREALS FROM THE POINT OF VIEW OF PRODUCT QUALITY
MICHAL ANGELOVIČ, KRISTIÁN FIALA, JÁN JOBBÁGY, TOMÁŠ GIERTL, KOLOMAN KRIŠTOF 54

COMPUTER MODELLING OF THERMAL STRESS ON GLASS SHEET DURING LASER ENGRAVING
TOMÁŠ ZOUBEK, ROMAN BUMBÁLEK, FRANTIŠEK ŠPALEK, KAREL ŠRAMHAUSER, ZBYNĚK HAVELKA 64

VERIFICATION OF THE FUNCTIONALITY OF THE GLASS SURFACE TREATMENT IN TERMS OF PROVIDING A VISIBLE BARRIER TO FREE-CHEWING BIRDS
TOMÁŠ ZOUBEK, ROMAN BUMBÁLEK, MARTIN FILIP, ONDŘEJ TUPÝ, PAVEL OLŠAN 76

USE OF DRONES WITH MULTISPECTRAL CAMERAS IN AGRICULTURE
ONDŘEJ TUPÝ 84

PREDICTION OF TRACTOR REPAIR AND MAINTENANCE COSTS
ANTONÍN DOLAN, MARTIN FILIP 90

DESIGN AND DEVELOPMENT OF SOFTWARE TO DETECT BIRD COLLISIONS WITH GLASS OBSTACLES

ROMAN BUMBÁLEK, TOMÁŠ ZOUBEK, RADIM STEHLÍK, RADIM KUNEŠ, JEAN DE DIEU MARCEL UFITIKIREZI

Faculty of Agriculture and Technology, University of South Bohemia, Department of Technology and Cybernetics, Na Sádkách 1780, 37005 České Budějovice, Czech Republic

Abstract: The paper is focused on the problem of image processing. Its output is software for the identification of bird collision with a glass obstacle using the detection of changes in the image with implemented basic algorithms in this area, which is created in MATLAB programming language. The first part, oriented to the theoretical introduction to the topic, is divided into image segmentation focusing on edge detection. The second part of the paper contains an introduction to software development, including its flowchart and examples of selected parts of the pseudocode of the applied algorithms, with a short description. Subsequently, the functionality of the developed system is verified on test video frames and the implemented methods and settings are compared based on data processing speed and reliability of image change detection

Keywords: Image processing, image segmentation, edge detection

INTRODUCTION

Computer vision algorithms involving convolutional neural networks have opened up new possibilities for extracting information from image data in the field of image processing, where the application of these methods can detect objects or segment instances to obtain their exact boundaries even in complex compositions (Gui et al., 2024). Their main advantages are their robustness to the variability of the observed features and low image quality, but compared to conventional image processing methods, they require high computational power and often also a high-quality training dataset, which can be very time-consuming, and therefore it is not optimal to use these technologies for every task related to image data (Münke et al., 2024; Ofir and Nebel, 2021), for example to detect changes in an image by segmenting it in the case of a not very complicated scene. Segmentation is an essential operation in image processing to extract the information contained in the image, to divide the image into regions with a certain probability, corresponding to the structural units of the image scene, into contiguous regions composed of essential elements with similar properties, to detect objects of interest and to separate this objects from an uninteresting background (Ciecholewski, 2024; Gao et al., 2022). Segmentation is sometimes described in analogy to the vision process as a foreground-background distinction, where human vision interprets an image based on the relationships between elements formed unconsciously at lower levels of the visual system; it is therefore appropriate even in computer image analysis systems to proceed from low-level elements in ascending order, creating initial criteria at the pixel level (Yu et al., 2024). The presented software was designed to identify bird's glass obstacle collisions using image change detection while implementing selected conventional image processing methods.

MATERIAL and METHODOLOGY

In general, image segmentation algorithms are based on two elementary properties of luminance values: discontinuity and similarity. Image segmentation approaches based on abrupt changes in luminance values, such as edges in an image, fall into the first category, i.e. methods based on the detection of contours that mark the boundaries of individual objects (Gonzales and Woods, 2002). The main approaches of the second category are based on the partitioning of an image into regions of similarity according to specified criteria. These approaches include, for example, thresholding, where an image is extracted based on a given threshold (Amiriebrahimabadi et al., 2024). Another widely used method of image segmentation based on similarity scores is the K-means segmentation algorithm, which is used to

segment the image into clusters or groups representing selected categories (Guo et al., 2023). At the beginning of the segmentation, points are randomly assigned to clusters, then the clusters are continuously updated and points are reassigned between clusters so that the similarity of point values increases within the same cluster and decreases between different clusters (Liang et al., 2022).

One of the fundamental features that occur in an image and provide important information for its interpretation are edges, which can be described as a distinct local change in the brightness intensity of image pixels or also as a transition between dark and light pixels corresponding to the local contour of an object (Magnier et al., 2018). These brightness discontinuities are classified according to their one-dimensional profile into a) jump discontinuities, where sharp, abrupt changes in the values of adjacent pixels occur, and b) oblique discontinuities, also called ramp edges, which form a smooth transition whose slope is inversely related to the edge blur, c) line edges, which are characterised by a step change in values and a steep return to the original values, d) roof edges, which are characterised by a smooth change in values and their smooth return, e) noise edges, which contain fluctuations of values within the course of the edge. In real images, jump and line edges are rare, with noise edges being the most common (Ruslau et al., 2020).

Edge filters are used to detect edges and are divided into several groups. The basic groups are gradient edge detection methods, also called first derivative methods, which are detectors based on approximating the maximum values of the first derivative of the image function, as shown in Figure 3.3 c), and second derivative methods, which consist in finding the passes of the second derivative through zero, as shown in Figure 3.3 d) (Amorim et al., 2023). Another group consists of methods based on evolutionary algorithms (Mousavi et al., 2019).

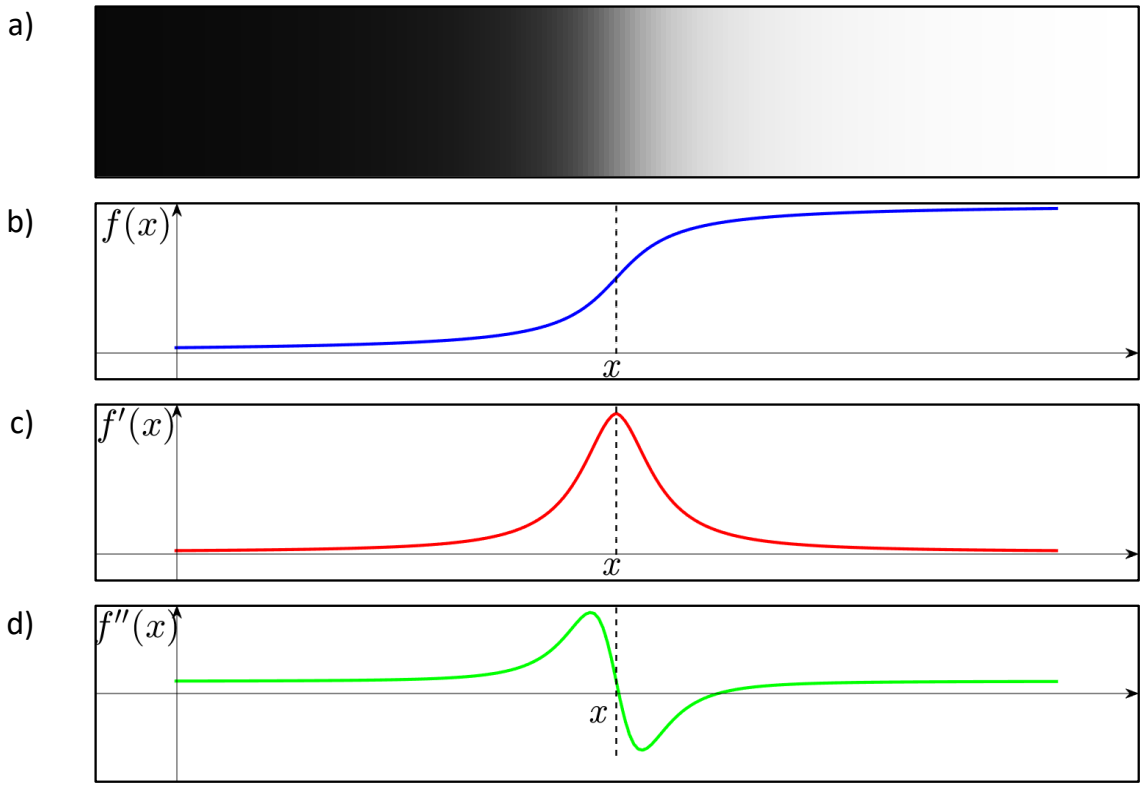

Figure 1 a) Illustration of the brightness transition, b) representation of the image function of the brightness transition, c) first derivative of the image function, d) second derivative of the image function

First-order derivative edge detection algorithms

Gradient operators used for edge detection consist of approximating the results of the first derivative of the image function when its values are high in the edge region. The gradient expressing the change in the values of the image function $f(x,y)$ is defined as a vector

$$\nabla f(x,y) = \begin{bmatrix} e_x(x,y) \\ e_y(x,y) \end{bmatrix} = \begin{bmatrix} \frac{\partial f(x,y)}{\partial x} \\ \frac{\partial f(x,y)}{\partial y} \end{bmatrix}. \quad (1)$$

An important property of the gradient, essential for finding edges, is its magnitude, which gives the maximum rate of increase of the function per unit distance in the direction of the gradient and is given by

$$E(x,y) = |\nabla f(x,y)| = \sqrt{e_x(x,y)^2 + e_y(x,y)^2}\,. \quad (2)$$

The magnitude of the gradient can also be approximated by the sum of the absolute values of its components or their maximum value (Muntarina et al., 2022), thus

$$E(x,y) \approx |e_x(x,y)| + \left|e_y(x,y)\right|, \quad (3)$$

$$E(x,y) \approx \max\left(|e_x(x,y)|, \left|e_y(x,y)\right|\right). \quad (4)$$

The direction of the gradient, which is perpendicular to the edge direction, is given by

$$\alpha(x,y) = \arctan\left(\frac{e_y(x,y)}{e_x(x,y)}\right), \quad (5)$$

the α angle is taken as the angle between the gradient direction and the x-axis (Meester et Baslamisli, 2022). Since the image function $f(x,y), x = 0,1,\dots,M-1, y = 0,1,\dots,N-1$, of the real image, is discontinuous, changes in brightness intensity can be computed by differencing adjacent points so that

$$e_x(x,y) = f(x+1,y) - f(x,y), \quad (6)$$

$$e_y(x,y) = f(x,y+1) - f(x,y). \quad (7)$$

The calculation of e_x and e_y values for all points of the image can be realized by convolution of the image with kernels g_x in the x-axis direction and g_y in the y-axis direction, hence

$$e_x(x,y) = f(x,y) * g_{x,} \quad (8)$$

$$e_y(x,y) = f(x,y) * g_y. \quad (9)$$

To suppress less pronounced edges, a threshold can be set; the resulting pixel is displayed if its value is greater than the threshold; if its value is less than the threshold, it is assigned a value of 0 and is replaced by black. The primary edge detection operators include the Roberts, Sobel, Robinson, Kirsch and Prewitt operators, which differ in the form of convolution kernels (Ali et al., 2023; Petrou and Petrou, 2010).

Second-order derivative edge detection algorithms

The standard gradient operators described above suffer from some sensitivity to noise. Using the second derivative to find edges is more convenient due to the higher reliability, which is due to the steepness of

the second derivative of the function around its zero crossing (Versaci et Morabito, 2021). In 1980, Marr and Hildreth introduced a procedure that can suppress the negative effect of noise by implementing a Gaussian smoothing filter, the Laplacian of Gaussian, also known as LoG (Gironés and Julià, 2020). The operator is based on the second derivative of the convolution of the image with the Gaussian filter, thus

$$\nabla^2 h(x,y) = \nabla^2[f(x,y) * G(x,y)], \tag{10}$$

after reversing the order of application of the second derivative and the convolution, which is possible because of the linearity of the two operations, we obtain

$$\nabla^2 h(x,y) = [\nabla^2 G(x,y)] * f(x,y). \tag{11}$$

A Gaussian two-dimensional filter is defined as

$$G(x,y) = \frac{1}{2\pi\sigma^2} e^{-\left(\frac{x^2+y^2}{2\sigma^2}\right)} \tag{12}$$

and the formula for the Laplace operator is

$$\nabla^2 f = \frac{\partial^2 f}{\partial x^2} + \frac{\partial^2 f}{\partial y^2}. \tag{13}$$

To obtain the relation for the LoG operator, we need to sum the second derivatives of the Gaussian filter function according to x and y

$$\nabla^2 G(x,y) = \frac{\partial^2 G(x,y)}{\partial x^2} + \frac{\partial^2 G(x,y)}{\partial y^2}, \tag{14}$$

$$\nabla^2 G(x,y) = \frac{x^2-\sigma^2}{2\pi\sigma^6} e^{-\left(\frac{x^2+y^2}{2\sigma^2}\right)} + \frac{y^2-\sigma^2}{2\pi\sigma^6} e^{-\left(\frac{x^2+y^2}{2\sigma^2}\right)}, \tag{15}$$

from there we get

$$\nabla^2 G(x,y) = \frac{x^2+y^2-2\sigma^2}{2\pi\sigma^6} e^{-\left(\frac{x^2+y^2}{2\sigma^2}\right)}, \tag{16}$$

after adjustment, we obtain the following equation

$$\nabla^2 G(x,y) = \left(-\frac{1}{\pi\sigma^4}\right)\left(1 - \frac{x^2+y^2}{2\sigma^2}\right) e^{-\left(\frac{x^2+y^2}{2\sigma^2}\right)}. \tag{17}$$

LoG is also expressed in the literature by the relation

$$\nabla^2 G(x,y) = \frac{x^2+y^2-2\,\sigma^2}{\sigma^4} e^{-\left(\frac{x^2+y^2}{2\sigma^2}\right)}, \tag{18}$$

the difference between the LoG expressions of equations 17 and 18 is due to the use of a Gaussian function of the form

$$G(x,y) = e^{-\left(\frac{x^2+y^2}{2\sigma^2}\right)}, \tag{19}$$

in the case of relation 18 instead of the prescribed Gaussian normal distribution (Gonzales et al., 2009; Zhang 2021).

After the convolution of the image with the LoG operator kernel, a zero-crossing search must be performed because a pixel belongs to an edge if the values between it and its neighbours change from positive to negative or vice versa. For example, the zero-crossing detector can take the form of a mask of size 2×2, where a representative point is chosen with a fixed position relative to the mask, and edge detection occurs when the sign within the mask changes relative to the representative point (Sonka et al., 2008). Marr and Hildreth (1980), before detecting the zero crossing, create a binary image from the convolution result by assigning the white colour, i.e. the value 255, to positive values and the black colour to negative values, the zero values do not change, then the boundary pixels in the immediate vicinity of which the value change occurs must be detected. Petrou and Petrou (2010) describe a zero crossing search procedure which is divided into a search in the x-axis direction, along the rows, and in the y-axis direction, along the columns, where for each point (x, y) from the interval $x \in \langle 1; M-1 \rangle$, $y \in \langle 1; N-1 \rangle$ of the resulting image of size $M \times N$ a product is performed with the point following in the direction, i.e. $(x+1, y)$ or $(x, y+1)$. If the product is less than or equal to zero, the point (x, y) belongs to the edge and gets the value 0 in the new output image, otherwise it gets the value 255. In the default display of found edges, where edges are white and other pixels are black, the values are reversed.

Algorithm design and implementation of selected operators

The image change detection algorithm consists of several main parts, the first of which is aimed at obtaining input values and generating the parameters or empty sets necessary for its correct operation. The activity of the other parts, aimed at modifying and comparing the individual frames of the video file, is cyclic, the number of repetitions depending on the total number of frames of the video, the frame rate and the chosen time interval between each frame. Input image adjustments include loading a frame with a given order, adjusting it from RGB colour space to greyscale levels, and scaling the image if necessary. This is followed by the ability to remove noise by smoothing the image with a Gaussian filter whose mask size is automatically determined according to the σ value, or whose size is precisely defined by the user. The next step is to search for edges by applying one of the six operators included in the algorithm; the Sobel, Robinson, Kirsch, Prewitt, LoG and Canny edge detectors are implemented. Uložení výsledků

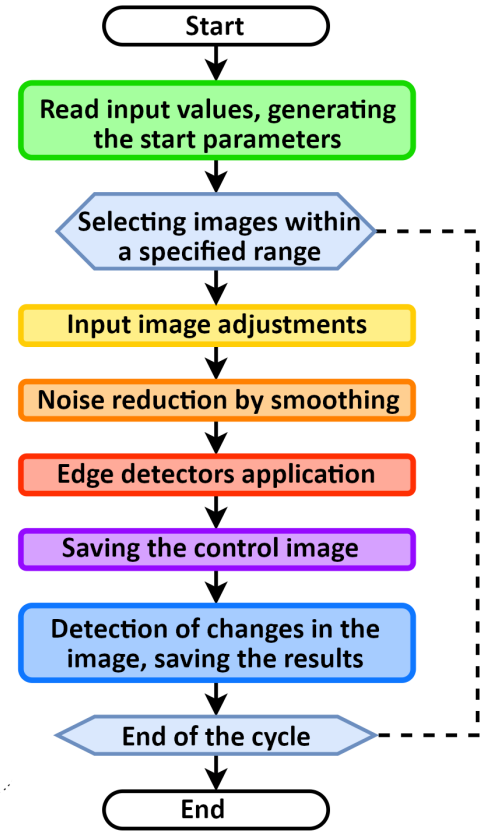

Figure 2 Basic scheme of the algorithm for detecting changes in the image

The downstream partition stores the control images in their original or modified form in the folder created in the selected directory during the first stage. The last stage is concerned with the detection of changes in the image by comparing two frames with a range of 1 to 20 frames, or the current frame with the first frame of the video, where the relative difference of their values is evaluated and a change is detected if a predefined threshold is exceeded, which should be calibrated on a short section of the video examined. The basic simplified scheme is shown in Figure 1, with separate stages arranged in sequence according to the programme flow. The implemented algorithms were developed using MATLAB commands and syntax.

Example implementation of the Canny edge detector

The Canny edge detector contains most of the input values of the above operators, outside the image they are σ and the lower and upper thresholds. After converting the image to grey levels, if necessary, the image is smoothed using the Gaussian filter and edge detection is performed using the Sobel operator. The detected edges are narrowed by non-maximum suppression, where the magnitudes of the edge points are compared with two neighbouring points in the gradient direction, and if the feature under consideration has a higher value than the two features it is compared with, its value is transferred to the zero matrix at the same position, otherwise no feature value transfer takes place. The process of the Canny operator action is completed by the hysteresis thresholding, which involves a parameter p that affects the number of repetitions of the process, in which elements with a value between the lower and upper thresholds are recognised as an edge point only if there is an element with a value greater than the upper threshold in its neighbourhood of size 3×3.

Table 1 Example of the Canny edge detector pseudocode

	CANNY EDGE DETECTOR
1	**start**
2	READ ($image, \sigma, threshold_L, threshold_U$);
3	$p \leftarrow number\_of\_repeating$;
4	**if** SIZE ($image$,3) $\neq$ 1 **then**
5	**start**
6	$image \leftarrow$ RGB_TO_GRAYSCALE ($image$) ;
7	**end**
8	$A \leftarrow$ GAUSSIAN_FILTER ($image, \sigma$) ;
9	$[A_s, M_\theta] \leftarrow$ SOBEL_EDGE_DETECTOR ($A, threshold_L$)
10	$A_\theta \leftarrow$ N-M_SUPPRESSION (A_s, M_θ) ;
11	$A_{out} \leftarrow$ HYSTERESIS_THRESHOLDING ($A_\theta, p, threshold_L, threshold_U$) ;
12	**end**

Table 2 Example of the hysteresis thresholding pseudocode

	HYSTERESIS THRESHOLDING
1	**start**
2	READ $(A_\theta, p, threshold_L, threshold_U)$
3	$rows \leftarrow$ SIZE $(A_\theta, 1)$;
4	$columns \leftarrow$ SIZE $(A_\theta, 2)$;
5	**for** i **from** 1 **to** $rows$
6	**start**
7	**for** j **from** 1 **to** $columns$
8	**start**
9	**if** $A_\theta \geq threshold_U$ **then**
10	**start**
11	$A_{out}(i,j) \leftarrow 255$;
12	**end**
13	**end**
14	**end**
15	**for** o **from** 1 **to** p
16	**start**
17	**for** i **from** 2 **to** $rows - 1$
18	**start**
19	**start**
20	**for** j **from** 2 **to** $columns - 1$
21	**start**
22	**if** $A_\theta(i,j) \geq threshold_L \wedge A_\theta(i,j) < threshold_U$ **then**
23	**start**
24	$B \leftarrow \sum_{b=-1}^{1} A_{out}(i+b, j+b)$;
25	**if** $B \geq 255$ **then**
26	**start**
27	$A_{out}(i,j) = 255$;
28	**end**
29	**end**
30	**end**
31	**end**
32	**end**
33	**end**

RESULTS and DISCUSSION

The proposed software can be evaluated according to several criteria; the results of this paper focus on the assessment of the speed of the selected algorithms and the reliability of the detection of changes in the image. The evaluation of the speed of the software was carried out on the basis of the time interval required to process a FullHD video file of 60 seconds in length at a frame rate of 25 fps. Table 3 shows the values of the time consumption in seconds as a function of the time interval between the video frames processed and the size of the convolution mask of the filters used, which depends on the size of the σ a value; the settings of other parameters, such as the threshold or the relative difference between frames, are insignificant in terms of time dependence, since they do not affect the number of operations performed. The measurements for each pair of parameters were performed ten times and the resulting values are their arithmetic mean. The computer setup on which the program was run includes a 14-core Intel Core i9 10940X processor complemented by 64 GB of RAM; CPU utilisation during software operation was only in the range of 6–7 %.

Table 3 Processing time of a 60 s video file using a) Sobel filter, b) LoG filter, c) Kirsch filter, d) Canny filter [s]

a)

	The time interval between processed video frames [s]					
	1/25	0.1	0.2	0.5	1	2
K=3	141.98	52.83	34.49	18.53	17.24	17.18
K=5	142.02	53.05	34.61	18.82	17.75	17.60
K=7	142.68	53.10	34.61	18.74	17.62	18.04
K=9	144.98	53.86	35.16	19.13	17.70	17.78
K=11	146.54	54.48	35.39	18.97	17.31	17.93
K=13	149.21	55.24	35.98	19.46	17.83	17.17
K=15	152.22	56.26	36.49	19.56	17.67	17.69
K=17	155.67	57.34	36.92	19.61	17.75	17.91
K=19	158.92	58.05	37.43	19.88	18.47	17.58
K=21	161.81	58.94	37.92	20.05	18.26	18.21

b)

	The time interval between processed video frames [s]					
	1/25	0.1	0.2	0.5	1	2
K=3	235.86	90.89	58.69	30.17	21.59	17.06
K=5	246.57	90.83	58.42	29.98	21.56	17.09
K=7	227.00	83.78	54.16	28.22	20.66	16.57
K=9	228.98	83.19	52.91	27.85	21.44	19.02
K=11	233.90	85.74	55.52	29.03	20.89	16.84
K=13	254.01	92.67	59.67	30.49	21.74	17.01
K=15	257.32	93.82	60.05	30.60	21.85	17.08
K=17	261.02	94.90	60.48	30.74	21.71	17.08
K=19	264.61	95.83	60.90	30.97	22.03	17.44
K=21	269.96	97.02	61.80	31.12	22.05	17.23

c)

K=3	673.76	232.67	141.11	63.68	40.30	28.18
K=5	672.99	232.18	141.68	63.80	40.40	28.10
K=7	673.97	231.25	140.83	63.48	40.71	28.70
K=9	674.67	232.16	141.78	64.09	40.19	27.66
K=11	675.55	232.69	141.85	63.76	40.54	28.03
K=13	679.47	233.30	142.01	63.81	40.50	28.45
K=15	680.78	234.01	142.53	64.00	40.72	28.22
K=17	682.76	235.26	143.48	64.19	40.86	28.51
K=19	688.25	236.76	143.95	64.49	40.92	28.46
K=21	692.73	238.11	145.37	65.15	41.01	29.33

d)

K=3	451.49	156.99	97.06	45.88	31.16	23.88
K=5	457.68	159.37	98.70	46.38	31.37	23.68
K=7	456.15	159.24	98.42	46.38	31.53	24.15
K=9	457.47	159.79	98.43	46.36	31.29	24.31
K=11	461.04	160.72	99.32	46.70	31.55	23.90
K=13	464.17	161.68	99.87	46.82	31.57	23.95
K=15	468.30	163.23	101.56	47.08	31.57	23.33
K=17	470.96	163.85	101.03	47.37	31.99	24.00
K=19	475.54	165.12	102.14	47.33	31.92	23.65
K=21	478.13	165.99	102.16	47.59	32.36	23.84

The measured data clearly show that the time taken to process the video increases as the time difference between frames decreases, i.e. as the number of frames processed increases. The size of the convolution mask used by the filters has a negligible effect on the speed of the programe at higher frame intervals, its effect is more pronounced for values less than 0.5 s, which is directly related to the greater number of frames evaluated. The time difference between the values K = 3 and K = 21 in processing each frame of the video, over a range of 1/25 s, is 13.97 % for the Sobel operator, 2.81 % for the Kirsch operator, 14.46 % for the LoG operator and 5.90 % for the Canny operator. Comparing the speeds of the selected edge detectors, the Sobel operator performs best with an average time of 149.6 s for the frame-to-frame interval of 1/25 s, and the Kirsch operator performs worst with an average time of 679.5 s. The average time for the LoG operator is 247.9 s and 464.1 s for the Canny operator at the same values. It is also clear from these values that none of the selected operators can be used for real-time evaluation of the video file if every frame of it is processed; the Sobel operator could be used for this activity from 0.1 s,

the Kirsch operator from up to 1 s, the LoG operator from 0.2 s and the Canny operator from 0.5 s. The speed of the Prewitt operator was not measured because it performs the same number of operations as the Sobel operator, so the difference in time between them would be negligible; the same situation exists between the Kirsch and Robinson filters.

The reliability of detecting changes in the image depends on more factors than the size of the convolution mask and the range between the processed frames, the threshold value of the operators and the value of the relative difference between the compared frames are also very important parameters, the size of which must be determined experimentally with respect to the form of the scenes to be evaluated and the properties of the objects causing their changes. The value expressing the reliability of the image evaluation is defined as

$$s_p = \frac{I_s}{I_o + I_n}, \tag{20}$$

where $I_s$is the number of correctly evaluated frames, I_o is the number of frames in which a change should be defined, and I_n indicates the number of incorrectly identified frames. Using the proposed software, test videos were created to determine the reliability of the program under given conditions, simulating a situation where spherical objects with diameters of 5 and 10 cm are incident on a relatively homogeneous background without significant irregularities; video 1 contains black objects in order to achieve a high contrast with respect to the light background, while test video 2 contains grey objects, so the contrast with respect to the background is lower. To be fully successful, all 15 objects that appear in sequence in the frames must be detected, while those frames in which the objects are not present or in which the objects shown in the frames have already been detected are also scored as correct. In the frames, there is a grey square in the upper left corner, which acts as a reference edge, which is important for the normalisation of each frame that takes place during the output of the edge operators. In the absence of a reference edge, otherwise insignificant edges are highlighted because the normalisation is always based on the highest gradient value in a given image, i.e. in the case of an image containing only background, edges with subtle transitions between background shades are detected despite their low gradient value compared to gradient values in images with objects.

The test videos were processed for frame-to-frame time ranges from 1/25 s to 2 s and Gaussian filter convolution mask sizes from 3 to 21. The relative difference between frames parameter was set to 0.01 for all edge detectors, a threshold of 10 for the Sobel, Kirsch and LoG operators, and a lower and upper threshold of 10 and 30 for the Canny operator.

The output of the program at the given values for the selected video can be evaluated as quite reliable at time intervals between the processed frames of 0.1, 0.2 and 0.5 s, where for the selected edge detectors the image changes were evaluated absolutely correctly in at least ten cases for each of them, depending on the size of the convolution mask of the Gaussian filter, which influences the effect of the image smoothing. The reliability of the results over the time range of 1/25 s is low for most of the selected filters, despite the correct detection of all objects, due to the incorrect evaluation of changes in a larger number of frames, e.g. for the Sobel operator at K = 13, the change was detected in 28 frames instead of 15, an extreme fluctuation occurred for the LoG operator at K = 7, when changes were detected in 140 frames. One of the main causes is probably the high number of consecutive frames in which the same object appears with a different position due to its motion. Another source of these discrepancies could be a low threshold that does not filter out less distinct edges caused by the blurring of objects due to their rapid motion. Also, for a time range of 2 s, the accuracy of the correct evaluation is low, the total number of evaluated frames is small due to the size of the time gaps between the frames so that the object to be detected does not appear very often in the processed frames, since the frames in which the object is present may fall within the time gap. When averaging all the values found for each operator, the Canny operator with an average reliability of 80.8 % is the most reliable option, while the LoG operator with an average reliability of 64.6 % appears to be the least reliable, but this value is biased by the zero success rate at K = 3, when the values of the LoG convolution mask take on a very high range, and thus no edges are crawled in all frames, i.e. no image change is detected. The average success rates of the Sobel and Kirsch operators are 72.8 % and 71.7 %, respectively.

Table 4 Reliability of image change detection using a) Sobel filter, b) LoG filter, c) Kirsch filter, d) Canny filter – video 1 [%]

a)

	Time interval between processed video frames [s]					
	1/25	0.1	0.2	0.5	1	2
K=3	71.4	100.0	100.0	100.0	80.0	40.0
K=5	57.7	100.0	100.0	100.0	86.7	40.0
K=7	57.7	100.0	100.0	100.0	86.7	40.0
K=9	55.6	100.0	100.0	100.0	86.7	40.0
K=11	55.6	100.0	100.0	100.0	86.7	40.0
K=13	53.6	100.0	100.0	100.0	86.7	40.0
K=15	57.7	100.0	100.0	73.3	46.7	26.7
K=17	71.4	93.3	86.7	53.3	40.0	20.0
K=19	78.9	80.0	66.7	40.0	33.3	13.3
K=21	53.6	100.0	87.5	66.7	53.3	20.0

b)

	Time interval between processed video frames [s]					
	1/25	0.1	0.2	0.5	1	2
K=3	0.0	0.0	0.0	0.0	0.0	0.0
K=5	93.3	93.3	80.0	66.7	53.3	26.7
K=7	9.9	11.1	16.3	12.1	20.3	15.4
K=9	60.0	100.0	100.0	100.0	86.7	40.0
K=11	68.2	100.0	100.0	100.0	80.0	40.0
K=13	88.2	100.0	100.0	80.0	80.0	40.0
K=15	83.3	100.0	93.3	80.0	80.0	40.0
K=17	83.3	100.0	93.3	86.7	80.0	40.0
K=19	88.2	100.0	93.3	80.0	73.3	33.3
K=21	83.3	100.0	93.3	86.7	80.0	40.0

c)

K=3	75.0	100.0	100.0	93.3	80.0	40.0
K=5	71.4	100.0	100.0	100.0	80.0	40.0
K=7	57.7	100.0	100.0	100.0	86.7	40.0
K=9	55.6	100.0	100.0	100.0	86.7	40.0
K=11	55.6	100.0	100.0	100.0	86.7	40.0
K=13	51.7	93.8	93.8	93.8	86.7	40.0
K=15	78.9	86.7	73.3	53.3	46.7	26.7
K=17	62.5	87.5	93.3	66.7	40.0	20.0
K=19	82.4	66.7	53.3	40.0	33.3	13.3
K=21	53.6	100.0	93.8	66.7	53.3	20.0

d)

K=3	88.2	100.0	100.0	80.0	80.0	40.0
K=5	88.2	100.0	100.0	80.0	80.0	40.0
K=7	78.9	100.0	100.0	100.0	80.0	40.0
K=9	68.2	100.0	100.0	100.0	86.7	40.0
K=11	68.2	100.0	100.0	80.0	80.0	40.0
K=13	88.2	100.0	100.0	80.0	80.0	40.0
K=15	57.7	100.0	100.0	100.0	86.7	40.0
K=17	55.6	100.0	100.0	100.0	86.7	40.0
K=19	51.7	100.0	100.0	100.0	86.7	40.0
K=21	51.7	100.0	100.0	100.0	86.7	40.0

The reliability values were also checked in the same way for video 2, in which the grey objects appear randomly so that the contrast between them and the background is lower than in video 1; the appearance of the objects is the same in terms of their quantity as in the previous test video, but they differ in time and order. The results in Table 5 correspond with some similarity to the values obtained by evaluating the changes in the image for the high-contrast objects, with the lower reliability being evident from a difference of 0.5 s between frames. This may be due to the different times at which each object enters the frame, or it may be due to their movement, in which case the imaginary trace created by the blurring of the objects as they change position in time takes on lighter shades of grey than the trace of darker objects, and therefore the contrast between it and the background is lower. The operator with the highest reliability in detecting changes is the Kirsch operator, with an average value of 70,1 %, followed by the Sobel and Canny operators, with average values of 70.0 % and 69.7 % respectively, with the worst result

being obtained by the LoG operator with an average reliability of 49.7 %, which, however, gives excellent results in lower time ranges and with more significant image smoothing.

Table 5 Reliability of image change detection using a) Sobel filter, b) LoG filter, c) Kirsch filter, d) Canny filter – video 2 [%]

a)

	Time interval between processed video frames [s]					
	1/25	0.1	0.2	0.5	1	2
K=3	83.3	100.0	100.0	53.3	46.7	26.7
K=5	75.0	100.0	100.0	60.0	60.0	33.3
K=7	71.4	100.0	100.0	60.0	66.7	40.0
K=9	55.6	100.0	100.0	80.0	66.7	40.0
K=11	55.6	100.0	100.0	80.0	66.7	40.0
K=13	51.7	100.0	100.0	86.7	66.7	40.0
K=15	71.4	100.0	93.3	46.7	33.3	20.0
K=17	83.3	100.0	100.0	33.3	53.3	33.3
K=19	83.3	100.0	100.0	33.3	60.0	33.3
K=21	62.5	100.0	100.0	60.0	60.0	33.3

b)

	Time interval between processed video frames [s]					
	1/25	0.1	0.2	0.5	1	2
K=3	0.0	0.0	0.0	0.0	0.0	0.0
K=5	93.3	80.0	46.7	13.3	13.3	6.7
K=7	10.7	17.2	19.5	7.7	13.2	12.2
K=9	78.9	93.8	93.8	43.8	60.0	33.3
K=11	93.8	100.0	100.0	46.7	53.3	33.3
K=13	93.3	93.3	80.0	26.7	26.7	13.3
K=15	100.0	100.0	93.3	26.7	40.0	20.0
K=17	100.0	100.0	93.3	33.3	40.0	20.0
K=19	93.3	93.3	80.0	26.7	33.3	13.3
K=21	100.0	100.0	93.3	26.7	40.0	20.0

c)

K=3	100.0	100.0	93.3	33.3	40.0	20.0
K=5	83.3	100.0	100.0	53.3	46.7	26.7
K=7	75.0	100.0	100.0	60.0	60.0	33.3
K=9	62.5	100.0	100.0	80.0	66.7	40.0
K=11	62.5	100.0	100.0	80.0	66.7	40.0
K=13	86.2	93.8	93.8	93.3	66.7	46.7
K=15	81.3	66.7	66.7	33.3	40.0	20.0
K=17	55.6	100.0	88.2	60.0	73.3	46.7
K=19	68.2	100.0	100.0	60.0	66.7	40.0
K=21	57.7	100.0	100.0	73.3	66.7	40.0

d)

K=3	100.0	100.0	100.0	33.3	40.0	20.0
K=5	100.0	100.0	100.0	33.3	40.0	20.0
K=7	93.8	100.0	100.0	33.3	40.0	20.0
K=9	83.3	100.0	100.0	60.0	46.7	26.7
K=11	88.2	100.0	100.0	46.7	53.3	26.7
K=13	65.2	100.0	100.0	66.7	53.3	33.3
K=15	68.2	100.0	100.0	73.3	60.0	33.3
K=17	62.5	100.0	100.0	73.3	60.0	33.3
K=19	60.0	100.0	100.0	80.0	66.7	40.0
K=21	53.6	100.0	100.0	86.7	66.7	40.0

Figure 3 shows the application of the developed software to real video composition, with the original frames on the left and the postprocessed frames on the right showing the detection of changes in the image in the form of birds passing in front of a glass obstacle.

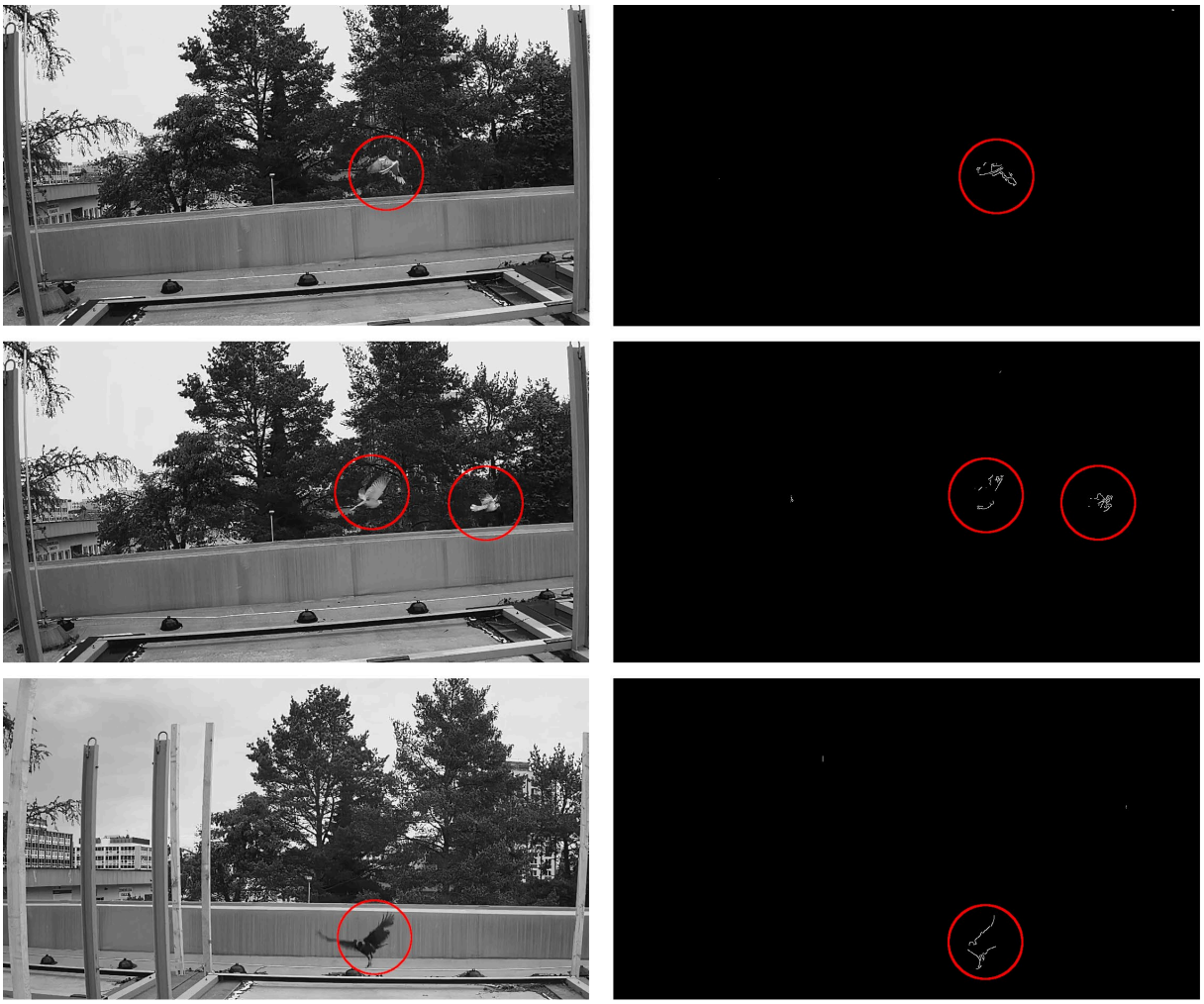

Figure 3 Identification of birds by detecting changes in the image

CONCLUSION

The developed software uses selected basic methods of image processing and segmentation, which are very important for the initial work with image data, but there is a wide range of procedures for their modification and subsequent acquisition of the required information, of which this article deals with only a fraction. For further elaboration and implementation in software, methods based on histogram processing, adaptive thresholding, K-means clustering or other more advanced segmentation techniques can be proposed, or some of the symptom detectors can be applied. From the point of view of usability, the developed program seems to be a decent tool for detecting changes in the image, but the relevant settings of the given parameters should be taken into account with respect to the characteristics of the video file and the detected objects.

REFERENCES

ALI, A.A.I.M., JAMALUDIN, S., IMRAN, M.M.H., AYOB, A.F.M., AHMAD, S.Z.A.S., AKHBAR, M.F.A., SUHRAB, M.I.R., RAMLI, M.R. 2023. *Computer Vision and Image Processing Approaches for Corrosion Detection.* J. Mar. Sci. Eng., 11, 10, 1954. https://doi.org/10.3390/jmse11101954

AMIRIEBRAHIMABADI, M., ROUHI, Z., MANSOURI, N. A. 2024. *Comprehensive Survey of Multi-Level Thresholding Segmentation Methods for Image Processing.* Arch Computat Methods Eng. https://doi.org/10.1007/s11831-024-10093-8

AMORIM, M., DIMURO, G., BORGES, E., DALMAZO, B. L., MARCO-DETCHART, C., LUCCA, G., BUSTINCE, H. 2023. *Systematic Review of Aggregation Functions Applied to Image Edge Detection.* Axioms, 12, 4, 330. https://doi.org/10.3390/axioms12040330

CIECHOLEWSKI, M. 2024. *Review of Segmentation Methods for Coastline Detection in SAR Images.* Arch Computat Methods Eng, 31, 2, 839–869. https://doi.org/10.1007/s11831-023-10000-7

GAO, M., ZHENG, F., YU, J.J.Q., SHAN, C., DING, G., HAN, J. 2023. *Deep learning for video object segmentation: a review.* Artif Intell Rev, 56, 1, 457–531. https://doi.org/10.1007/s10462-022-10176-7

GIRONÉS, X. ET JULIÀ, C. 2020. *Real-time localization of multi-oriented text in natural scene images using a linear spatial filter.* Journal of Real-Time Image Processing, 17, 5, 1505–1525. https://doi.org/10.1007/s11554-019-00911-9

GONZALES, R. C. A WOODS R. E. 2002. *Digital Image Processing.* Second Edition. New Jersey: Prentice Hall, 793. ISBN 0-201-18075-8.

GONZALES, R. C., WOODS, R. E., EDDINS, S. L. 2009. *Digital Image Proicessing using MATLAB.* Second Edition. Knoxville: Gatesmark Publishing, 827. ISBN: 978-0-9820854-0-0.

GUI, S., SONG, S., QIN, R., TANG, Y. 2024. *Remote Sensing Object Detection in the Deep Learning Era—A Review.* Remote Sensing, 16, 2, 327. https://doi.org/10.3390/rs16020327

GUO, Y., NIE, G., GAO, W., LIAO, M. 2023. *2D Semantic Segmentation: Recent Developments and Future Directions.* Future Internet, 15, 6, 205. https://doi.org/10.3390/fi15060205

LIANG, R.,HAN, L., LIU, P., LIU, M. 2022. Research on Improved K-means Image Segmentation Algorithm Based on HSV Space. In: *2022 International Conference on Image Processing, Computer Vision and Machine Learning (ICICML)*, 28-30 Oct. 2022. Xi'an, China: 116-122. https://doi.org/10.1109/ICICML57342.2022.10009682

MAGNIER, B., ABDULRAHMAN, H., MONTESINOS, P. 2018. *A review of supervised edge detection evaluation methods a an objective comparison of filtering gradient computations using hysteresis thresholds.* Journal of Imaging, 4, 6, 74. https://doi.org/10.3390/jimaging4060074

MARR, D. ET HILDRETH, E. 1980. *Theory of edge detection.* Proc. R. Soc. Lond. B., 207, 1167, 187–217. https://doi.org/10.1098/rspb.1980.0020

MEESTER, M. J. ET BASLAMISLI, A. S. 2022. *SAR image edge detection: review and benchmark experiments.* International Journal of Remote Sensing, 43, 14, 5372–5438. https://doi.org/10.1080/01431161.2022.2131480.

MOUSAVI, S. M. H., LYASHENKO, V., PRASATH, V. S. B. 2019. *Analysis of a robust edge detection system in different color spaces using color a depth images.* Computer Optics, 43, 4, 632–646. https://doi.org/10.18287/2412-6179-2019-43-4-632-646

MÜNKE, F. R., SCHÜTZKE, J., BERENS, F., REISCHL, M. 2024. *A review of adaptable conventional image processing pipelines and deep learning on limited datasets.* Machine Vision and Applications, 35, 2, 25. https://doi.org/10.1007/s00138-023-01501-3

MUNTARINA, K., SHORIF, S.B., UDDIN, M.S. 2022. *Notes on edge detection approaches.* Evolving Systems, 13, 1, 169–182. https://doi.org/10.1007/s12530-021-09371-8

OFIR, N. ET NEBEL, J. CH. 2021. *Classic versus deep approaches to address computer vision challenges. CoRR, 2101.09744.* https://doi.org/10.48550/arXiv.2101.09744

PETROU, M. M. P. ET PETROU C. 2010. *Image Processing: The Fundamentals.* Second Edition. Chichester: Wiley, 832. ISBN: 978-0-470-74586-1.

RUSLAU, M. F. V., PRATAMA, R. A., MEIRISTA, E. 2020. *Edge detection of digital image with different edge types.* Journal of Physics: Conference Series, 1569, 4, 42069. https://doi.org/10.1088/1742-6596/1569/4/042069

SONKA, M., HLAVAC, V., BOYLE, R. 2008. *Image Processing, Analysis, and Machine Vision.* Third Edition. Toronto: Thomson Learning, 829. ISBN: 978-0-495-08252-1.

VERSACI, M., MORABITO, F. C. 2021. *Image Edge Detection: A New Approach Based on Fuzzy Entropy and Fuzzy Divergence.* Int. J. Fuzzy Syst., 23, 4, 918–936. https://doi.org/10.1007/s40815-020-01030-5

YU, Y., WANG, C., FU, Q., KOU, R., HUANG, F., YANG, B., YANG, T., GAO, M. 2023. *Techniques and Challenges of Image Segmentation: A Review.* Electronics, 12, 5, 1199. https://doi.org/10.3390/electronics12051199

ZHANG, Y. J. 2021. *Handbook of Image Engineering.* Singapore: Springer, 1967. ISBN 978-981-15-5873-3.

DESIGN OF A LONG-TERM PERIODIC MEASUREMENT DEVICE FOR REMOTE LOCATIONS USING AN ARDUINO BOARD

MATĚJ KOHÚTEK, JIŘÍ MARČAN, FRANTIŠEK KUMHÁLA, JITKA KUMHÁLOVÁ

Czech University of Life Sciences Prague, Faculty of Engineering, Department of Agricultural Machines

Abstract: This paper presents the design and development of a low-cost, low-power measurement device for long-term periodic data collection in remote locations, utilizing an Arduino board. The primary objective is to create a robust solution suitable for environmental monitoring in the field of hops. Commercial measurement devices often come with high costs and limited flexibility, necessitating the development of custom solutions for budget-constrained projects. By optimizing the power consumption and employing a combination of Arduino Nano and Mega boards, the proposed system ensures reliable data collection and transmission over extended periods. Key features include the use of solar-powered batteries, RS485 communication for long-distance sensor integration, and GSM modules for data relay to cloud storage.

Keywords: Environmental Monitoring, Low Power, Arduino, Remote Data Collection, Autonomous System

INTRODUCTION

Reliable long-term measurement is a cornerstone of robust research. In the context of monitoring the environment in the field of hops, the reliability and the accuracy of the data is paramount. Means of measurement greatly affects the frequency of the measurement. Measurements can be done manually by a person or automatically by an automatic measuring station. Manual measurements require a person to be personally in the proximity of the measured environment. That is not usually possible for long-term measurement with high frequency. That is when automatic measurement is used. For automatic measurement, there needs to be a power source available like from a battery or a solar panel. These sources have limited capacity, so the measuring device needs to be low-powered. Commercial grade measuring devices last up to several years just on battery power. But researchers often need many of these devices with limited budgets, that is when they must create their own solutions. This paper focuses on the creation of a low power data logger, leveraging the capabilities of an Arduino board to facilitate long-term and periodic measurement in a remote location.

Literature review

The usage of microcontrollers as data acquisition devices is not a new invention, as Emory Zimmers writes in his paper from the year 1980, with the cost of computing power rapidly lowering, computers find their usage in systems like data acquisition that previously utilized less sophisticated devices (Zimmers, Brown 1980). Even in the present one must find a balance between execution efficiency and implementation difficulty. Arduino boards are a popular choice for rapid development of data acquisition devices, for example gas sensing (Goyal, Patra, Sapre, Kaur, Ramgir 2024), cycling space environment measuring (Luo, Hui, Shang, Wang, Jin, Wang, Li 2024), High-Speed Cylinder Pressure Measurement (Celislami, Rawashdeh, DelVescovo 2024), photovoltaic panel monitoring (Khaleel, Al-Naib, Atyia 2024), haemodialysis monitoring (Sulayman, Araromi, Ayodele, Araromi, Osuolale 2024). There are projects like the Open Source Building Science Sensors (Ali, Zanzinger, Debose, Stephens 2016) that provide frameworks and guidance for creating a custom low-cost data acquisition system. For wireless data acquisition systems with multiple sensing nodes energy conservation is a necessity, there are many ways to extend the battery lifetime like duty-cycling and data compression as discussed in (Anastasi, Conti, Di Francesco, Passarella 2009). Approaches to reducing the power consumption of Arduino boards are documented on the official Arduino documentation website (Chung, Bagur 2024),

some of these include putting the Arduino into sleep mode, removing unused components from the board or lowering the supply voltage and frequency of the processor.

Objectives

The primary objective of this paper is to develop and validate effective data collection methods using low-cost methods suitable for the developing countries or projects with low budget, tailored for monitoring the environment in the field of hops. Specifically, we aim to design a system that ensures accurate, long-term, and periodic data gathering in remote locations, overcoming the limitations of the current approaches. Another objective is to design a system using open-source software and hardware easily programmable by researchers.

Theoretical Framework

Multipurpose boards like the Arduino board contain various components, which consume considerable amounts of electric energy. The out of the box availability of these components is useful for the prototyping stage, when rapid development is key, but in case of low-power systems only the necessary components can be left behind to minimize the power consumption and in hand increase the battery life of the device. The nonessential components for this project that are by default on the Arduino board are for example the USB bridge, linear voltage regulator and inbuilt LEDs, as mentioned in the official Arduino documentation (Chung, Bagur 2024). The documentation mentions other ways of lowering the power consumption like lowering the supply voltage and reducing the clock speed.

There are many development boards on the market to consider when developing a custom measuring system like Arduino, Pro Micro, Teensy or ESP. Important attributes to consider when choosing a suitable development board are the microchip voltage, power consumption, number of programmable input/output pins, supported communication protocols, means of programming the microchip, size of the community, and so on.

Saving data persistently is important when working with low power devices. Popular options for saving data are SD Card and EEPROM. While they both have limited number of writes an SD card usually has a higher storage capacity of up to several terabytes compared to EEPROM which usually has a capacity of several kilobytes to several hundred megabytes. When considering the ease of use, the SD card is easily removable and replaceable, that is why it is often chosen as the primary data storage option.

Real time data monitoring requires data to be transferred from the data acquisition (DAQ) device to a server located in the cloud or on-site. Transferring data wirelessly consumes considerable amount of energy. For energy efficient data transmission low power wide area networks (LPWAN) are attracting a lot of attention (Raza, Kulkarni, Sooriyabandara 2017). The leading LPWAN technologies according to (Mekki, Bajic, Chaxel, Meyer 2018) are Sigfox, LoRaWAN, and NB-IoT.

MATERIALS and METHODOLOGY

System Architecture

The system, which can be seen on the fig. 1, consists of multiple sensing modules and a single backup and relay module. The sensing modules sense the environment using sensors that are connected to the sensing module over the I2C bus or to the analogue IO pin. The measured data is then transferred over the RS485 bus to the backup and relay module, which saves the data locally as a backup and sends it over the internet to a remote server over GSM. Power is supplied to the system from a solar charged battery pack. The data needs to be timestamped with real time timestamp, for this purpose there is a real time clock (RKT) connected to the backup and relay module.

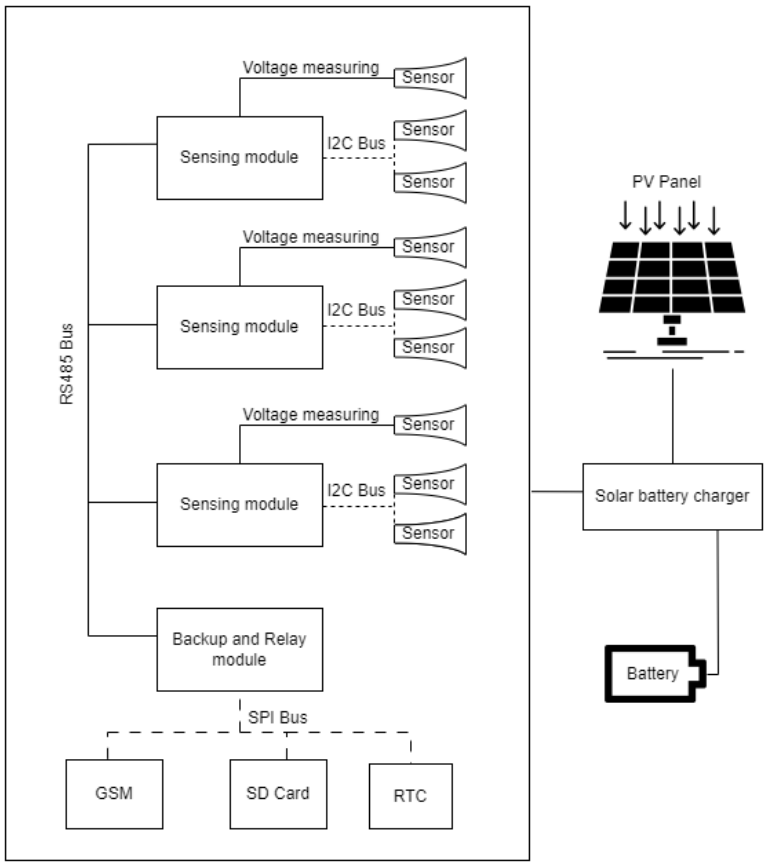

Figure 1 System Architecture comprising of the three sensing modules that collect data from sensors and send it to the backup and relay module which saves a backup on an SD card in case of connection outage and sends the timestamped data over the GSM on a server over the internet. The whole system is powered by a solar panel charged battery located in a separate container.

Hardware

We used the Arduino Nano and Arduino Mega boards. The Arduino Nano as a sensing device and the Arduino Mega which acts as a data relay and data backup. A single Arduino board would normally be enough to collect measurements and save them to a micro-SD card, but there are several reasons, why this simple setup would not be sufficient for our measurement requirements. The first reason is that the chosen sensors communicating over the I2C bus have a static address, which limits the number of sensors of one type on a single I2C bus to one. Another reason is that the I2C line can reliably extend to a maximum of 0.5 meters with lower speed to 1 meter, and the distance between sensors needed for our research is 2 to 4 meters. The last reason is because one of the sensors has a voltage output, with a higher length of a wire between the sensor and the microcontroller adds unwanted induced noise, because the wire acts as an antenna, picking up passing signals. The sensing and data relay Arduinos communicate over RS485 bus which allows for communication up to 1200 meters. The data relay Arduino saves the received data on a micro-SD card using a SD card module and relays the data to the cloud using a GSM communication module. The communication between the backup and relay module and the GSM and SD Card module is over the SPI Bus.

Software and Cloud

The Arduinos are programmed in an Arduino IDE, which is the standard development environment when working with Arduino development boards. Other editors can be used as well, for example VS Code, but these editors require plugins to be installed for them to be able to program the Arduino boards.

The data will be sent to a cloud storage like AWS, Google Firebase or Microsoft Azure. With access to the raw and aggregated data over a website, a user will be able to view the data anywhere on their phone and check the status of the automatic measurement system like the battery status.

Future Work

The system is built with Arduino boards that contain many unnecessary parts, which consume power. In the next steps we will design a custom PCB will contain only the necessary part, thus lowering the power consumption and extending the measurement period. We expect to lower the power consumption to a point at which a solar panel will not be needed for measurements lasting up to two years. This would make the at site installation easier, because mounting the solar panels and wiring the whole setup requires a lot of time and is not cheap.

Communication wise, we are planning to test a solution that uses wireless communication instead of communication over the RS485 bus. This would further decrease the need for wires, making the system truly modular and easy to use.

The solution can be modified to specific needs. In case of a project Exploring of context between growing plants and change in soil with using IoT lead by Ing. Jiří Marčan, there is no need for measurements spread up by several meters. On the fig. 2 it is visible that the sensing module and backup and relay modules were merged, and the result is a single DAQ device capable of measuring and saving the data on its own, saving power and space.

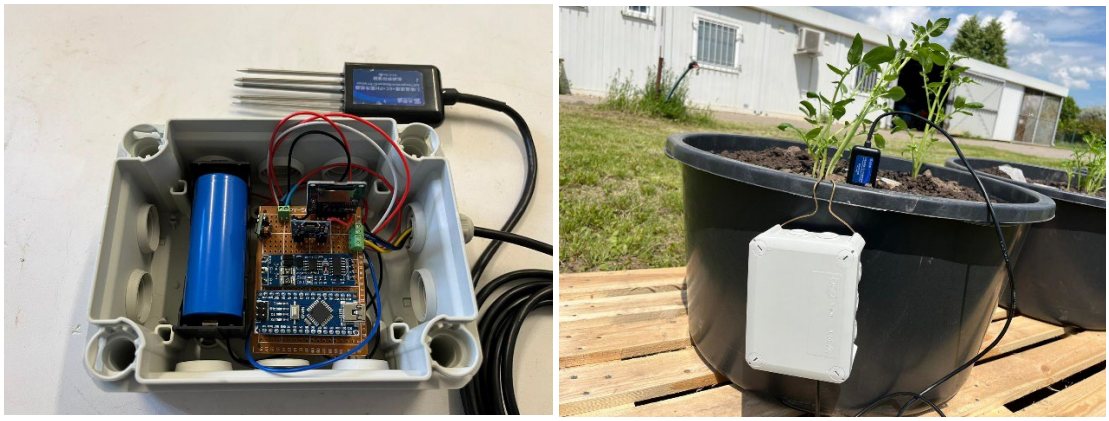

Figure 2 Data acquisition device with the sensing module and backup and relay modules merged. One the left image is the inside of the device with the battery on the left and Arduino Nano board, micro-SD card module, solar charger module, RS485 to UART bridge and regulator on the right. On the right image is the DAQ with a connected soils sensor automatically collecting data and saving it on an micro-SD card.

CONCLUSION

In conclusion, the developed Arduino-based measurement device offers a cost-effective and reliable solution for long-term environmental monitoring in remote locations. The system's design addresses key challenges such as power consumption, sensor integration, and data transmission. By leveraging open-source hardware and software, the solution is accessible and customizable, making it suitable for various research applications, particularly in budget-constrained settings. Future work will focus on field testing, further optimization of power management, and exploring additional sensor integrations to enhance the system's versatility and reliability.

ACKNOWLEDGEMENTS

We would like to express gratitude to our supervisor and the head of the department of agricultural machines at the Czech University of Life Sciences Prague prof. Dr. Ing. František Kumhála for his support of this project.

REFERENCES

ALI, S., ZANZINGER, Z., DEBOSE, D., STEPHENS, B., 2016. Open Source Building Science Sensors (OSBSS): A low-cost Arduino-based platform for long-term indoor environmental data collection. *Building and Environment*. May 2016. Vol. 100, p. 114–126. DOI 10.1016/j.buildenv.2016.02.010.

ANASTASI, G., CONTI, M., DI FRANCESCO, M., PASSARELLA, A., 2009. Energy conservation in wireless sensor networks: A survey. *Ad Hoc Networks*. May 2009. Vol. 7, no. 3, p. 537–568. DOI 10.1016/j.adhoc.2008.06.003.

CELISLAMI, E., RAWASHDEH, O., DELVESCOVO, D., 2024. Low-Cost Open-Source Data Acquisition for High-Speed Cylinder Pressure Measurement with Arduino. In: . 9 April 2024. DOI 10.4271/2024-01-2390.

CHUNG, T., BAGUR, J., 2024. The Arduino Guide to Low Power Design. *Arduino docs*. Online. 2024. Available from: https://docs.arduino.cc/learn/electronics/low-power/ [Accessed 5 June 2024].

GOYAL, D., PATRA, S., SAPRE, A., KAUR, M. and RAMGIR, S., 2024. Design and Development of Arduino-Based Four-Channel Data Acquisition System with Digital Temperature Control for Chemiresistive Sensors. *Sensing and Imaging*. 25 May 2024. Vol. 25, no. 1, p. 30. DOI 10.1007/s11220-024-00477-2.

KHALEEL, K., AL-NAIB, I., ATYIA, H., 2024. An efficient wireless monitoring system for photovoltaic panels using bluetooth technology. In: . 2024. p. 020001. DOI 10.1063/5.0182370.

LUO, Ch., HUI, L., SHANG, Z., WANG, Ch., JIN, M., WANG, X., LI, N., 2024. Portable Arduino-Based Multi-Sensor Device (SBEDAD): Measuring the Built Environment in Street Cycling Spaces. *Sensors*. 13 May 2024. Vol. 24, no. 10, p. 3096. DOI 10.3390/s24103096.

MEKKI, K., BAJIC, E., CHAXEL, F., MEYER, F., 2018. Overview of Cellular LPWAN Technologies for IoT Deployment: Sigfox, LoRaWAN, and NB-IoT. In: *2018 IEEE International Conference on Pervasive Computing and Communications Workshops (PerCom Workshops)*. IEEE. March 2018. p. 197–202. ISBN 978-1-5386-3227-7. DOI 10.1109/PERCOMW.2018.8480255.

RAZA, U., KULKARNI, P., SOORIYABANDARA, M., 2017. Low Power Wide Area Networks: An Overview. *IEEE Communications Surveys & Tutorials*. December 2017. Vol. 19, no. 2, p. 855–873. DOI 10.1109/COMST.2017.2652320.

SULAYMAN, A., ARAROMI, O., AYODELE, E., ARAROMI, O., OSUOLALE, N., 2024. Arduino microcontroller based real-time monitoring of haemodialysis process for patients with kidney disease. *e-Prime - Advances in Electrical Engineering, Electronics and Energy*. March 2024. Vol. 7, p. 100403. DOI 10.1016/j.prime.2023.100403.

ZIMMERS, E., BROWN, L., 1980. The selection of microcomputers for industrial data acquisition. *Computers & Industrial Engineering*. January 1980. Vol. 4, no. 4, p. 293–302. DOI 10.1016/0360-8352(80)90006-6.

BIOGAS PRODUCTION FROM FOOD PRODUCTION WASTE

TOMÁŠ GIERTL[1], JÁN GADUŠ[2], MICHAL ANGELOVIČ[1]

[1] SPU v Nitre, Ústav poľnohospodárskej techniky, dopravy a bioenergetiky

[2] SPU v Nitre, Ústav práva a udržateľného rozvoja

Abstract: The search for new input materials for biogas production is a very current topic. Many operators of biogas stations are forced to limit the consumption of corn silage simply because of the high price of the input raw material. The paper deals with the possibilities of using alternative input materials for biogas production. We compared corn silage, potatoes and cocoa bean husks. The results show that cocoa bean husks are a very interesting material for biogas production. Biogas production is 150% higher than from corn silage and the methane content of biogas is 13% higher.¶

Keywords: waste, electricity, energy, biogas

INTRODUCTION

Slovenská republika sa v rámci záväzkov plynúcich z jej členstva v Európskej únii zaviazala k uhlíkovej neutralite do roku 2050 s cieľom zvrátiť nežiadúce dopady klimatickej krízy spôsobenej emisiami skleníkových plynov. Udržateľný manažment odpadov je jedným z nástrojov ako môžu krajiny významne prispieť k naplneniu tohto cieľa. Kým zdrojov skleníkových plynov existuje niekoľko, za najvýznamnejšie skleníkové plyny sa považuje oxid uhličitý (CO_2), metán (CH_4) a oxid dusný (NO_2). Práve produkcia metánu a jeho koncentrácia v atmosfére v roku 2020 zalarmovovala vedecký svet, nakoľko nové zistenia ukázali, že jeho koncentrácia mnohonásobne prekračuje predošlé namerané hodnoty, pričom väčšina má antropogénny pôvod, teda pochádza z ľudskej aktivity (University of Rochester, 2020). Podľa odhadov EDF antropogénny metán v súčasnosti prispieva ku globálnemu otepľovaniu až 25-imi percentami (Katz, 2021). Metán je mnohonásobne škodlivejší než oxid uhličitý kvôli jeho schopnosti zachytávať teplo, a teda prispievať k otepľovaniu našej planéty. Teplo zadržiava približne 28- až 36-krát účinnejšie než oxid uhličitý v časovom horizonte 100 rokov, v krátkodobom horizonte je to až 80-krát, pričom relatívne výhodnou je jeho krátka životnosť v atmosfére v trvaní 9 rokov (IPPC, 2014). Práve vďaka týmto vlastnostiam môže mať zo strednodobého hľadiska zníženie emisií metánu najvýznamnejší dopad v zmierňovaní globálneho otepľovania a klimatickej krízy (Mathew, 2020).

Najväčším zdrojom antropogénneho metánu je potravinový systém, najmä živočíšna výroba, produkcia určitých plodín, ako napríklad ryža a v neposlednom rade odpad z potravín. Nielenže sa poľnohospodárska výroba celosvetovo zintenzívňuje, ale aj množstvo skládkovaného odpadu celosvetovo rastie a stáva sa globálnym problémom, ktorý môže do významnej miery ohroziť nielen kvalitu ovzdušia, ale aj kvalitu čoraz vzácnejších prírodných zdrojov - vody a pôdy. Práve spotrebitelia a domácnosti sú významným producentom potravinového odpadu. Slovensko nie je výnimkou. Na jedného Slováka podľa štúdie FUSIONS (2017) pripadá celkovo 163 kg, pričom domácnosti sú zodpovedné za 53 %. Väčšina z tohto odpadu sa pritom nachádza v zmesovom komunálnom odpade.

To, že Slovenská republika si uvedomuje dôsledky skládkovania organického odpadu, sa odrazilo aj na jednom z cieľov Programu predchádzania vzniku odpadov SR pre roky 2014 – 2018 „Znižovať vznik BRKO (biologicky rozložiteľný komunálny odpad) a znižovať podiel BRKO v ZKO (zmesový komunálny odpad)“ (MŽP, 2014, str.40). Tento cieľ sa však v danom rámcovom období naplniť nepodarilo, naopak, množstvo BRKO zaznamenalo nárast (Odpady Portál, 2021). Napriek relatívne náhlemu plošnému zavedeniu zberu BRKO ide o komplexnú problematiku zhodnocovania významných zdrojov energie a živín, ktorá nemá len lokálny, ale aj regionálny, či dokonca národný a nadnárodný význam.

MATERIALS and METHODOLOGY

Pre účely realizovania porovnávacích testov výdatnosti rôznych zmesí vstupnej biomasy na SPU v Nitre sú využívané experimentálne fermentory pre tzv. dávkové (batch) pokusy s nasledovnými základnými parametrami: fermentor s dvojitým plášťom, čistým objemom 100 dm^3, s elektrickým ohrevom vykurovacej vody, s digitálnou reguláciou teploty s presnosťou ± 0,5 °C a elektrickým pomalobežným miešadlom s možnosťou nastavovania času miešania a prestávok (12 cyklov za deň v trvaní 20–30 minút).

Vyprodukované množstvo bioplynu sa kontinuálne meria a zaznamenáva plynomerom pre malé prietoky Ritter s automatickým záznamom využívajúc software RIGAMO. Fermentor je vybavený uzávermi umožňujúcimi odber substrátu počas experimentu k realizovaniu chemických rozborov, ako aj na analyzovanie zloženia produkovaného bioplynu (Obrázok 1). Usporiadanie experimentálnych fermentorov s plynomermi je znázornený na Obrázku 2.

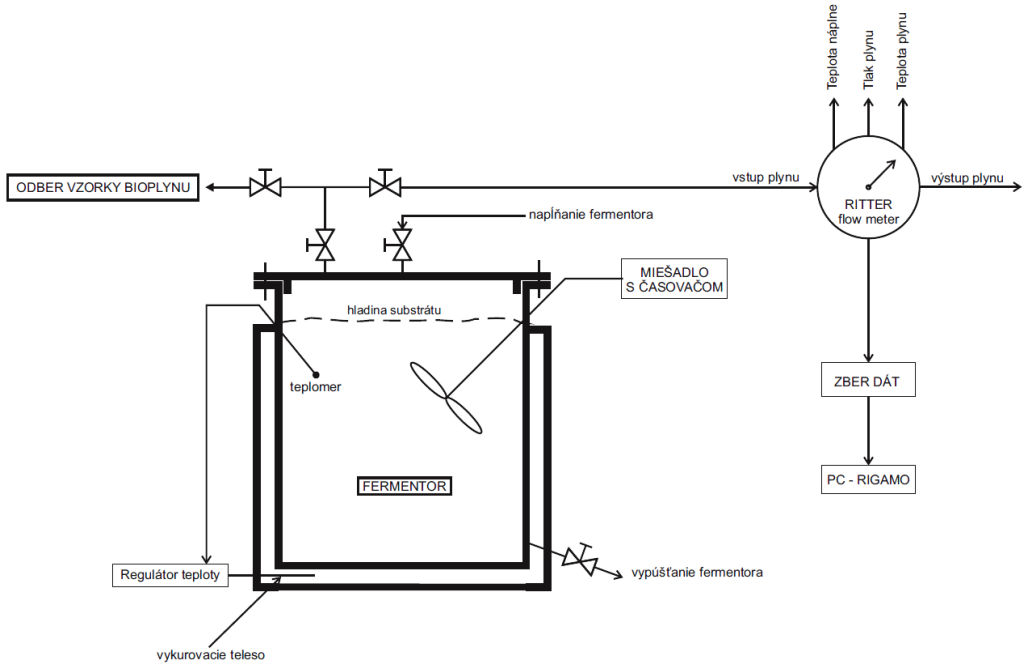

Obrázok 1 Technologická schéma experimentálneho fermentora 100 l

Každý experiment zameraný na zisťovanie výdatnosti bioplynu skúmaného substrátu je realizovaný v dĺžke 600 hodín. Po nadávkovaní skúmaného materiálu do fermentora a doplnení inokulom (odobratým z prevádzkového fermentora bioplynovej stanice) sú realizované analýzy vzoriek bioplynu z bioreaktora – merané sú nasledovné parametre v zmysle prijatej metodiky:

a. TF – teplota vo fermentore (°C).

a v každý deň pokusu sú realizované analýzy zloženia produkovaného bioplynu:

a. CH_4 – metán (obj.%),
b. CO_2 – oxid uhličitý (obj.%),
c. H_2S – sírovodík (ppm),
d. O_2 – kyslík (obj.%).

Okrem toho denne je stanovovaná produkcia bioplynu:

a. PBP – prietok bioplynu ($dm^3.h^{-1}$),
b. KPBP – kumulatívna produkcia bioplynu (dm^3), realizovaná automaticky,

Obrázok 2 Usporiadanie 100 l fermentorov s plynomermi

S cieľom hľadať možné alternatívne vstupné materiály pre produkciu bioplynu boli výskumu podrobené ako vstupné materiály odpady z potravinárskej výroby a porovnávali sa s produkciou bioplynu z kukuričnej siláže (Tabuľka 1).

Tabuľka 1 Testovaná vstupná biomasa pre produkciu bioplynu

Biomasa	**Zemiaky**	**Šupy kakaových bôbov**	**Kukuričná siláž**
Množstvo (kg)	2	2	2

Vstupné suroviny boli bez úprav nadávkované do fermentorov a doplnené inokulom odobratým z fermentora bioplynovej stanice v objeme 98 dm^3. Po uzavretí fermentora bol nastavený automatický režim kontroly ohrevu na teplotu 40 °C ± 1 °C, ako aj automatický režim záznamu kumulatívnej produkcie bioplynu v riadiacom programe plynomeru pre malé množstvá. Hodnota produkcie bioplynu sa zaznamenávala každú hodinu. Raz denne boli uskutočňované analýzy produkovaného bioplynu. Výsledkom experimentu je grafické znázornenie produkcie bioplynu a grafické znázornenie chemického zloženia bioplynu.

RESULTS and DISCUSSION

Kumulatívnu produkciu bioplynu (KPBP) vybraných materiálov je vidieť Obrázku 3. Celkovo bolo z testovanej vstupnej biomasy „Zemiaky 2 kg + inokulum 98 dm^3“ vo fermentore vyprodukovaných za 600 hodín 260 dm^3 bioplynu. Zo vstupnej biomasy „Šupy kakaových bôbov 2 kg + inokulum 98 dm^3“ bolo celkovo vyprodukovaných 1231,5 dm^3 [a] zo vstupnej biomasy „Kukuričná siláž 2 kg + inokulum 98 dm^3“ bolo celkovo vyprodukovaných 590 dm^3 bioplynu.

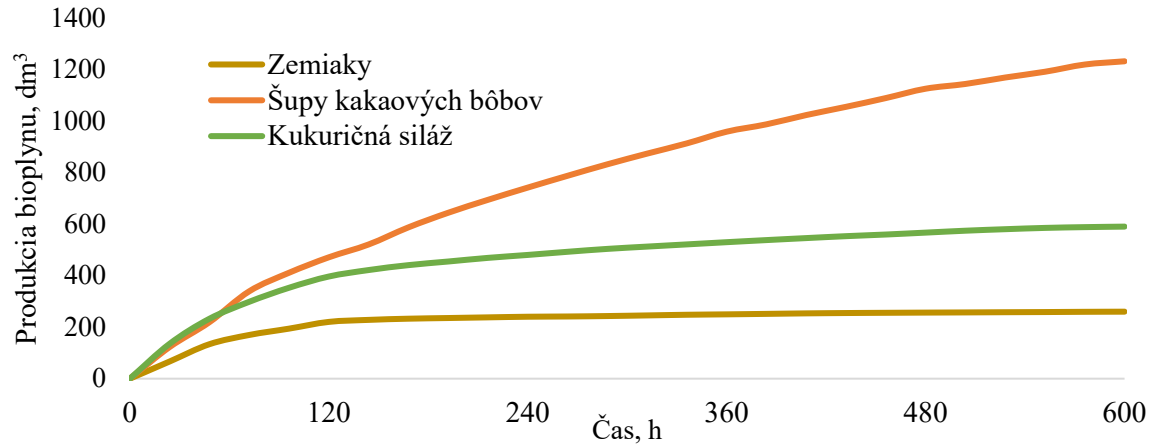

Obrázok 3 Kumulatívna produkcia bioplynu

Obrázok 4 znázorňuje prietok bioplynu (PBP) počas experimentu. Maximálny prietok bioplynu nastal vo všetkých prípadoch v priebehu prvých 72 hodín. V prípade kukuričnej siláže to bolo 5,64 $dm^3.h^{-1}$, v prípade šúp kakaových bôbov 5,6 $dm^3.h^{-1}$ a v prípade zemiakov 2,61 $dm^3.h^{-1}$. Následne prietok bioplynu klesal a nedochádzalo k výrazným zmenám v prietoku až do ukončenia experimentu.

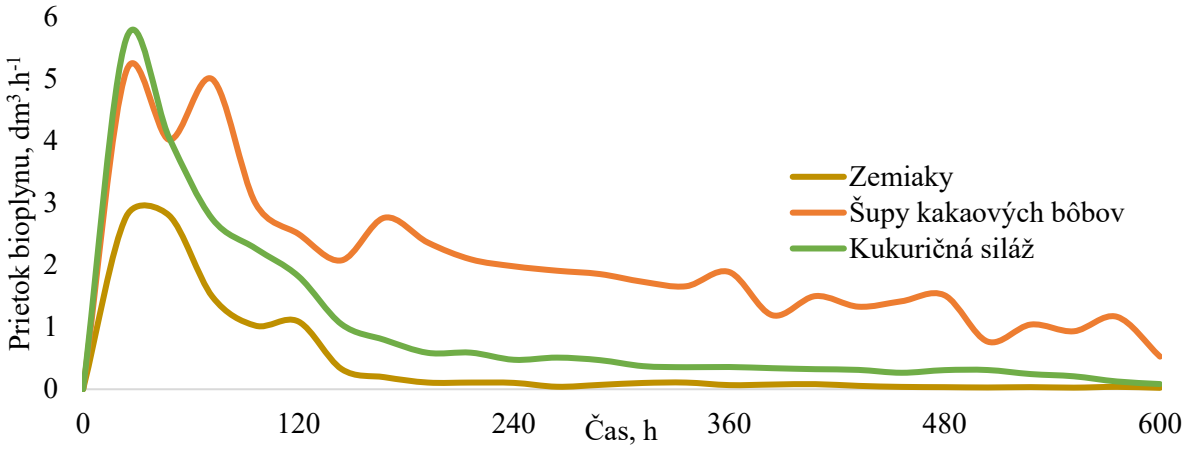

Obrázok 4 Prietok bioplynu

Obrázok 5 znázorňuje obsah metánu v bioplyne. Obsah metánu v bioplyne sa vyvíjal odlišne vo všetkých troch prípadoch. V prípade zemiakov sa obsah CH_4 zvyšoval prvých 120 hodín na hodnotu 70 % CH_4. Ďalších 120 hodín bol obsah CH_4 v rozsahu 68 až 72 %. Od 240-tej hodiny obsah CH_4 klesal až do ukončenia experimentu, na hodnotu 56 % CH_4. V prípade šúp kakaových bôbov sa obsah CH_4 zvýšil počas prvých 120 hodín na hodnotu 62 %. Maximálny obsah CH_4 bol dosiahnutý po 240-tich hodinách, kedy bola dosiahnutá hodnota 69,8 %. V štúdii o alternatívnej energii Redjeki (2013) vhodnou kombináciou čokoládovej kôry a vody dosiahol obsah metánu 74,22 %, čo je približne o 4 % viac v porovnaní s nami dosiahnutými výsledkami. Ďalej, až do ukončenia experimentu sa obsah CH_4 pohyboval medzi hranicami 67,3 % až 68,9 %. Kukuričná siláž dosiahla maximálny obsah CH_4 62,5 % po 72 hodinách od začiatku experimentu. Ďalej obsah CH_4 klesal a po 240-tich hodinách, až do ukončenia experimentu sa pohyboval medzi hranicami 48 % a 52,8 %. Podobný obsah metánu (54,6 %) stanovil Thiago Da Silva (2016).

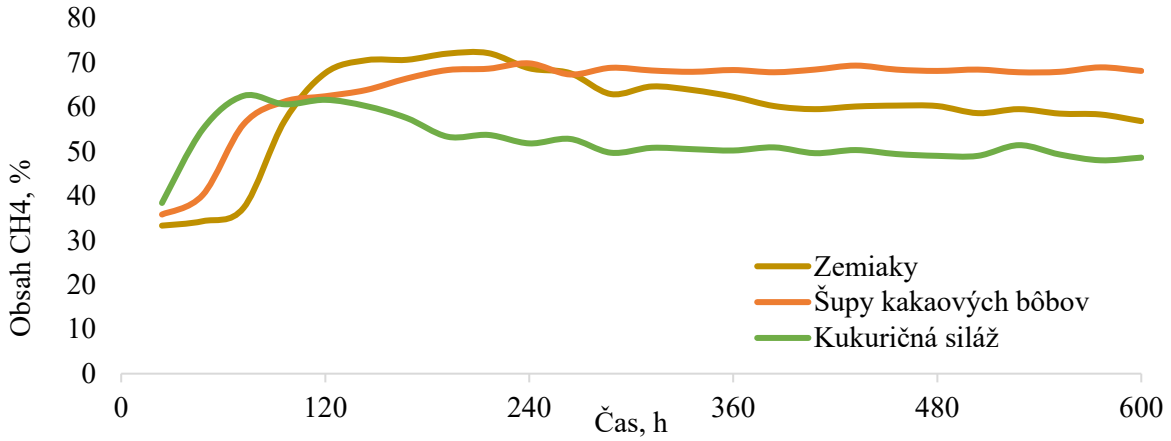

Obrázok 5 Obsah CH_4 v bioplyne

Obrázok 6 znázorňuje obsah CO_2 v produkovanom bioplyne. Na začiatku experimentu dosahuje obsah CO_2 hodnoty okolo 62 % vo všetkých troch skúmaných materiáloch. Uvádzaný vývoj produkcie CO_2 v bioplyne korešponduje s vývojom tak, ako ho popisuje Straka (2003).

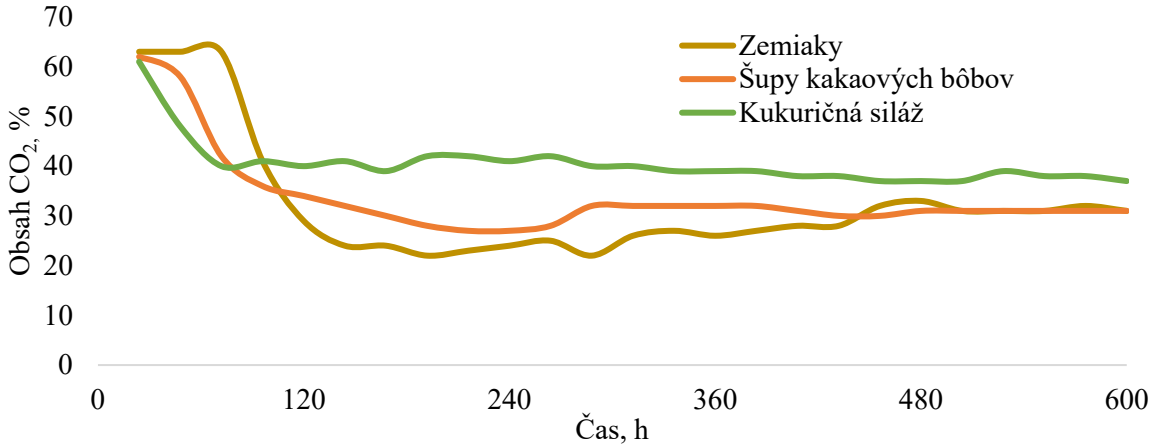

Obrázok 6 Obsah CO_2 v bioplyne

Proces tvorby bioplynu sa uskutočnil v anaeróbnych podmienkach, to znamená bez prístupu kyslíka. Analýzy bioplynu preukázali, že počas experimentov bol kyslík prítomný do 0,5 % (Obrázok 7).

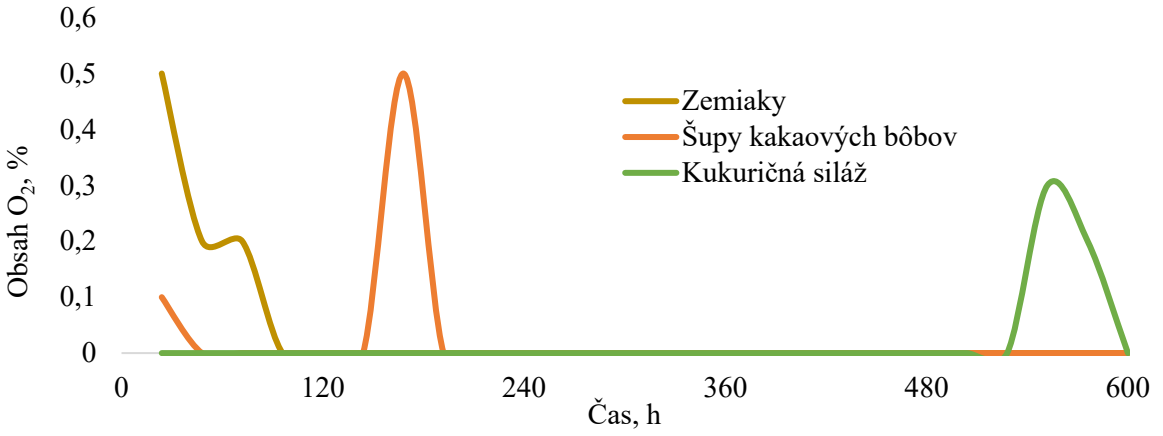

Obrázok 7 Obsah O_2 v bioplyne

Nežiadúcim komponentom v bioplyne je H_2S. Spôsobuje koróziu a znižuje životnosť spaľovacích motorov. Ako je znázornené na Obrázku 8, na začiatku experimentov boli zaznamenávané vyššie hodnoty. Bioplyn zo zemiakov obsahoval 1 500 ppm H_2S, bioplyn z šúp kakaových bôbov 1 300 ppm H_2S a bioplyn z kukuričnej siláže obsahoval 874 ppm H_2S. V priebehu 120 hodín bol obsah H_2S pod 1 000 ppm pri všetkých troch skúmaných vzorkách. V ďalších hodinách už nebol zistený prudký pokles H_2S. Priemerný obsah H_2S v bioplyne zo zemiakov bol 601 ppm, z šúp kakaových bôbov 446 ppm, z kukuričnej siláže 409 ppm.

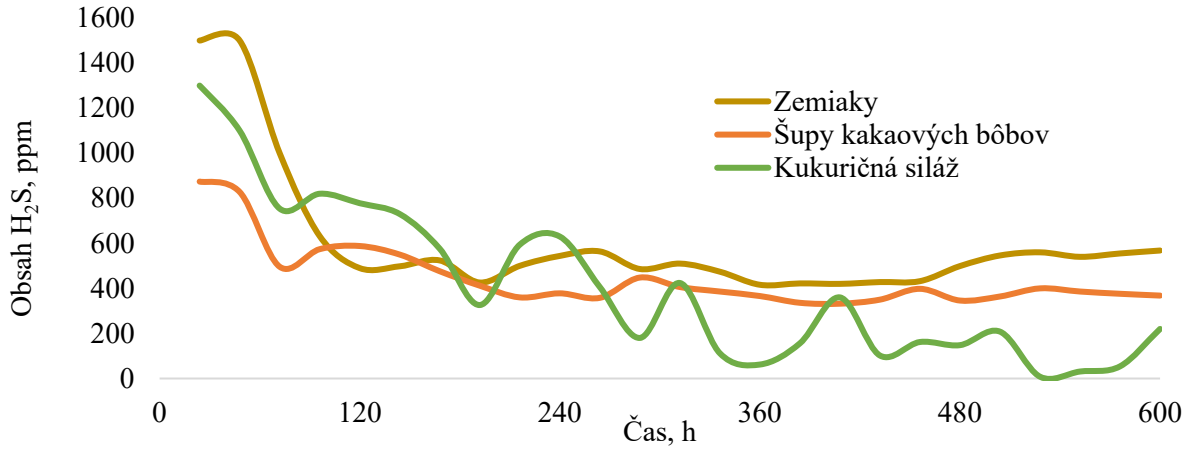

Obrázok 8 Obsah H_2S v bioplyne

CONCLUSION

V súčasnosti sa na produkciu bioplynu na Slovensku využíva najčastejšie kukuričná siláž (podľa štatistík viac ako 80 %), a to spôsobuje opakované pestovanie kukurice na tých istých poliach niekoľko rokov. Jeden z problémov je, že pri monokultúrnom pestovaní kukurice (na zrno, siláž, bioplyn) sa zvýšil podiel burín, na ktoré nedostatočne zaberajú herbicídy. Preto je dôležité hľadať iné vstupné suroviny, ktoré nebudú narušovať striedanie plodín (osevný postup) a nebudú v konkurencii s potravinami. Z uvedených experimentov vyplýva, že je možné použiť ako náhradu za kukuričnú siláž aj odpadové zemiaky a šupy kakaových bôbov, ktoré nie je možné použiť ako potraviny. Zemiaky produkovali menej bioplynu ako kukuričná siláž, čo znamená, že pre dosiahnutie rovnakého výkonu kogeneračnej jednotky je potrebné vyššie množstvo vstupnej suroviny. Pozitívne je, že priemerný obsah metánu je o 8 % vyšší ako pri kukuričnej siláži. Výhodou použitia šúp kakaových bôbov je, že je vyššia produkcia bioplynu v porovnaní s kukuričnou silážou a aj obsah metánu v bioplyne je o 13 % vyšší, čo pozitívne ovplyvňuje spotrebu plynu spaľovacieho motora. Vzhľadom k vyššiemu obsahu sírovodíka v bioplyne vo všetkých troch skúmaných materiálov, je potrebné zabezpečiť odsírovanie bioplynu.

REFERENCES

KATZ, CH., 2021. *The search for the world's largest methane sources*. Online. Dostupné na: https://www.bbc.com/future/article/20210805-the-search-for-the-worlds-largest-methane-sources [dátum citovania 2024-05-19]

MATHEW, R., 2020. *A Rising Problem: Methane More Dangerous than Previously Thought*. Online. Dostupné na: https://ramapolookout.blogspot.com/2020/04/a-rising-problem-methane-more-dangerous.html [dátum citovania 2024-04-09]

MŽP SR, 2014. *Program predchádzania vzniku odpadu SR na roky 2014-2018* . Online. Dostupné na: https://www.minzp.sk/files/sekcia-enviromentalneho-hodnotenia-riadenia/odpady-a-obaly/regi stre-a-zoznamy/ppvo-vlastnymaterial.pdf [zobrazené 2024-05-09]

ODPADY PORTÁL, 2021. *Slovensko stále nespĺňa európske ciele o odpadoch*. Online. Dostupné na: https://www.odpady-portal.sk/Dokument/105873/slovensko-stale-nesplna-europske-ciele-o-odpadoch.aspx [zobrazené 2024-04-09]

REDJEKI, S., TRIANA, N.W., IRIANI, UTAMI, I., 2013. *Alternative energy biogas from chocolate rind*. Procedia - Social and Behavioral Sciences. Online. Volume 103. 13th International Educational Technology Conference. Dostupné na: https://doi.org/10.1016/j.sbspro.2013.10.312 [dátum citovania 2024-04-09]

STRAKA, F., 2003. *Bioplyn*. Říčany: GAS s.r.o. 517s. ISBN 80-7328-029-9

DA SILVA, T., SANTOS, E.M., 2016. *Advances in Silage Production and Utilization*. Online. London: IntechOpen. 206 s. Dostupné na: http://dx.doi.org/10.5772/61574. ISBN 978-953-51-2777-2 [dátum citovania 2024-04-09]

UNIVERSITY OF ROCHESTER, 2020. *Methane emitted by humans vastly underestimated.* Online. Dostupné na: https://www.sciencedaily.com/releases/2020/02/200219113746.htm [dátum citovania 2022-04-09]

MANAGEMENT OF THE WINE FILTRATION PROCESS IN A WINERY

ZUZANA LAUKOVÁ[1], JÁN JOBBÁGY[1], KOLOMAN KRIŠTOF[1], MICHAL ANGELOVIČ[1], ZUZANA BAJUSOVÁ[2]

[1] Ústav poľnohospodárskej techniky, dopravy a bioenergetiky, TF, SPU v Nitre

[2] Ústav ekonomiky a manažmentu, FEM, SPU v Nitre

Abstract: The article is focused on assessing the efficacy of two different types of wine filtration equipment. The measurements were carried out on a plate filter (Jolly 30) and diatomaceous earth filter (Velo FOB 2). The chosen company is Velkeer 1113, s.r.o., which is based in the village of Velky Kyr in the Nitra wine region. Four varieties of wine were used as samples (Devin, Gewurztraminer, Dunaj and Alibernet). Filtration of these varieties were further carried out on wine in various stages of processing (initial filtration, primary fermentation, fined with bentonite, malolactic fermentation, final filtration). In the present work we introduced time-frames for the different operations (primetime filtration, time to overcharge filter, time for maintenance or machine preparation, time to remove defects, time for rest). Comparing the results, we found that the best wines were achieved through single filtration and that the diatomaceous earth filter was more efficient than the plate filter.

Keywords: filtration, wine, plate filter, diatomaceous earth filter

INTRODUCTION

Účelom lisovania je oddelenie muštu od rmutu, ktoré môže byť vykonané mechanicky – tlakom alebo odstredivou silou. Účinnosť procesu je ovplyvnená predovšetkým druhom lisovacieho zariadenia, konzistencie lisovaného materiálu (odroda), stupňom zrelosti, spôsobom spracovania pred lisovaním (drvenie, odstopkovanie, macerácia), hrúbkou lisovacej vrstvy a počtom lisovacích cyklov (Burg, Zemánek, 2014). Ošetrovanie a školenie vína sú všetky úpravy, ktoré zlepšia trvanlivosť, chuť, vzhľad a buket vína (Jobbágy, Findura, 2013).

Filtrácia je technologická operácia, ktorej účelom je odstrániť z vína nežiaduce častice (kaly, kalotvorné látky, koloidy a i.), ktoré sa vo víne nachádzajú. Filtrácia znamená cedenie vína cez jemné pórovité materiály (Kunová, Lopašovský, 2015). Pre filtráciu sa aplikujú rôzne filtre ako napr. tlakové naplavovacie, tlakové vložkové a pod. (Filtrácia, 2018). Na materiál použitý na filtráciu vína sa kladú veľké nároky. Dôležitá je jeho indiferentnosť t.j. nesmie vplyvom alkoholu alebo kyselín nič odovzdávať do vína a z druhej strany, nesmie víno ochudobňovať o chuťové a aromatické látky. Okrem použitia vhodného druhu filtračnej látky je rozhodujúci aj typ filtračného zariadenia a druh vína. Nezanedbateľným faktorom je tiež výkon filtrácie a spotreba filtračného materiálu. Filtračná látka musí byť ľahká, aby pri nanášaní na filtračný element nedochádzalo k sedimentácii. Aby mala filtračnú schopnosť, musí byť tiež mikropórovitá a mať také zloženie, aby nevyžadovala nákladné úpravy. Musí byť dobre súdržná, ale nemôže byť mastná ani lepkavá (Kunová, Lopašovský, 2015).

Hlavným cieľom príspevku bolo posúdiť celkový proces riadenia výroby vína vo vybranom vinárskom podniku.

MATERIALS and METHODOLOGY

Vinársky podnik Velkeer 1113, s.r.o.

Rodinné vinohradníctvo a vinárstvo Velkeer 1113, s.r.o. je slovenská vinárska spoločnosť zameriavajúca sa výrobou prémiových vín. Spoločnosť pôsobí na trhu od roku 2011 a opiera sa o viacgeneračnú tradíciu výroby vína rodiny, ktorá siaha až do 18 - teho storočia.

Celková výmera vlastných vinohradov predstavuje viac ako 10 ha, pričom sa tieto vinohrady nachádzajú v jednej z najlepších oblastí na pestovanie hrozna na Slovensku – v Nitrianskej vinohradníckej oblasti. Najväčšiu rozlohu vo vinohradoch predstavujú odrody Rizling Rýnsky a Rizling Vlašský, ktoré sú pre túto oblasť historicky významné. V mladej výsadbe má vinárstvo vysadené aj slovenské novošľachtence ako Dunaj a Devín, ktoré sa prezentujú vysokým potenciálom.

Priemerná ročná produkcia vinárstva je 40 000 fliaš vína, tieto fľaše sú vďaka distribučným kanálom umiestňované na celom svete. Na základe filozofie rodiny a manažmentu podniku sa produkty neumiestňujú do nákupných reťazcov, fľaše s logom Velkeer 1113 je možné si zakúpiť len v špecializovaných predajniach, vo vinotékach, a v HORECA zariadeniach.

Filtrácia

Filtrovanie sa vykonáva buď na kremelinovom filtri Velo Fob 2 alebo na doskovom filtri Jolly 30. Technické parametre sú uvedené v tabuľke 1 a v tabuľke 2. Časové snímky sa vykonávali pre tieto pracovné operácie:

t_1 – hlavný čas filtrácie,
t_2 – čas na prebitie filtra,
t_3 – čas na údržbu alebo prípravu stroja,
t_4 – čas na odstránenie porúch,
t_5 – čas na odpočinok.

Tabuľka 1 Technické parametre filtračného zariadenia

Filter	**Kremelinový filter Velo FOB 2**
Výrobca	VeloAcciaiS.r.l
Priemerný prietok, $l.h^{-1}$	3000
Maximálny pracovný tlak	6 atm.
Filtračná plocha, m^2	2
Maximálny výkon	3,25 kW
Rozmery (d . š . v), mm	1650 x 900 x 1710
Hmotnosť, kg	200
Požitý filtračný materiál	KremelinaBecoGur 3500

Tabuľka 2 Technické parametre filtračného zariadenia

Filter	**Doskový filter Jolly 30**
Výrobca	MORI-TEM Srl
Model	Jolly 30
Počet dosiek	31
Rozmer dosiek, cm	20x20
Filtračná plocha, m^2	1,2
Výkon, Prietok, $l.h^{-1}$	900
Hmotnosť, kg	43
Požitý filtračný materiál	Filtračné dosky BecoPad 450

Obrázok 1 Vinohrady Velkeer 1113, s.r.o.

RESULTS and DISCUSSION

Charakteristika odrôd hrozna

Odrody, ktoré sme použili ako vzorky pri filtrovaní sú Devín, Tramín červený, Dunaj a Alibernet.

Devín. Vína odrody Devín sú aromatické, muškátovo – kvetinovo–korenisté. Vznikla v roku 1958 krížením Tramínu červeného s Veltlínskym červeno-bielym, ktoré na Výskumnou ústave vinohradníckom a vinárskom v Bratislave uskutočnila pani Ing. Dorota Pospíšilová PhD. V súčasnosti sa na Slovensku pestuje na približne 75 ha, čo predstavuje 0,49 % plochy. Uznaná bola u nás v roku 1997 a v Českej republike od roku 1998.Pre výsadbu sú vhodné svahovité pozemky, s veľmi dobrou expozíciou na slnečné žiarenie. Je náročná na pôdne podmienky, neznáša suché lokality. U Devínu s stretávame i s akostnými vínami. Pre túto odrodu sú však vhodnejšie prívlastkové vína a nezriedka sa vyskytujú aj najvyššie kvalitatívne stupne s hroznom napadnutým ušľachtilou formou šedej hniloby. K výrobe vína sa odporúča metóda krátkej macerácie za účelom zvyšovania uvoľňovania aromatických muškátovo-kvetinových látok obsiahnutých v šupkách bobúľ. Aromatický prejav môže byť zvýraznení výberom vhodného kmeňa kvasiniek. U suchých vín býva aróma často nevýrazná a zastretá vysokým obsahom alkoholu (14–16 obj. %). Preto je pri vínach vyrobených s hrozna o vysokej cukornatosti vhodné nenechať prekvasiť víno do sucha a tým smerovať k dosiahnutiu harmónie medzi cukrom, kyselinami a aromatickým charakterom vín (Devín, 2018).

Obrázok 2 Kremelinový a doskový filter

Tramín červený. Vína z Tramínu červeného sú výrazne aromatické s ovocnými tónmi pripomínajúcimi tropické plody. Pôvod tejto starej kultúrnej odrody je značne nejasný. Prvotným predpokladom bolo, že sa jedná o starú odrodu pochádzajúcu z Grécka. V 15. storočí je potvrdený jej výskyt v obci Tramino v južnom Tirolsku. Je typickou odrodou severných vinohradníckych oblastí. V Európe je rozšírený vo francúzskom Alsasku, v Nemecku, Rakúsku, severnom Taliansku, Slovinsku, Chorvátsku, Maďarsku, Rumunsku, na Ukrajine a v Moldavsku. Na Slovensku sa pestuje na 2 % z vinohradníckych plôch, čo predstavuje 318 ha. Zaregistrovaný bol v roku 1941. Požiadavky na pestovateľskú polohu sú veľmi

vysoké. Vyžaduje polohy chránené pred vetrom a najmä v období kvitnutia vyžaduje dostatok tepla. Má vysoké nároky aj na pôdu. Vyžaduje hlboké, ľahko záhrevné a úrodné pôdy. Najlepšie sú hlinité pôdy s nízkym obsahom vápnika. Tramín červený je odrodou pre vína všetkých akostných kategórií a predovšetkým pre odrodové vína.Pri technológií výroby je opäť veľmi dôležité prevedenie krátkodobej macerácie pri riadených teplotách, ktorá napomôže lepšej extrakcií aromatických a chuťových látok. Výroba vína u Tramínu by mala smerovať i k dosiahnutiu vysokého extraktu vo vínach. Preto je vhodné iba jemné odkalenie, aplikácia čistej kultúry kvasiniek a kvasenie pri teplotách okolo 20 °C.Výrazne aromatické vína sa môžu získať metódou chladného kvasenia. U týchto vín však často chýba chuťová plnosť, preto je vhodná predovšetkým pre akostné a kabinetné vína (Tramín, 2018).

Dunaj. Dunaj je veľmi kvalitná odroda. Dáva vína tmavočervenej farby, s výraznou chuťovou plnosťou. V chuti a vôni sú tóny prezretých čerešní a višní, ktoré prechádzajú až do veľmi zaujímavých čokoládových tónov. Odrodu vyšľachtila vo Výskumnom ústave vinohradníckom a vinárskom v Bratislave D. Pospíšilová. Pochádza z trojitého kríženia odrôd (Muškát Bouchet x Oportox Svätovavrinecké). Pestuje sa iba u nás a okrajovo v ČR. Na Slovensku tvorí 0,024 % vinohradov. Uznaná bola v roku 1997. Na polohu je nenáročný. Vo vynikajúcich lokalitách však poskytuje veľmi kvalitné červené vína. Na pôdu je stredne náročný. Nie sú vhodné vyložene výsušné pôdy, ale tiež ani veľmi výživné a vodozdržné. Hrozno odrody Dunaj sa často zberá vo vyšších prívlastkových stupňoch. Vhodné je zrenie vína v dubových sudoch. Vína majú výrazný ovocný charakter a preto je menej vhodné využitie barikových sudov. Dunaj je veľmi kvalitná odroda. Dáva vína tmavočervenej farby, s výraznou chuťovou plnosťou (Dunaj, 2018).

Alibernet. Alibernet je modrá muštová odroda, ktorú zaradujeme do skupiny farbiarok, t.j. odrôd, ktoré obsahujú antokyaninové farbivá nielen v šupke ale aj v dužine. Vznikla v roku 1950 v Ukrajinskom vedeckom ústave vinohradníckom a vinárskom v Odese, krížením odrôd AlicanteBouschet x CabernetSauvignon.Alibernet sa doposiaľ veľmi nerozšíril. V súčasnosti zaberá 0,63 % celkovej plochy vinohradov v SR. Zaregistrovaná bola v roku 1975.Patrí medzi odrody náročné na stanovište. Ideálne sú svahovité pozemky s južnou alebo juhozápadnou expozíciou. Hodí sa iba do teplejších oblastí. Vyžaduje pôdy dobre zásobené živinami, dostatočne záhrevnéa s dobrým vodným hospodárením. Pri kvalitne vyzretej surovine je možné využiť i priame lisovanie hrozna, bez akejkoľvek macerácie. V ostatných prípadoch potom dĺžku macerácie určujeme podľa charakteru vína ktoré chceme získať. Pri výrobe vína musí ísť najmä o harmóniu farebnosti a chuťového dojmu vína, nie o získanie čo najtmavšieho vína, avšak s veľmi ostrou trieslovinou v chuti. Alibernet je farbiarka, ale je v nej cítiť kabernetový charakter. Preto je vhodná iba na prifarbovanie kabernetových odrôd. Používa sa aj na výrobu odrodových vín, čo je rozšírené najmä u nás (Alibernet, 2018).

Zhodnotenie filtrácie

Devín: Z vypočítaných ukazovateľov vyplýva, že celkový čas filtrácie bol pri odrode Devín – viac ako 2,5 h (stočený z kvasenia), z čoho čistý čas filtrácie činil 1,5 h. Zostatkový čas pozostával z rôznych pracovných operácií ako napr. čas na úvodnú sanitáciu, príprava a inštalácia stroja, organizačné prestoje, čas potrebný na prebitie filtra, technické poruchy a koncová sanitácia stroja. Výkonnosť pri tomto vybranom víne bola u doskového filtra 0,67 $m^3.h^1$. Na druhej strane, výkonnosť u kremelinového filtra pri odrode Devín bola 1,82 $m^3.h^{-1}$ (stočený z kvasenia). V porovnaní s tou istou odrodou a úprave vína, ale už filtrovanom na kremelinovom filtri, činil celkový čas úkonu vyše 4 h a čistý čas filtrácie bol vyše 2 h. Z týchto nameraných výsledkov sme zistili, že hoci nám jednotlivé operácia a samotná filtrácia u kremelinového filtra trvala dlhšie, výkonnosť bola skoro trikrát vyššia (obr. 4a). Výkonnosť, pri filtrácii kremelinovým filtrom u vína jedenkrát filtrovanom, bola efektívnejšia o 70 %, u vína stočeného z bentonitu o 68 % a u vína stočeného z kvasenia o 63 %. Najdlhší pracovný úkon sa zaznamenal pri filtrácii vína stočeného z kvasenia na kremelinovom filtri. Pri tejto filtrácii neprišlo k žiadnym technickým alebo technologickým poruchám. Čas t5 bol nulový pri každej filtrácii (obr. 5a).

Tramín červený: Výkonnosť pri filtrácii kremelinovým filtrom u vína jedenkrát filtrovanom bola efektívnejšia o 71 %, u vína stočeného z bentonitu o 68% a u vína stočeného z kvasenia o 65% (obr. 4b). Najdlhší pracovný úkon činila filtrácia vína stočeného z kvasenia na doskovom filtri. Podrobnejšie výsledky sú uvedené na obr. 5b.

Dunaj: Výkonnosť pri filtrácii kremelinovým filtrom u vína jedenkrát filtrovanom bola efektívnejšia o 68 %, u vína dvakrát stočeného o 63% a u vína stočeného z jablkovo – mliečnej fermentácie o 62 % (obr. 6a). Pri uvedenej odrode činil najdlhší pracovný úkon pri filtrácii vína stočeného z jablkovo – mliečnej fermentácie na kremelinovom filtri. Najdlhšia bola operácia samotnej filtrácie. Pri tejto filtrácii neprišlo k žiadnym technickým alebo technologickým poruchám, preto čas t4 je nulový.

Alibernet: Na obr. 6b je uvedené porovnanie výkonností u kremelinového a doskového filtra pre odrodu Alibernet. Výkonnosť pri filtrácii kremelinovým filtrom u vína jedenkrát filtrovanom bola efektívnejšia o 74 %, u vína dvakrát stočeného o 72 % a u vína stočeného z jablkovo – mliečnej fermentácie o 70 %. Opäť bola najdlhšie operácia samotnej filtrácie, za ňou pokračuje samotná príprava a údržba stroja. Najmenšie zastúpenie mala časová zložka odstránenia porúch. Čas t5 bol nulový aj pri tejto vykonanej filtrácii.

V súčasnosti sa však čoraz viac začína používať tangenciálna filtrácia tzv. cross-flow filtrácia. Patrí k najprogresívnejším postupom separačných techník, pretože umožňuje dosiahnuť produkt vysokej čistoty a kvality. Veľký vplyv na kvalitu filtrácie má zloženie a stav vína. Staršie vína, v ktorých je už väčšina koloidných častíc vyzrážaná, sa filtruje pomerne jednoducho. Možno tu dosiahnuť maximálny výkon a rýchlosť. Mladé vína s vysokým obsahom bielkovín a slizovitých látok sa filtrujú horšie a na filtráciu sa používa filtrácia kremelinou (Íllešová, 2010).

Obrázok 3 Odrody hrozna (zľava, Devín, Tramín červený, Dunaj, Alibernet)

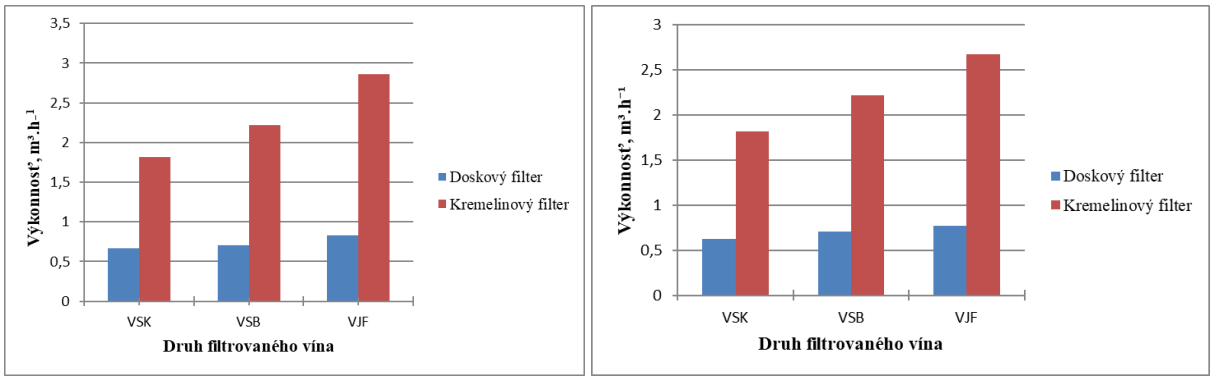

Obrázok 4 Výkonnosť, doskový a kremelinový filter pre tri rôzne stavy filtrovaného vína pre odrody: a) Devín, b) Tramín červený, VSB - víno stočené z bentonitu, VJF - víno jedenkrát filtrované, VSK - víno stočené z kvasenia

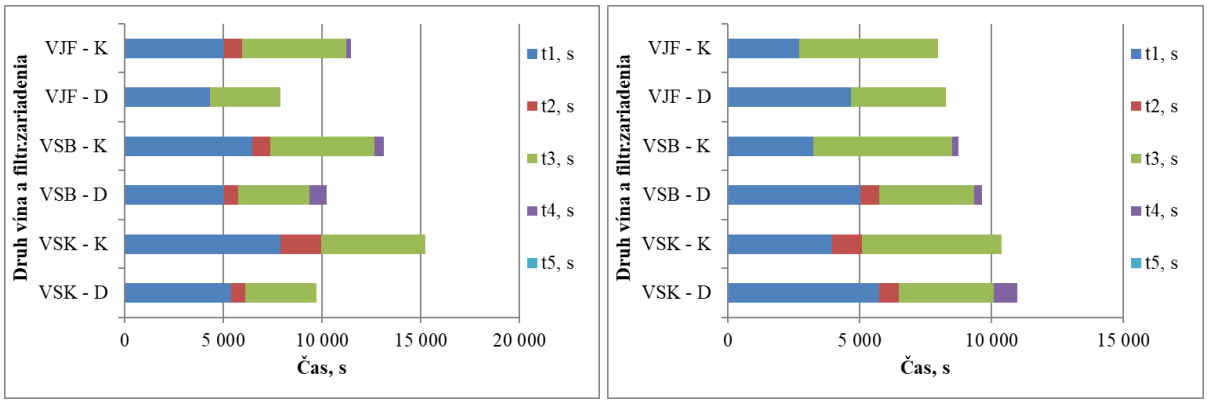

Obrázok 5 Časové snímky pre jednotlivé pracovné operácie pre odrody Devín (a) a Tramín (b) červený pri jednotlivých stavoch filtrovaného vína. VJF – K – víno jedenkrát filtrované / kremelinový filter , VJF – D – víno jedenkrát filtrované / doskový filter, VSB – K – víno stočené z bentonitu / kremelinový filter, VSB –D – víno stočené z bentonitu / doskový filter, VSK – K – víno stočené z kvasenia / kremelinový filter, VSK – D – víno stočené z kvasenia / doskový filter, t_1 – hlavný čas filtrácie, t_2 – čas na prebitie filtra, t_3 – čas na údržbu alebo prípravu stroja, t_4 – čas na odstránenie porúch, t_5 – čas na odpočinok.

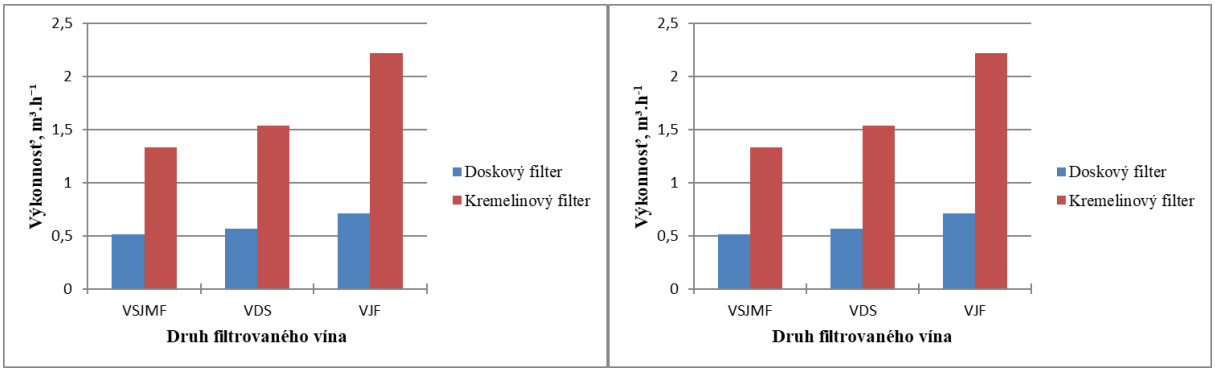

Obrázok 6 Výkonnosť, doskový a kremelinový filter pre tri rôzne stavy filtrovaného vína pre odrody: a)Dunaj, b) Alibernet , VSB - víno stočené z bentonitu, VJF - víno jedenkrát filtrované, VSK - víno stočené z kvasenia

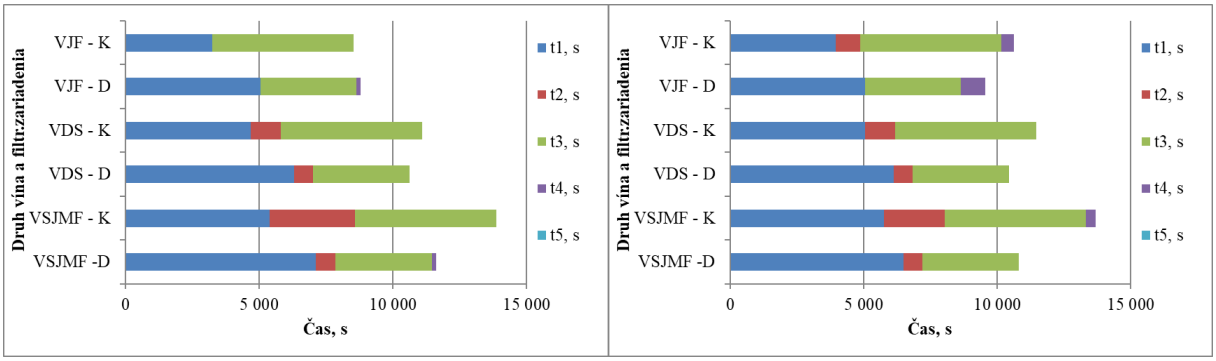

Obrázok 7 Časové snímky pre jednotlivé pracovné operácie pre odrody Devín (a) a Alibernet (b) pri jednotlivých stavoch filtrovaného vína. VJF – K – víno jedenkrát filtrované / kremelinový filter , VJF – D – víno jedenkrát filtrované / doskový filter, VSB – K – víno stočené z bentonitu / kremelinový filter, VSB –D – víno stočené z bentonitu / doskový filter, VSK – K – víno stočené z kvasenia / kremelinový filter, VSK – D – víno stočené z kvasenia / doskový filter, t_1 – hlavný čas filtrácie, t_2 – čas na prebitie filtra, t_3 – čas na údržbu alebo prípravu stroja, t_4 – čas na odstránenie porúch, t_5 – čas na odpočinok.

Filtrácia je separačná až vysoká technika, pričom pomocou nej možno rozdeliť pevné častice suspenzie od tekutého podielu prietoku cez poréznu vrstvu filtračného materiálu (Balík, Stávek, 2017). Prietok kvapaliny je zaistený rozdielom tlakov vznikajúcich na oboch stranách filtračnej vrstvy. Tlak závisí od typu filtra a účelu filtrácie, rovnako ako na koncentrácii a vlastnosti filtrované suspenzie. Ide prakticky o posledné manipulácie s vínom pred jeho plnením do fliaš. Vložková filtrácia sa používa k ostrej filtrácii priamo pred plnením do fliaš (Farkaš, 1980). V oblasti vinárstva sa využíva filtrácia k oddeleniu kalov, kalotvorných látok nebo mikroorganizmov. Podľa spôsobu snímania pevných častíc na povrchu filtračného materiálu sa filtrácia delí povrchovú a hĺbkovú (Fic, 2015). Na materiál použitý k filtrácii sa kladú veľké nároky. Dôležitá je jeho indiferentnosť t.j. nesmie vplyvom alkoholu alebo kyselín nič odovzdávať do vína a z druhej strany, nesmie víno ochudobňovať o chuťové a aromatické látky (Hronský 2006). Podľa Šauera (1966) znamená filtrácia cedenie vína cez jemne pórovité materiály. Filtrácia má za účel víno vyčistiť, aby bolo víno iskrivo čisté. Rýchlosť filtrácie závisí od pórovitosti a kvality používaných filtračných hmôt. Malík (1994) tvrdí že na fľaškovanie sa vyžaduje dokonalé, vyškolené, iskrivé a stabilizované víno. Plnenie je označované ako stáčanie tekutín do fliaš, pri ktorom je treba v krátkom časovom období dosiahnuť plnenie fľaše požadovaným množstvom tekutiny, bez strát a všetkých škodlivých vplyvov.

CONCLUSION

V podniku Velkeer 1113 s.r.o. bolo naším cieľom zhodnotiť efektívnosti doskového a kremelinového filtra, kde sme sa zamerali na časové a výkonnostné parametre. Pri porovnávaní odrôd a vín, ktoré boli rôzne filtrované (jedenkrát filtrované, dvakrát filtrované, stočené z kvasenia a pod.) sme sa zamerali na odlišné časy (hlavný čas filtrácie, čas na prebitie filtra, čas na údržbu alebo prípravu stroja, čas na odstránenie porúch, čas na odpočinok), z ktorých sme uviedli aj časové snímky. U všetkých štyroch odrôd (Devín, Tramín červený, Dunaj a Alibernet) bol čas t_2 pri víne jedenkrát filtrovanom nulový, pretože sa tam nemusel prebíjať filter, či sa jednalo o doskový alebo kremelinový filter. Počas filtrovania sa u niektorých odrôd vyskytli aj technické poruchy napr. zle uzatvorené dvierka na nádrži, čo bol dôsledok zlého tesnenia, kde sa všetko muselo vyčerpať a znova zavrieť. Čas t5, ktorý bol určený ako čas na odpočinok, bol počas nášho merania vždy nulový.

V podniku Velkeer 1113, s.r.o. sa zameriavajú na výrobu kvalitných prémiových vín a preto sa snažia filtráciu robiť čo najšetrnejšiu. Pri porovnaní výkonností filtračných zariadení bola výkonnosť u kremelinového filtra vždy vyššia, hoci tam boli aj vyššie objemy.

REFERENCES

ALIBERNET [s.a.] [online] [cit.22.4.2016] Dostupné na: http://www.vino.sk/encyklopedia-vina/odrody-vinica/alibernet/

BALÍK, J., STÁVEK, J. 2017. Vinařská technologie. Valtice: Národní vinařské centrum, 2017. ISBN 978-80-87498-77-4.

BURG, P., ZEMÁNEK, P., 2014. Stroje a zariadenia pre vinárstvo. Olomouc, Agriprint s.r.o., Baštan 2014, 254 s., ISBN 978-80-87091-49-4.

DEVÍN [s.a.] [online] [cit.22.4.2016] Dostupné na: http://www.vino.sk/encyklopedia-vina/odrody-vinica/devin/

DUNAJ [s.a.] [online] [cit.22.4.2016] Dostupné na: http://www.vino.sk/encyklopedia-vina/odrody-vinica/dunaj-vino/

FARKAŠ, J., 1980. Technologie a biotechnologie vína. Státní nakladatelství technické literatury.

FIC, V., 2015 Víno: analýza, technologie, gastronomie. Český Těšín: 2 THETA, 2015. ISBN 9788086380773.FILTRÁCIA. [online] [s.a.] [cit. 2018-04-15] Dostupné na internete: https://is.mendelu.cz/eknihovna/opory/index.pl?fit_w=1;cast=58507

HRONSKÝ, Š., 2006. Vinárstvo. Nitra: SPU, 2006. 108 s. ISBN-80-8069-010-3

ÍLLEŠOVÁ, P., 2010. Technika a technológia spracovania hrozna a filtácia vína. Nitra, SPU 2010, 64 s., Diplomová práca.

JOBBÁGY, J., FINDURA, P., 2013. Mechanizácia vinárstva. Nitra, SPU 2013, 165 s., ISBN 978-80-522- 0996-8.

KUNOVÁ, S., LOPAŠOVSKÝ, Ľ., 2015. Hygiena a sanitácia vo vinárstve. Nitra, SPU 2015, 134 s., ISBN 978-80-552-1384-2.

MALÍK, F., 1994. Dobré víno. Bratislava 1994, 326 s., Polygrafia SAV

ŠAUER, Z., 1966. Filtrace nápojú. Praha: SNTL,1966, 181 s.

TRAMÍN ČERVENÝ [s.a.] [online] [cit.22.4.2016] Dostupné na: http://www.vino.sk/encyklopedia-vina/odrody-vinica/tramin-cerveny

POSSIBILITIES OF USING BIOCHAR FROM BIOMASS

ĽUBOŠ KÚDEĽA, JURAJ MAGA, JÁN JOBBÁGY, ADAM TKÁČ

Ústav poľnohospodárskej techniky, dopravy a bioenergetiky, TF, SPU v Nitre

Abstract: The aim of the paper was to assess the possibilities of using biochar from biomass, where the input products were material from wood chips of basket willow from a school farm in Kolíňany. The object of the investigation was the substrate for the cultivation of sown pickling cucumbers (Charlotte F1 variety) and sown salad cucumbers (Superstar F1 variety). The study was carried out for 55 days and biochar was mixed with the substrate at concentrations of 0%, 5%, 10%, 15%, 20% and 25%. Cucumbers were sown in prepared mixed substrates with biochar. The retention capacity of the prepared substrate and the response of the crop were also monitored. The results show that the constituent status of the substrate (percentage of biochar) has a significant effect on the growth of the seedlings. The greatest effect (pickling cucumbers) was observed at 20% biochar content. In the case of sown cucumbers, the highest influence was observed when the growth was grown with 5 % biochar in the soil.

Keywords: biochar, biomass, water retention, cucumbers

INTRODUCTION

Biouhlie je forma dreveného uhlia, ktorá je bohatá na uhlík, produkovaná ohrievaním organickej hmoty v prostredí bez prístupu kyslíka, prípadne s jeho veľmi nízkym obsahom (Lehmann, et al. 2011). Tento proces sa zjednodušene nazýva pyrolýza. Biouhlie má nespočetné kvantum predností pre poľnohospodárstvo, vrátane zlepšeného zadržiavania vody, zvýšenej prístupnosti živín a klesania emisií skleníkových plynov, čo z neho prakticky robí pútavú možnosť pre udržateľné poľnohospodárstvo, pôdne hospodárenie, ale takisto vytvára čo najprijateľnejšie prostredie pre pôdne baktérie (Tan et al., 2017). Biouhlie je druh dreveného uhlia ako aj organické palivo, vyrábané zahrievaním organického materiálu, ako je napríklad drevo či zvyšky plodín. Spravidla obsahuje nie menej než 50 percent uhlíka (Ahmad a kol., 2014). Biouhlie má množstvo fyzikálnych vlastností a možno ho použiť pre rôzne aplikácie. Hlavné fyzikálne vlastnosti biouhlia sú pórovitosť, povrchová plocha, hustota, pH a elektrická vodivosť (Lehmann a Joseph, 2009). Jedným z najdôležitejších aspektov tejto aplikácie je zvýšenie produktivity pôdy, najmä vďaka zvýšenej dostupnosti pôdnych živín pre rastliny. Účinky, ktoré biouhlie vyvoláva v pôde, môžu spôsobiť mechanizmy, ktoré vedú ktransportu živín k rastlinám a tým k zlepšeniu úrodnosti. Je zrejmé, že jedným z hlavných mechanizmov, ktorými biouhlie ovplyvňuje prísun živín, je zvýšenie obsahu organických živín vo forme nestabilných organických zlúčenín. Biouhlie sa spája s pôdou a poskytuje vysoko využiteľné živiny. Vzhľadom na to, že pôdy obvykle obsahujú pomerne veľké množstvo pôdnych organických nutrientov, biouhlie obvykle prispieva len obmedzeným množstvom živín vzhľadom na ich celkový obsah (Chan a kol. 2007).

Rastliny môžu využívať len malú časť z celkového množstva pôdnych živín, ale aj takýto krátkodobý prísun dostupných živín môže zvýšiť produktivitu rastlín, zlepšiť kvalitu rastlinných tkanív a v konečnom dôsledku ovplyvniť kvalitu a množstvo organickej hmoty vstupujúcej do pôdy (Major et al., 2010).

Hlavným cieľom príspevku bolo analyzovať možnosti využitia biouhlia z drevných štiepok vŕby košikárskej zo školského podniku v Kolíňanoch. Okrem toho sa sledoval vplyv podielu biouhlia na zadržiavanie vody v pôde, ďalej rast priesad a dĺžku respektíve objem koreňového systému.

MATERIALS and METHODOLOGY

Pre dosiahnutie stanoveného cieľa sme si museli stanoviť metodiku, ktorá pozostáva z nasledovných bodov (technické parametre prístrojov tabuľka 1 a tabuľka 2):

- príprava substrátu s rôznym obsahom biouhlia,
- váženie jednotlivých pomerov daných vzoriek za pomoci váhy Momert 6000 (obr.1),
- sejba vybraných plodín do pripravených zmesí substrátu a biouhlia (množstvo bolo postupne vypočítané objemovo – 0 %; 5 %; 10 %, 15 %; 20 %; 25 %),
- podpora rastu uhoriek – UV lampa Gardloy (obr.1), chladné mesiace (január, február, marec – nepriaznivé počasie, nedostatok svetla, kratšie dni), 12hodinové intervaly počas tmy dokázala rastlinám vynahradiť slnečné žiarenie,
- aplikácia závlahy (konkrétne bolo zaznamenaných presne 11 meraní pri polievaní zo začiatku každý deň, postupom času cca každý 2–3 deň pri presnom množstve 10 ml vody za pomoci injekčnej striekačky),
- sledovanie vplyvu biouhlia na uhorky počas siedmych dní bez závlahy (pri tomto procese bola koreňová sústava starostlivo vybratá, umytá a následne skenovaná),
- sledovanie koreňovej sústavy uhoriek po siedmych dňoch bez závlahy,
- spracovanie jednotlivých výsledkov v programe Microsoft Excel.

Obrázok 1 Digitálna váha Momert 6000, UV lampa Gardloy

Tabuľka 1 Technické parametre vreckovej digitálnej váhy Momert 6000

Parameter	Hodnota
Automatická kalibračná funkcia	Áno
Rozsah váženia	500 g
Presnosť váženia	0,1 g
Jednotky váženia	g/oz/ozt
Displej	LCD (8cm)
Šírka	120 cm
Výška	20 cm
HĺbkA	85 cm

Tabuľka 2 Technické parametre vreckovej digitálnej váhy Momert 6000

Parameter	Hodnota
Časovač	3, 9, 12 hod.
Počet LED diód	40
Napájanie	USB
Flexibilné ramená	Áno
Farba vyžarovania	Červená a modrá
Výkon	20 W 2 svetelné panely
Uhol sklonu	Do 180°
Rozmery	68 x 12 x 7 cm

RESULTS and DISCUSSION

Charakteristika riešenej problematiky, príprava substrátu

Biouhlie je jemnozrnný materiál podobný drevenému uhliu a vyrába sa procesom pyrolýzy. Pridáva sa napr. do pôdy, aby sa zlepšila jej kvalita. Jeho zloženie je veľmi podobné vstupnej biomase, s výnimkou dusíka. Väčšinu tvorí čistý uhlík, ktorý je vo veľmi stabilnej forme a len zriedka sa udeje proces následného čo i len čiastočného rozkladu. Má výrazný dosah na rast rastlín a ich úrodnosť, čo bolo preukázané v rôznych štúdiách (Ameloot, 2013).

Presnú aplikačnú dávku drevného biouhlia (5%, 10%, 15%, 20% a 25%, obr. 2) sa zabezpečila do jednotlivých zmesí množstvom daného substrátu prostredníctvom valcovej odmerky (priemer 3,6 cm a výška 2,4 cm). Používané biouhlie bolo vyrobené zo štiepky z rýchlorastúcich drevín v školskom podniku SPU, Kolíňany. Použitá štiepka bola vyhotovená konkrétne z vŕby košikárskej.

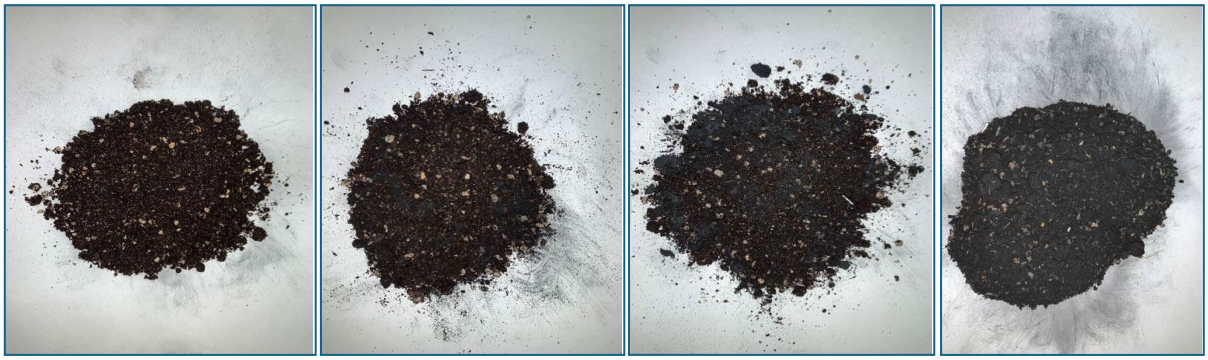

Obrázok 2 Príprava substrátu, kontrola, podiel biouhlia 5%, 10%, 15%, 25 %

Typy pestovaných uhoriek

Pre naše výskumné práce sme si vybrali ako objekt skúmania druh uhorky siatej nakladačky, konkrétne odrodu Charlotte F1 a druh uhorky siatej šalátovej, konkrétne odrodou Superstar F1. Uhorky boli po zasiatí polievané „v prvotnej fáze“ tj. prvých cca 10–15 dní v každodennom intervale rovnakým množstvom vody 10 ml. Následne dochádzalo k miernemu zaplesneniu pôdy aj sledovaných uhoriek siatych a z tohto dôvodu bolo potrebné obmedziť prísun vody na väčší rozostup dní v týždni (cca 3–4 dni). Počas pokusov sa realizovalo aj jeden krát do týždňa mierne prekyprenie pôdy, aby sa na vrchu nevytvárala už spomínaná pleseň, čo by mohlo rast a vývin ovplyvniť. Presné množstvo vody bolo aplikované pomocou injekčnej striekačky. Pracovná teplota v miestnosti bola udržovaná po celý čas výskumu nad 20 °C. Poloha rastlín bola každý deň menená, z dôvodu rovnakého prísunu svetla.

Sledovanie vývinu priesad uhoriek

Uhorky siate oboch druhov, teda druh Charlotte F1 aj druh Superstar F1, sme sledovali po dobu 55 dní, počas ktorých sa vykonalo celkovo 11 meraní. Počas meraní bol pomocou metra pozorovaný postupný rast všetkých sadeníc od téglika až po korunku a tento proces bol tiež fotograficky zdokumentovaný (obr. 3). Merané parametre rastových dĺžok sú uvedené v tabuľkách 3 a 4. V deň siatia bola teplota 21 °C a vlhkosť externého prostredia bola 67 %. V 15.deň rastu bola teplota 20 °C a vlhkosť vzduchu 68 %. V 30.deň rastu bola teplota 20 °C a vlhkosť sa zvýšila na 76 %. V 45.dni rastu sa teplota nezmenila, ale vlhkosť ovzdušia klesla na 71 %. V 55 deň rast sa teplota opäť nezmenila, ale vlhkosť stúpla na 73 %.

Zhruba na štyridsiaty piaty až päťdesiaty deň od zasadenia bolo možné pozorovať jemné zožltnutie spodných lístkov. Zožltnutie bolo viditeľne voľným okom na uhorkách siatych nakladacích s každým percentuálnym pomerom biouhlia. Výnimkou boli len tégliky s 0% biouhlia, teda rastlina, ktorá neobsahovala prakticky žiadne biouhlie. Počas výskumu (35. deň od sejby, pri 0% obsahu biouhlia odumrela jedna z piatich meraných rastlín, z toho dôvodu priemerná veľkosť uhorky siatej mierne klesla). Podľa dovtedy zistených údajov sa dá predpokladať, že by priemerná veľkosť uhoriek siatych pri nulovom pomere v 55. deň od siatia bola určite vyššia).

Výsledky získané pri pestovaní priesad uhoriek siatych naznačujú, že použitie biouhlia pri pestovaní záhradných plodín môže mať ako pozitívne, tak aj negatívne výsledky. Sporné až diskutabilné výsledky boli získané pri použití substrátov. Výsledky získané sledovaním rastu uhoriek siatych poukázali na pozitívny vplyv aplikácie drevného biouhlia na rast priesad, pričom je treba sledovať jeho percentuálny obsah. Podobné výsledky odzrkadľujú aj záverečné práce Ing. Mateja Holana a Ing. Daniela Kovácsa a ďalšie výskumné práce z praxe (Atkinson et all., 2013; Basu, 2010; Elad, 2010; Graber, 2010). Nnadmerná aplikačná dávka biouhlia teda nemusí mať nutne priaznivý vplyv na rast priesad. Ich výskum bol zameraný na rozdielny druh záhradnej zeleniny, môžeme s istotou povedať, že výsledky sú si viacmennej podobné. Príliš veľké množstvo totiž môže brániť potrebnému prísunu určitých živín, ktoré sú nevyhnutné k rastu plodiny. Priesady uhorky siatej nakladacej s obsahom biouhlia 20% dosiahli najväčší prejav rastu. Pri priesadách uhoriek siatych šalátových dosahovali najvišší vplyv na rast uhorky s 5% pomerom biouhlia. Výsledkom teda je, že vplyv biouhlia na dva druhy uhoriek siatych je rozličný.

Obrázok 3 Uhorky (nakladačky-horný riadok, šalátovky-dolný riadok),
zľava – deň siatia, 15 deň rastu, 30 deň rastu, 45 deň rastu)

Obrázok 4 Uhorky (nakladačky-vľavo, šalátovky-vpravo, 55 deň rastu)

Tabuľka 3 Dĺžka nadzemnej časti po vysiatí uhoriek siatych nakladacích (Charlotte F1), mm

Počet dní od sejby	**Pomery biouhlia v substráte nakladačiek**					
	0%	5%	10%	15%	20%	25%
0	0,0	0,0	0,0	0,0	0,0	0,0
5	1,0	0,0	0,0	0,0	0,0	0,0
10	67,0	63,3	66,7	50,6	6,0	60,5
15	71,0	68,6	71,3	59,6	81,3	72,0
20	82,3	75,3	77,3	65,0	91,0	77,5
25	85,3	77,6	80,3	66,3	94,3	80,5
30	86,3	82,3	83,6	69,0	100,3	84,9
35	89,0	84,3	89,6	75,0	102,3	89,7
40	90,3	85,6	90,0	75,6	102,6	90,5
45	91,3	86,6	90,6	76,3	100,3	91,0
50	98,3	91,0	106,3	88,6	109,6	97,5
55	105,3	96,0	110,3	94,0	111,0	101,8

Tabuľka 4 Dĺžka nadzemnej časti po vysiatí uhoriek siatych šalátových (Superstar F1), mm

Počet dní od sejby	Pomery biouhlia v substráte nakladačiek					
	0%	5%	10%	15%	20%	25%
0	0,0	0,0	0,0	0,0	0,0	0,0
5	2,3	1,0	0,0	0,0	0,0	0,0
10	96,3	99,6	83,0	72,0	92,6	91,3
15	100,6	107,3	92,5	98,5	106,6	106,0
20	123,0	125,6	106,0	103,5	124,3	115,0
25	138,0	136,3	112,5	106,5	134,6	123,5
30	145,0	138,6	121,5	111,5	137,6	127,5
35	145,0	141,6	124,5	115,5	145,6	135,5
40	141,5	144,0	127,5	117,5	147,0	138,0
45	143,0	145,3	128,5	118,0	147,6	138,5
50	149,5	169,6	154,0	137,0	152,3	144,0
55	151,0	172,3	156,0	140,0	154,3	146,5

Obrázok 5 Koreňová sústava – uhorky siate nakladacie, obsah biouhlia v substrátoch (0, 5, 10; 15; 20, 25 %)

Obrázok 6 Koreňová sústava – uhorky siate šalátové, obsah biouhlia v substrátoch (0, 5, 10; 15; 20, 25 %)

Biouhlie má ďalej schopnosť zlepšiť retenciu vody v pôde, čo bolo pozorované aj pri našich vzorkách Pri použití substrátu bolo viditeľné určité zlepšenie retencie vody (Elad, 2010; Steiner, 2010). Pri nedostatku vody, ktorej bola vystavená nami skúmaná záhradná pôda a biouhlie bol prejav retencie vody evidentne zlepšený. Rôzne štúdie o vplyve drevného biouhlia na zlepšenie retencie vody v pôde nám len potvrdili, že aj uhorky siate „šalátovky“ pri vyšších aplikačných dávkach ako sú v našom prípade 20% a 25% obsah biouhlia prežili dlhšie počas obdobia sucha. Avšak, na rozdiel od uvedených pokusov, sa pri uhorkách siatych „nakladačkách“ prejavil skôr presný opak. Priesady s 0% pomerom biouhlia boli tie, ktoré sa držali najlepšie v období bez závlahy. Bolo by veľmi zaujímavé sa uvedenej problematike venovať podrobnejšie a dokázať respektíve vyvrátiť uvedené konštatované výsledky.

Tabuľka 5 Dĺžka nameraných koreňov rastlín uhorky siatej, D-dĺžka koreňov, O_{bio}-obsah biouhlia

O_{bio}, %	**D, mm (Uhorky siate nakladacie)**	**D, mm (Uhorky siate šalátové)**
0	18	33
5	27	25
10	20	44
15	40	37
20	26	56
25	21	61

Zhodnotenie stavu koreňovej sústavy pri rôznych koncentráciách obsahu biouhlia

Poslednou súčasťou výskomov prezentovaného prispevku bolo aj posúdenie stavu koreňovej sústavy uhoriek siatych nakladacích a šalátových. Najviac rozvinuté koreňové sústavy mali uhorky siate „nakladačky“ a to sadenice s pomerom 5% biouhlia a z hľadiska celkovej dĺžky to bola sadenica s pomerom 15% biouhlia (40 mm). Pri uhorkách siatych „šalátovky“ mala najviac rozvinutú koreňovú sústavu a rovnako aj najdlhší koreň rastlina s pomerom 25% (61 mm). Meranie prebiehalo rovnakým spôsobom u všetkých rastlín a to od stonky po koreň.

CONCLUSION

Využitie biouhlia z biomasy predstavuje veľký potenciál v oblasti poľnohospodárstva, pričom pomáha zvýšiť obsah organických látok a mikroorganizmov (zlepšuje jej štruktúru a živiny), pH a znížiť

množstvo ťažkých kovov v pôde. Výsledky ukázali, že biouhlie môže mať pozitívny vplyv na zlepšovanie rastových podmienok pre rastliny. V rámci výskumu (55 dní) sledovania a merania rastlín s zistilo, že pri uhorkách siatych nakladacích mal najväčší vplyv 20% pomer biouhlia a pri uhorkách siatych šalátových mal 5% pomer biouhlia. Výsledky poukázaly na fakt, že uhorky siate nakladacie najlepšie reagujú na retenciu vody priesady s nulovým pomerom biouhlia a pri uhorkách siatych šalátových to boli priesady s najväčším pomerom biouhlia (15%, 20% a 25%). Optimálna dávka biouhlia závisí od konkrétneho typu pôdy a druhu rastliny. Bolo by vhodné sa v budúcnosti zamerať na presnejšie určenie optimálnej dávky a aplikácie biouhlia v rôznych druhoch pôd a plodín, čím by sa skúmaný problém posunul vpred. Biouhlie z biomasy môže byť užitočným nástrojom pre zlepšenie a kvalitu plodín v poľnohospodárstve. Výstupy z príspevku poslúžia ako zdroj informácií a inšpirácie pre ďalšie výskumy a aplikácie v praxi.

REFERENCES

AHMAD, M., RAJAPAKSHA, A.U., LIM, J.E., ZHANG, M., BOLAN, N., MOHAN, D., VITHANAGE, M., LEE, S.S., OK, Y.S., 2014. Biochar as a sorbent for contaminant management in soil and water: a review. Chemosphere. 2014 Mar; 99:19–33. https://doi.org/2010.1016/j.chemosphere.2013.10.071.

AMELOOT N., GRABER, E.R., VERHEIJEN, F.G.A., DE NEVE, S., 2013. Interactions between biochar stability and soil organisms: review and research needs. European Journal of Soil Science. 2013, 64(4), 379–390. https://doi.org/10.1111/ejss.12064

ATKINSON, C., FITZGERALD, J.D., HIPPS, N.A., 2010. Potential Mechanisms for Achieving Agricultural Benefits from Biochar Application to Temperate Soils: A Review. Plant and Soil. vol. 337, 2010, Pages 1–18, ISSN 0032-079X, https://doi.org/10.1007/s11104-010-0464-5

BASU, P., 2010. Biomass gasification and pyrolysis: practical design and theory. In: Vliv pH na extrakci látek z komplexu biouhel–půda Amsterdam: Elsevier, ISBN 978-0-12-374988-8.

ELAD, Y., DAVID, D.R., HAREL, Y.M., BORENSHTEIN, M., KALIFA, H.B., SILBER, A., GRABER, ER., 2010. Induction of systemic resistance in plants by biochar, a soil-applied carbon sequestering agent. Phytopathology. vol. 100, no. 9, Pages 913–921, https://doi.org/10.1094/PHYTO-100-9-0913.

GRABER, E. R., 2010. Biochar impact on development and productivity of pepper and tomato grown in fertigated soilless media. Plant Soil. Vol. 337, Pages 481–496, https://doi.org/10.1007/s11104-010-0544-6.

LEHMANN, J., JOSEPH, S., 2009 Biochar for Enviromental Management: Science and Technology. London: Earthscan. ISBN: 978-1-84407-658-1.

LEHMANN, J., RILLIG, M.C., THIES, J., MASIELLO, C.A., HOCKADAY, W.A., CROWLEY, D., 2011. Biochar effects on soil biota – A review. Soil Biology and Biochemistry. 2011, 43(9), 1812–1836. https://doi.org/10.1016/j.soilbio.2011.04.022.

MAJOR J., LEHMANN, J., RONDON, M., GOODALE, CH., 2010. Fate of soil-applied black carbon: downward migration, leaching and soil respiration. Global Change Biology. 2010, 16(4), 1366–1379. ISSN 13541013. https://doi.org/10.1111/j.1365-2486.2009.02044.x

STEINER, CH., GLASER, B., TEIXEIRA, W.G., LEHMANN, J., BLUM W.E.H., ZECH, W., 2008. Nitrogen retention and plant uptake on a highly weathered central Amazonian Ferralsol amended with compost and charcoal. J Plant Nutr Soil Sci. vol. 171, 2008, Pages 893–899, https://doi.org/10.1002/jpln.200625199

TAN, Z., LIN, C.S.K., JI, X., RAINEY, T,J. 2017. Returning biochar to fields: A review. Applied Soil Ecology. 2017, 116, 1–11. https://doi.org/10.1016/j.apsoil.2017.03.017.

EVALUATION OF THE PRODUCTION POTENTIAL OF BIOMASS FROM VINEYARDS

KOLOMAN KRIŠTOF, MARTIN SELICKÝ, JÁN JOBBÁGY, MICHAL ANGELOVIČ, BEÁTA NOVOTNÁ

Institute of Agricultural Engineering, Transport and Bioenergetics, Slovak University of Agriculture in Nitra, Tr. A. Hlinku 2, 949 76 Nitra, Slovakia

Institute of Landscape Engineering, Slovak University of Agriculture in Nitra, Tr. A. Hlinku 2, 949 76 Nitra, Slovakia

Abstract: In today's world, a large portion of the population relies on fossil fuels, but the problem lies in the constantly increasing cost of these fuels. Therefore, new solutions are being sought through renewable energy sources. The demand for these energy sources is becoming a necessity in the construction of family homes. The main goal of the study was to utilise and analyse biomass from vineyard cuttings during winter pruning in a selected enterprise. The work is divided into several parts, where we focused on processing the waste biomass material, selecting a suitable procedure for the final product (pellets). We tested the quality of the pellets and subjected them to several tests. The final part of the study is focused on evaluating and efficiently utilizing waste biomass for heating family homes.

Keywords: biomass, pellets, vineyard, calorific value.

INTRODUCTION

Na Zemi sa biomasa teší povesti jedného z najvšestrannejších a najpočetnejších zdrojov energie. Ľudstvo siahlo po tomto palive ako po prvom. Drevo, suchá tráva a šachoriny boli s najväčšou pravdepodobnosťou prvotnými energetickými surovinami a teplo prvou formou, akú si ľudia osvojili najprv náhodne a neskôr aj cielene. Od pravekého ohňa v jaskyni až po moderné biomasové elektrárne prešla biomasa fascinujúcim vývojom, ktorý odzrkadľuje neustálu snahu človeka o zdokonaľovanie a zefektívňovanie energetických zdrojov. Biomasa si tak drží pozíciu kľúčového hráča v energetickej hre a jej dostupnosť, obnoviteľnosť a nízky dopad na životné prostredie ju predurčujú k tomu, aby aj v budúcnosti zohrávala dôležitú úlohu v tomto strategickom odvetví (Sarvaš a Inašová, 2013).

Biomasa je tretím najväčším zdrojom energie na svete zo všetkých zdrojov. Pre tri štvrtiny ľudí v rozvojových krajinách je tiež hlavným zdrojom energie na varenie a vykurovanie. Predstavuje približne 14 % celkovej svetovej spotreby energie. Viac ako 80 % národnej spotreby energie je zabezpečené biomasou vo väčšine týchto krajín. Napríklad, v Etiópii tradícia spaľovania biomasy sleduje viac ako 92 % spotreby energie, viac ako 64 % v Ghane, 70 % v Keni, 78 % v Nigérii a 60 % v Bangladéši a 7 % elektriny v Brazílii (A Review of Technical and Economic Aspects of Biomass Briquetting, 2020).

Na redukciu veľkosti biomasy pred briketovaním sa používajú kladivové mlyny, nožové mlyny, mriežky s lineárnymi nožmi a diskové mlyny. Najvhodnejšie sú kladivové mlyny, nasledované nožovými mlynmi (A Review of Technical and Economic Aspects of Biomass Briquetting, 2020).

Zhutnená biomasa v podobe brikiet ponúka niekoľko výhod. Jednou z nich je zvýšená hustota energie, čo znamená, že brikety obsahujú viac energie v porovnaní s rovnakým objemom voľnej biomasy. Ďalšou výhodou je jednoduchá manipulácia, preprava a skladovanie vďaka ich kompaktnej forme. Brikety tiež vynikajú zlepšenou horľavosťou, pretože horia rovnomernejšie a s menším dymom ako voľná biomasa. Okrem toho produkujú nižšie emisie častíc, čím sú šetrnejšie k životnému prostrediu ako fosílne palivá. Brikety majú tiež nízku prchavosť, čo znamená, že sa ľahko nerozpadávajú a nestrácajú na hmotnosti. V neposlednom rade je dôležitá aj rovnomernosť brikiet, ktorá sa prejavuje v konzistentnej veľkosti, hustote a kvalite (A Review of Technical and Economic Aspects of Biomass Briquetting, 2020).

Cieľom štúdie bolo hodnotenie produkčného potenciálu biomasy z vinohradníctva so zameraním na kvantifikáciu objemu odpadu s následným návrhom spracovania a využitia na energetické účely.

MATERIAL and METHODOLOGY,

Predmetný vinohrad sa nachádza v katastrálnom území obce Komjatice. Táto oblasť patrí do vinohradníckej oblasti Južné Slovensko, pod zóny Podunajská. Vinohradníctvo má v Komjaticiach dlhú históriu a miestne vína sú známe svojou kvalitou. V obci sa koná aj viacero vinárskych podujatí. Vinohrad sa rozprestiera na miernom svahu orientovanom na juhozápad. Táto orientácia umožňuje optimálne využitie slnečného žiarenia, ktoré je dôležité pre fotosyntézu a dozrievanie hrozna. Mierny sklon terénu znižuje riziko erózie pôdy a umožňuje lepšiu drenáž vody. Klimatické podmienky v oblasti sú vhodné pre pestovanie viniča. Priemerná ročná teplota sa pohybuje okolo 9 °C a priemerný ročný úhrn zrážok okolo 550 mm. Vegetačné obdobie je dostatočne dlhé na dozrievanie hrozna.

Zimný rez viniča predstavuje neoddeliteľnú súčasť jeho pestovateľskej stratégie a významne ovplyvňuje jeho celkové zdravie, rast a úrodu. V tejto časti práce sa zameriame na podrobný opis základných krokov zimného rezu. Optimálne obdobie pre vykonanie zimného rezu viniča sa datuje do vegetačného pokoja, obvykle v rozmedzí od decembra do februára. V chladnejších klimatických oblastiach sa odporúča odložiť rez do konca januára alebo februára s cieľom predísť poškodeniu púčikov mrazom. Naopak, vykonávanie rezu počas vegetačného obdobia sa neodporúča, nakoľko môže oslabiť vinič a zvýšiť jeho náchylnosť na choroby. Vzdialenosť, ktorú sme strihali pre záverečnú prácu: 100 m z jedného radu. Po dostrihaní sme odrezky dali do vriec: 13,8 kg. Z celého vinohradu by bolo približne 241,5 kg.

Efektivita zhutňovania ovplyvňuje pevnosť a stabilitu materiálu. Úprava veľkosti a tvar materiálu podľa použitej technológie. Dosušenie materiálu na správnu vlhkosť pre lepšie zhutnenie. Bola vybraná vhodná technológia zhutňovania pre daný materiál a požadované vlastnosti. Dodržaním týchto krokov dosiahneme optimálne zhutnenie a požadované vlastnosti materiálu (Tulumuru et al., 2011). Na podrvenie biomasy bude použitý kladivkový drvič 9FQ40.

Sledovaný materiál bol následne zhutnený do formy peliet peletovacom lise: LPBB 2000 V2. Materiál na peletovanie musí mať optimálnu vlhkosť (približne 10 – 15 %) a na veľkosť vstupnej frakcie. Vlhkosť materiálu sa môže upraviť sušením alebo pridaním malého množstva vlhkého materiálu. Materiál sa nasype do zásobníka lisu. Podávací systém dopravuje materiál do lisovacej komory. V lisovacej komore sa materiál stláča medzi dvoma maticami a otáčajúcimi sa valcami. Tlak a trenie generuje teplo, ktoré napomáha k spekaniu materiálu a tvorbe peliet. Pelety sa vytlačia z lisu cez otvory v matici. Pelety sa po vytlačení z lisu ochladzujú na vzduchu alebo pomocou chladiaceho zariadenia. Po ochladení sa pelety preosejú cez sito, aby sa oddelili od prachu a drobných častíc (Matúš a Križan, 2009).

Následne boli pelety testované za účelom zhodnotenia: oteruvzdornosti, pevnosti v tlaku a stanovenie spalného tepla podľa (Pertuf, 2014), (Ilabo, 2022) a (Studený, 2022).

RESULTS and DISCUSSION

Vzdialenosť, ktorú sme strihali pre záverečnú prácu: 100 m z jedného radu, čo tvorí 140 m^2 z vinohradu. Po dostrihaní sme odrezky dali do vriec: 13,8kg. Z celého vinohradu by bolo pravdepodobne 241,5 kg. Hmotnosť, ktorú sme získali po procese peletovania, bola 12,55 kg, čo znamená, že straty na hmotnosti boli 9 %.

Tabulka 1 Oteruvzdornosť peliet

Meranie č.	hmotnosť na začiatku (g)	hmotnosť po skúške (g)	oteruvzdornosť (%)
1	200,29	191,27	4,50
2	201,13	194,65	3,22
3	200,76	191,48	4,62
		Aritmetický priemer:	4,12

Merali sme oteruvzdornosť vyrobených peliet na 3 vzorkách. Na základe týchto výsledkov je možné usúdiť, že hodnoty sa príliš nelíšili a pelety vyrobené z viničných odrezkov majú priemernú oteruvzdornosť 4,12 %. To naznačuje, že pelety sú odolné voči opotrebovaniu, manipulovateľnosťou a mali by vydržať dlhú dobu bez významného opotrebenia (Purohit a Chaturvedi, 2016).

Tabulka 2 Skúška pevnosti peliet v tlaku

Vzorka	Priemer (mm)	Sila (N)
1	6	1 845,5
2	6	1 623,3
3	6	1 970,1
4	6	1 492,0
5	6	1 676,4
6	6	1 742,5
7	6	1 892,1
8	6	1 614,3
9	6	1 735,7
10	6	1 795,0
Aritmetický priemer:		1 738,7

Z prevedených meraní vieme usúdiť, že priemerná pevnosť v tlaku peliet je 1 738,7 N a vieme povedať že pelety vyrobené z viničných odrezkov sú pevné a odolné voči tlaku. To naznačuje, že pelety by sa pri skladovaní mohli navŕšiť bez toho, aby spodné boli poškodené. Vďaka svojej pevnosti sa pelety budú dobre prepravovať a manipulovať s nimi. Taktiež by mali odolať bežnému opotrebovaniu a nárazom (Grover a Mishra, 1996).

Tabulka 3 Výsledky merania spalného tepla kalorimetrickou metódou

Meranie č.	Hmotnosť (g)	Spalné teplo (MJ.kg^{-1})
1	0,82	16,86
2	0,78	16,74
3	0,85	16,96
4	0,84	17,12
5	0,91	17,30
6	0,89	16,81
7	0,83	16,87
8	0,77	16,72
9	0,85	16,80
10	0,90	17,22
priemerné hodnoty $\bar{m}$ a QS	8,44	16,94

Priemerné spalné teplo peliet z viničných odrezkov bolo 16,94 MJ.kg^{-1}, zatiaľ čo priemerné spalné teplo komerčne dostupných peliet z dreveného odpadu bolo 16,58 MJ.kg^{-1} (Valorization of Wood-Based Waste from Grapevine, 2023). To znamená, že pelety z viničných odrezkov mali o 2 % vyššie spalné teplo ako pelety z dreveného odpadu. Rozdiel v spaľovacom teple medzi peletami z viničných odrezkov a peletami z dreveného odpadu nie je štatisticky významný. To naznačuje, že pelety z viničných odrezkov by sa mohli z hľadiska spaľovania považovať za ekvivalent peliet z dreveného odpadu (Lieth et al., 1975; Salano et al., 2016).

Na Slovensku sa nachádza 7 752,09 ha rodiacich viníc, z toho 3 332 ha v Nitrianskom kraji, (Štatistický úrad SR, 2021) čo predstavuje 43 % z celkovej plochy. V tejto práci sme analyzovali produkciu biomasy a peliet z viničných odrezkov na malej meranej ploche 0,245 ha. Zistili sme, že z 1 ha viničných odrezkov sa dá v priemere vyrobiť 911,66 kg biomasy a 831,2 kg peliet. Tieto výsledky naznačujú, že

produkcia biomasy a peliet z viničných odrezkov má na Slovensku značný potenciál. Je však dôležité poznamenať, že tieto výsledky sú založené na meraní malej vzorky viničných odrezkov a pre komplexnejšie posúdenie potenciálu biomasy na Slovensku by bolo potrebné vykonať rozsiahlejšie testovanie na väčšej vzorke.

Z uvedeného vieme určiť celkovú výhrevnosť viničných odrezkov v jednotlivých oblastiach z priemernej výhrevnosti ktorá bola 16,94 MJ.kg^{-1}. Vzhľadom na rozsiahlu plochu rodiacich viníc na Slovensku a použitie viničných odrezkov ako vedľajšieho produktu pestovania viniča by sa tieto odrezky mohli stať významným a udržateľným zdrojom bioenergie.

V dnešnej dobe sa často stretávame s kladením si otázky ohľadom obnoviteľných zdrojov, ktoré nám môžu poslúžiť v domácnosti napríklad pri vykurovaní rodinného domu. V práci som pracoval s viničnými odrezkami, ktoré môžeme získať pri zimnom strihu.

Na základe zistení (Valorization of Wood-Based Waste from Grapevine, 2023) môžeme povedať, že nami vyrobené pelety dosahovali mierne nižšiu odolnosť v otere. Autori uvádzajú priemerné hodnoty 5,9 %, pričom my sme namerali 4,12 %, čo znamená rozdiel 1,78 %. To znamená, že pelety budú mať veľmi podobné vlastnosti vzhľadom na skladovateľnosť, transport a podobne.

Výsledky mechanických skúšok peliet z viničnej révy sa pohybovali od 1 492 N až do 1 970,1 N, priemerná hodnota z vykonaných desiatich meraní bola 1 738,7 N, čo môžeme porovnať s ostatnými materiálmi, napríklad priemerná hodnota peliet zo slivky bola 2 146,52 N (Valovič, 2022), slama pšeničná 2 174,68 N (Kiss, 2019). Tieto hodnoty naznačujú, že pelety vyrobené pre potreby našej práce nie sú až tak náchylné na mechanické poškodenie pri manipulácií, nakoľko ich pevnosť je približne o 20 % nižšia ako porovnávané.

Podľa výsledkov (Valorization of Wood-Based Waste from Grapevine, 2023) drevené pelety majú hodnotu spalného tepla 16,58 MJ.kg^{-1}. Môžeme ich porovnať s našimi peletami z viničnej révy, ktoré dosiahli hodnotu 16,94 MJ.kg^{-1}, taktiež vieme porovnať s prácou, kde sa zaujímali spalným teplom viničných odrezkov s výsledkom 16,96 MJ.kg^{-1}, pri porovnaní s hodnotami v mojej práci výsledky sa od seba veľmi nelíšia. Energetický potenciál odrezkov viniča je porovnateľný s inými drevenými materiálmi. 20,70 MJ. kg^{-1} pre druhy Guaiac a Rose (Günther, 2012), hrubá výhrevnosť medzi brezou 17,9 MJ.kg^{-1} a palisanderom 20,5 MJ.kg^{-1} (Burg, 2016), drevený odpad z jednoročných zdrevnatených výhonkov z pestovania viniča odrôd Seyval Blanc, Solaris, Regent a Rondo. Štúdia ukázala, že materiál má vysoký energetický potenciál 15,88 – 16,19 MJ. kg^{-1}. (Maj, 2022)

Pri modelovom vykurovaní rodinného domu počas celého roka za použitia drevených peliet bolo odmeraná spotreba 3 700 kg. Za predpokladu, keby sme vykurovali rodinný dom s našimi peletani, spotreba by bola o 2 % nižšia ako pri použití drevených peliet. Pri použití kotla s vysokou výhrevnosťou 93,7 % od značky BIOPEL, model: MINI TOWER 21 kW, dosiahneme vysokú účinnosť energie o hodnote približne 15,9 MJ z 1 kilogramu (Kúrenie peletami).

Cena za 960 kg drevených peliet sa pohybuje okolo 299 € (prvotriednej kvality) (Palivové drevené pelety). Ak budeme brať do úvahy túto sumu aj pri výrobe peliet z viničnej biomasy, môžeme hovoriť o spotrebe 3 622 kg, ktorú domácnosť spotrebuje počas roka. Domácnosť zaplatí 1 128,10 € za rok ak bude kúriť peletami z viniču, ale ak by domácnosť kúrila drevenými peletami, zaplatia by o 23,05 € viac.

Na základe údajov štatistického úradu SR (Štatistický úrad SR, 2021), pri pracovaní viničnej biomasy z celej plochy slovenských plodiacich vinohradov, ktorá predstavuje oblasť 7 752,09 ha, by sme dokázali vykúriť 1 775 rodinných domov o štandardnej zastavanej / obytnej ploche 136 m^2. Celkový počet vyrobených peliet z viničnej révy z celého územia Slovenska je v priemerne 6 431 234 kg a celková suma peliet by sa mohla pohybovať okolo 1 922 939 € za celkový vyrobený počet peliet.

Z vinohradov, ktoré sa nachádzajú v Nitrianskom kraji, oblasť predstavuje rozlohu 3 332 ha, by sme vedeli vykúriť celkovo 763 rodinných domov. Z nášho vinohradu by sme vyrobili 219,76 kg peliet a ich hodnota by sa pohybovala okolo 65,7 € za celkový zber. Celkové množstvo odpadu, ktoré vzniká pri

zimnom reze viniča sa rok po roku mení. So spotrebou peliet je to tak isto, každým rokom je iná a nevieme dopredu povedať, koľko peliet spotrebujeme počas nasledujúceho vykurovacieho obdobia.

Celkovo môžeme konštatovať, že odpadová biomasa pri každoročnom reze viniča je vhodný obnoviteľný zdroj energie

CONCLUSION

Počas jednotlivých technologických procesov, ktoré je možné využiť na energetické účely, sme sa v našej práci snažili poukázať najmä na výhody a perspektívu zhutňovania materiálu z viniča. Výsledky práce nám ukázali niekoľko podstatných zistení. Po získaní a úprave materiálu, z ktorého sme vyrobili finálny produkt (pelety), sme vykonali niekoľko meraní určených vlastností. Proces peletovania je veľmi podobný ako pri ostatných biomasách. Vzorky prešli niekoľkými testami. Boli podrobené skúške odolnosti peliet voči oteru, z ktorej vyšiel výsledok s minimálnou hodnotou odolnosti voči oteru 4,50 % a s maximálnou hodnotou 4,62 %. Skúška pevnosti peliet v tlaku bola ďalší test, ktorý sme vykonávali na našich peletách s výsledkami od 1492 do 1970,1 N na jednu peletu. Pre túto prácu najdôležitejším meraním bolo meranie spalného tepla pomocou prístroja IKA C 5000. Na tomto prístroji sme vykonali 10 meraní individuálne. Pomocou aritmetického priemeru sme získali výslednú hodnotu spalného tepla 16,94 $MJ.kg^{-1}$. Podstatnou hodnotou bola aj vlhkosť pri tvorbe peliet. Pred začatím peletovania bola vlhkosť materiálu 15 %. Hotové pelety mali vlhkosť 10 %.

Výsledky štúdie, ktorá sa zaoberala tvorbou peliet a spalným teplom, vieme vyjadriť nasledovne: ak použijeme pelety na vykurovanie rodinného domu, spotrebujeme 3 622 kg ročne. Cena peliet, ktorú sme rátali, je 299 € za 960 kg a rodina by musela zaplatiť 1 128,10 €. Ak budeme rátať s číslami, ktoré nám poskytol Štatistický úrad, na Slovensku sa nachádza 7 811,07 ha plodných vinohradov, z čoho by sme mohli vyrobiť 6 480 165 kg peliet. Toto množstvo peliet by vedelo vykurovať 1 775 rodinných domov s rozlohou 136 m^2.

ACKNOWLEDGEMENTS

This project was supported by the Scientific Grant Agency of the Ministry of Education, Science, Research and Sport of the Slovak Republic and the Slovak Academy of Sciences (VEGA) no. Grant 1/0559/23: Assessment of the Production and Regulatory Function of Agricultural Ecosystems Affected by Climate Change.

REFERENCES

GROVER, P.D., MISHRA, S.K., 1996. Biomass Briquetting: Technology and Practices. Regional Wood Energy Development Programme In Asia; Field Document No 46; Food and Agriculture Organization: Rome, Italy, 1996.

GÜNTHER, B., GEBAUER, K., BARKOWSKI, R., ROSENTHAL, M., BUES, C.T., 2012. Calorific value of selected wood species and wood products. Eur. J. Wood Wood Prod., [cit. 2024-02-22] 70, 755–757. https://link.springer.com/article/10.1007/s00107-012-0613-z

ILABO, spol. s r. o., 2022. Kalorimeter C5000 Control. [Online] [cit. 2023-10-15] Dostupné na: https://www.ilabo.cz/.

KISS, M., 2019. Diplomová praca: Možnosti zhutňovania biomasy mobilným peletovacím zariadením [cit. 2024-03-15] Dostupné na: https://opac.crzp.sk/?fn=detailBiblioFormChildGCNEM&sid=9F8942B94996237AAAFB1EF666DC&seo=CRZP-detail-kniha.

KPALO, S.Y., ZAINUDDIN, M.F., MANAF, L.A., ROSLAN, A.M., 2020. A Review of Technical and Economic Aspects of Biomass Briquetting [cit. 2023-10 20] Dostupné na: https://www.mdpi.com/2071-1050/12/11/4609.

Kúrenie peletami: aké sú skúsenosti, spotreba a cena, 2021, [cit. 2024-01-18] Dostupné na : https://www.opop.sk/kurenie-peletami-ake-su-skusenosti-spotreba-cena.

LIETH, H., LIKENS, G.E., WHITTAKER, R.H., 1975. Primary Productivity of the Biosphere. Ecological Studies 14. New York: Springer-Verlag. 340 s. ISBN-13:978-3-642-80915-6.

MAJ, G., KLIMEK, K., KAPŁAN, M., WRZESIŃSKA-JĘDRUSIAK, E., 2022. Using wood-based waste from grapevine cultivation for energy purposes. Energies, 15, 890. [cit. 2024-02-18] Dostupné na: https://www.mdpi.com/1996-1073/15/3/890.

MATÚŠ, M., KRIŽAN, P., 2009. Identifikácia väzbotvorných mechanizmov v procese zhutňovania biomasy a ich vplyv na konštrukciu zhutňovacích strojov. In: Energie z biomasy X – Brno: Vysoké učení technické v Brně, 2009, s. 73-78, ISBN 978-80-214-40272.

PETRUF, A. 2014. Výskum procesu zhutňovania odpadov z biomasy. Diplomová praca. [cit. 2024-03-15] Dostupná na: https://opac.crzp.sk/?fn=detailBiblioFormChildG2N2HM&sid=18B0B0AA43959DC6DB56374321BD&seo=CRZP-detail-kniha.

PUROHIT, P., CHATURVEDI, V., 2016. Techno-Economic Assessment of Biomass Pellets for Power Generation in India; CEEW: New Delhi, India, 2016.

SARVAŠ, J., INAŠOVÁ, D., 2013. Paletovanie a briketovanie – efektívne využívanie biomasy. In Zborník vedeckých prác v rámci projektu Nové technológie pre energeticky enviromentálne a ekonomicky efektívne zhodnotenie biomasy. Bratislava: Ekonomická univerzita v Bratislave, s. 74–80. ISBN 978-80-225-3820-6.

SOLANO, D., VINYES, P., ARRANZ, P., 2016. Biomass Briquetting Process; UNDP-CEDRO Publication: Beirut, Lebanon, 2016.

STUDENÝ P., 2022. Meranie fyzikálno mechanických vlastností peliet vyrobených z Paulownie. Diplomová praca. [cit. 2024-03-15] Dostupné na: https://opac.crzp.sk/?fn=detailBiblioFormChildI2LDC7&sid=DD4AECDD61273E16FD3CF986B1FD&seo=CRZP-detail-kniha.

Štatistický úrad SR, 2021. Definitívne údaje o úrode poľnohospodárskych plodín a zeleniny v SR za rok 2021, [cit. 2024-01-18] Dostupné na: https://slovak.statistics.sk/wps/portal/c46a8a6a-48ed-4088-b775-2cacaebc7610/!ut/p/z0/jVDLTsMwEPyaHF1vUie2jymVqlb0UFWI4AtaOyY1SZ00MYH260nhAociLqN9zM6shipaUOVxdBUG13pspv5JZc87vhaLRZwD8HQJ683DcrfayxgY0P1Q0w1VVdPqb3rSb--2FVUdhgNx_qWlBWNCmJKVJE0tXtlOH2fv5jiDGeNxKiWHjEuRyPlVwL2eTiqnyrQ-2I9Ai1YPeCBDHcEQpr8M-dr4EEGJATVezhH0tnJDsD1p-wq9u6Bx7rdTnAiesSRmQibzqf7TinRvOoIJGldPUjaCcbChPv-cGJahwAwJE7YkDIQgmvOUJAYNWm14FsONQP512tWrR6J02oz3-Sc3LY4j/.

TUMULURU, J.S., WRIGHT, C.T., HESS, J.R., KENNEY, K.L., 2011. A review of biomass densification systems to develop uniform feedstock commodities for bioenergy application. In. Biofuels Bioproducts & Biorefining-Biofpr [online], vol. 5(6), pp. 683–707 [cit. 2024-04-18].

VALKOVIČ, J., 2022, Zhutnenie odpadovej biomasy, Diplomová praca, [cit. 2024-04-22] Dostupne na: https://opac.crzp.sk/?fn=detailBiblioFormChildWCHPS&sid=FE42652C724A629CC6634524874B&seo=CRZP-detail-kniha.

ANALYSIS OF THE SELECTED LINE OF MACHINES FOR POST-HARVEST PROCESSING OF CEREALS FROM THE POINT OF VIEW OF PRODUCT QUALITY

MICHAL ANGELOVIČ, KRISTIÁN FIALA, JÁN JOBBÁGY, TOMÁŠ GIERTL, KOLOMAN KRIŠTOF

Slovak University of Agriculture, *Institute of Agricultural Engineering, Transport and Bioenergetics*

Abstract: The objective of this thesis was to evaluate a selected line of machinery for the postharvest processing of cereals in terms of product quality. The machinery analyzed included the Schneider Jaquet & Cie SNST 1150 cleaner, the Mathews Company model 675 BEM-NG/HRS dryer, the MO 20 seed treater, conveyors, and storage facilities.

The results indicated that the quality of the processed wheat (Csillag variety) and barley (Casanova variety) met Slovak technical standards. Wheat achieved the highest classification (Class E), and barley was classified under Class A. The analysis showed that the highest percentage of the cereals by weight was found in the second fraction, with wheat exceeding 95% and barley over 50%, demonstrating that wheat grains were more uniform compared to the more varied barley grains. However, both the first and third fractions remained fully usable, satisfying the criteria for bulk density, impurity percentage, and moisture content.

Key words: Post-harvest treatment, machine line, cleaner, dryer, cereals

INTRODUCTION

V modernom svete zohráva poľnohospodárstvo kľúčovú úlohu v zabezpečovaní potravinovej bezpečnosti pre stále rastúcu globálnu populáciu. Zabezpečiť účinnú a bezpečnú produkciu obilnín, ktoré tvoria základnú časť ľudskej stravy, je preto kľúčovým cieľom poľnohospodárskeho sektora. V tejto súvislosti má pozberová úprava obilnín zásadný význam, pretože ovplyvňuje nielen kvalitu výsledného produktu, ale aj bezpečnosť práce pre tých, ktorí sa podieľajú na tejto kritické fáze poľnohospodárskej výroby. (MAREČEK, 2011)

Táto práca sa zameriava na analýzu vybranej linky strojov určených na pozberovú úpravu obilnín s dôrazom na kvalitu produktu. Kvalita produktu je neoddeliteľnou súčasťou úspešného poľnohospodárskeho procesu, pretože ovplyvňuje trhovú hodnotu obilnín, ich využitie v potravinárskom priemysle a celkovú spokojnosť spotrebiteľov. (**Z**IMOLKA, 2005)

Cieľom tejto práce je poskytnúť komplexnú analýzu vybranej linky strojov na pozberovú úpravu obilnín a identifikovať faktory, ktoré ovplyvňujú kvalitu výsledného produktu. Táto práca je rozdelená do viacerých kapitol, ktoré pokryjú rôzne aspekty analýzy linky strojov na pozberovú úpravu obilnín. Zahrnuté budú popisy vybraných strojov, analýzy kvality produktu a návrhy na vylepšenie. Celkovým cieľom je prispieť k efektívnejšiemu a bezpečnejšiemu poľnohospodárskemu procesu, ktorý bude zodpovedať súčasným a budúcim potrebám v oblasti potravinovej produkcie.

MATERIAL and METHODOLOGY

Charakteristika podniku

Podnik sídli v okrese Zlaté Moravce, pôdy na tomto území sú veľmi rôznorodé, ale zato priaznivé pre rastlinnú výrobu. Podielnické družstvo je v prevádzke od roku 1975 a disponuje vlastnou technikou pre rastlinnú výrobu a pozberovú úpravu. Vlastní kombajn značky New Holland, traktory Zetor, Massey Ferguson, New Holland a John Deere, nakladače Caterpillar, kypriče Väderstad, sejačky Väderstad a Monosem a rôzne iné náradia ako napr. rozmetadlá, mulčovače, plečky, pluhy atď. Z hľadiska

pozberovej linky podnik vlastní čističku od firmy Schneider Jaquet & Cie a sušičku Mathews Company, v prípade potreby majú aj moričku osív MO 20.

Základnou filozofiou firmy je priamy kontakt so zákazníkom. Svojím klientom sa snažia ku kvalitným produktom poskytnúť pridanú hodnotu. Spoločnosť ustavične vylepšuje svoje postupy a technológie z dôvodu zvýšenia kvality a konkurencieschopnosti na trhu.

Charakteristika vybraných meraných odrôd

Pšenica-Csillag. Vysoko výnosná odroda s veľmi dobrou adaptabilitou v rôznych klimatických podmienkach, rastie vyrovnane s vysokou úrodou a stabilnou potravinárskou kvalitou.

Jačmeň ozimný-Casanova. Dvojradá úrodná odroda sladovníckeho jačmeňa, najskoršia v sortimente s vysokým podielom predného zrna. Vyznačuje sa dobrým zdravotným stavom. (POSPÍŠILOVÁ, 2005).

Charakteristika vybranej linky strojov

Funkciou tejto linky je upravovať obilniny, ktoré si dopestoval podnik. Linka pozostáva z príjmového ústrojenstva, čistenia, sušenia a skladovania. (Obrázok 1).

Medzi hlavné časti príjmového ústrojenstva patrí príjmový kôš, čistička, dopravné pásy, sušička a skladovacie zásobníky. Na úpravu mikroklímy sú v skladoch využité ventilátory.

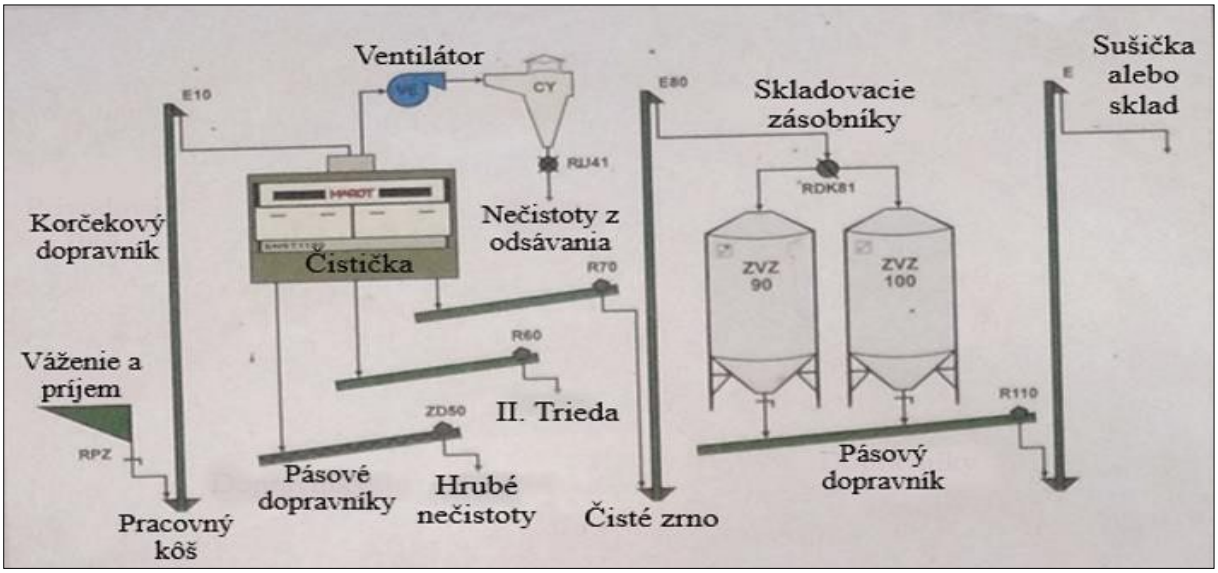

Obrázok 1 Schéma technologickej linky

– Čistička Schneider Jaguet & Cie SNST 1150

V rámci procesu pozberovej úpravy obilnín využíva podnik špecializovanú čističku Schneider Jaquet & Cie SNST 1150 (Obrázok 2). Čistička SNST 1150 je navrhnutá tak, aby zvládla čistenie všetkých typov obilnín, bez ohľadu na to, či sú vlhké alebo suché s vysokou spracovateľnosťou materiálu. Vďaka svojej vysokej výkonnosti a efektívnemu odstraňovaniu nečistôt je čistička Schneider Jaquet & Cie SNST 1150 neoceniteľnou súčasťou linky strojov na pozberovú úpravu obilnín, čo prispieva k udržaniu vysokej kvality produktu.

Obrázok 2 Čistička Schneider Jaquet & Cie SNST 1150

– Sušička obilnín Mathews Company 675 BEM-NG/HRS

Firma efektívne využíva sušičku obilnín Mathews Company 675 BEM-NG/HRS (Obrázok 3), ktorá je špeciálne navrhnutá pre potreby poľnohospodárstva. Sušička ponúka pokročilé funkcie, ako je sušenie v zrnových stĺpcoch širokých 30,5 cm, umožňujúce spracovanie širokého spektra zrnín a olejnín, začínajúc už pri veľkosti priemeru zrna 1,27 mm. Kľúčovým aspektom sušičky je jej schopnosť automaticky udržiavať sušiacu teplotu v rozmedzí od 25 do 110 °C, čo umožňuje presné nastavenie podmienok pre optimálne sušenie.

Obrázok 3 Sušička Mathews Company, 675 BEM-NG/HRS

– Moričkа osív MO 20

Firma úspešne využíva moričku osív MO 20 (Obrázok 4) na vlastnú úrodu, ktorá aplikuje osivá bežných druhov plodín pomocou moderného mokrého kontinuálneho procesu. Vďaka tejto technológii je moričkа vhodná aj pre ľahko poškoditeľné semená ako hrach, sója a kukurica, pričom minimalizuje riziko ich poškodenia počas procesu morenia.

Obrázok 4 Moričkа osív MO 20

RESULTS and DISCUSSION

Výsledky merania pozberovej úpravy

Pri posudzovaní linky sme sa zamerali na niekoľko kritérií a ukazovatele kvality obilnín. Prvým kritériom hodnotenia bola objemová hmotnosť v $kg.m^{-3}$. Nasledujúcim kritériom bola hmotnosť 1 000 zŕn (HTZ) v g, analýza podielu frakcií v %, analýza vlhkosti zrna v %.

– Analýza meraní objemovej hmotnosti

Pri meraní objemovej hmotnosti pšenice Csillag a jačmeňa Casanova sme postupovali podľa normy STN ISO 7971-3, pričom sme na určenie objemovej hmotnosti zŕn použili obilný skúšač OS-1.

Zistené meranie objemovej hmotnosti pšenice Csillag možno vidieť v nasledujúcej tabuľke 1. Tabuľka poskytuje detailné informácie o každom meraní**.**

Tabulka 1 Objemová hmotnosť pšenice Csillag pred čistením a po čistení

Objemová hmotnosť (kg.m^{-3}) pšenice Csillag					
Číslo merania	Pred čistením	Po čistení	Prímesi (g)	Prímesi (%)	Čisté zrno (%)
1	807,14	836,64	29,50	3,53	96,47
2	807,82	833,99	26,17	3,14	96,86
3	795,96	834,93	38,97	4,67	95,33
4	810,87	837,17	26,30	3,14	96,86
5	799,38	836,93	37,55	4,49	95,51
6	804,27	834,16	29,89	3,58	96,42
7	808,62	837,80	29,18	3,48	96,52
8	795,56	838,29	42,73	5,10	94,90
9	794,56	835,87	41,31	4,94	95,06
10	807,91	837,50	29,59	3,53	96,47
Min.	794,56	833,99	26,17	3,14	94,90
Max.	810,87	838,29	42,73	5,10	96,86
Rozsah	16,31	4,30	16,56	1,96	1,96
Priemer	803,21	836,33	33,12	3,96	96,04
Smer. odchýlka	6,22	1,52	6,32	0,75	0,75
Var. koeficient %	0,77	0,18	19,09	19,05	0,79

¶

Zvýšenie priemernej objemovej hmotnosti po čistení naznačuje, že čistenie odstránilo z obilia nečistoty a ľahké častice, čím sa zvýšila jeho hustota. Výrazný pokles rozsahu objemovej hmotnosti po čistení potvrdzuje, že čistenie viedlo k homogenizácii vzorky z hľadiska objemovej hmotnosti.

Tabulka 2 Objemová hmotnosť jačmeňa Casanova pred čistením a po čistení

Objemová hmotnosť (kg.m^{-3}) jačmeňa Casanova					
Číslo merania	Pred čistením	Po čistení	Prímesi (g)	Prímesi (%)	Čisté zrno (%)
1	663,13	671,95	8,82	1,31	98,69
2	658,45	673,20	14,75	2,19	97,81
3	665,14	674,22	9,08	1,35	98,65
4	660,45	671,76	11,31	1,68	98,32
5	667,52	672,53	5,01	0,74	99,26
6	665,91	671,87	5,96	0,89	99,11
7	660,23	671,67	11,44	1,70	98,30
8	661,01	672,16	11,15	1,66	98,34
9	662,14	672,46	10,32	1,53	98,47
10	661,19	669,83	8,64	1,29	98,71
Min.	658,45	669,83	5,01	0,74	97,81
Max.	667,52	674,22	14,75	2,19	99,26
Rozsah	9,07	4,39	9,74	1,45	1,45
Priemer	662,52	672,17	9,65	1,44	98,56
Smer. odchýlka	2,87	1,13	2,83	0,42	0,42
Var. koeficient %	0,43	0,17	29,29	29,24	0,43

Tak ako pri pšenici Csillag, tieto údaje naznačujú zvýšenie čistoty a zníženie variability po procese čistenia. Pokles rozsahu objemovej hmotnosti po čistení potvrdzuje, že čistenie viedlo k homogenizácii vzorky z hľadiska objemovej hmotnosti a zvýšenia hustoty.

– Analýza hmotnosti 1000 zŕn (HTZ)

Proces analýzy hmotnosti 1000 zŕn (HTZ) pšenice Csillag a jačmeňa Casanova prebiehal v laboratórnej súprave, kde nástrojom bolo laboratórne počítadlo zŕn NUMIREX.

Zistené údaje o hmotnosti 1000 zŕn pšenice Csillag a jačmeňa Casanova možno vidieť v tabuľke 3, ktorá obsahuje presné váhy pre jednotlivé vzorky.

Tabulka 3 Hmotnosť 1000 zŕn pšenice Csillag a jačmeňa Casanova

Hmotnosť 1 000 zŕn (HTZ) (g)		
Číslo merania	Pšenica Csillag	Jačmeň Casanova
1	33,12	36,72
2	34,61	36,62
3	34,32	35,90
4	34,44	37,27
5	35,13	36,09
6	35,15	36,23
7	34,68	35,62
8	34,51	36,24
9	34,28	36,78
10	35,46	35,40
Min.	33,12	35,40
Max.	35,46	37,27
Rozsah	2,34	1,87
Priemer	34,57	36,29
Smer. odchýlka	0,64	0,57
Var. koeficient %	1,86	1,57

Napriek tomu, že jačmeň Casanova mal v priemere ťažšie zrná ako pšenica Csillag, jeho rozsah hmotnosti bol menší, to naznačuje, že zrná jačmeňa Casanova boli jednotnejšej veľkosti a hmotnosti ako zrná pšenice Csillag.

– Triedenie zŕn podľa veľkosti

Pri analýze podielu frakcií v zrne pre pšenicu Csillag a jačmeň Casanova sa použila laboratórna sitová čistička značky Pfeuffer Sortimat, ktorá je navrhnutá na presné laboratórne rozdelenie zrnovej vzorky na rôzne veľkostné frakcie. Použité sitá pre pšenicu Csillag boli s priemerom otvorov 3,5, 2,0, 1,0 mm a pre jačmeň Casanova 2,8, 2,5, 2,2 mm.

Získané údaje z analýzy podielu frakcií v zrne pre pšenicu Csillag a jačmeň Casanova sú zaznamenané v tabuľke č.4 a 5, ktorá poskytuje hmotnosti jednotlivých frakcií po triedení.

Tabulka 4 Triedenie pšenice Csillag

Triedenie pšenice Csillag pri rozmeroch sít 3,5; 2,0; 1,0 mm										
Číslo merania	1. Frakcia		2. Frakcia		3. Frakcia		4. Frakcia		Spolu	
	g	%	g	%	g	%	g	%	g	%
1	2,43	2,43	96,31	96,31	1,25	1,25	0,01	0,01	100,00	100
2	2,23	2,23	96,39	96,41	1,34	1,34	0,02	0,02	99,98	100
3	2,86	2,86	95,62	95,59	1,53	1,53	0,02	0,02	100,03	100
4	5,00	5,00	93,24	93,28	1,70	1,70	0,02	0,02	99,96	100
5	2,90	2,90	95,35	95,28	1,78	1,78	0,04	0,04	100,07	100
Min.	2,23	2,23	93,24	93,28	1,25	1,25	0,01	0,01	99,96	100
Max.	5,00	5,00	96,39	96,41	1,78	1,78	0,04	0,04	100,07	100
Rozsah	2,77	2,77	3,15	3,13	0,53	0,53	0,03	0,03	0,11	0
Priemer	3,08	3,08	95,38	95,37	1,52	1,52	0,02	0,02	100,01	100
Smer. odchýlka	1,11	1,11	1,28	1,26	0,23	0,23	0,01	0,01	0,04	0
Var. koeficient %	35,93	35,96	1,34	1,33	14,91	14,89	49,79	49,75	0,04	0

Prvá a tretia frakcia majú menšie hmotnostné a percentuálne podiely, zatiaľ čo štvrtá frakcia, ktorou je prach alebo úlomky, má najmenší hmotnostný a percentuálny podiel.

Tabulka 5 Triedenie jačmeňa Casanova

Triedenie jačmeňa Casanova pri rozmeroch sít 2,8; 2,5; 2,2 mm										
Číslo merania	1. Frakcia		2. Frakcia		3. Frakcia		4. Frakcia		Spolu	
	g	%	g	%	g	%	g	%	g	%
1	14,89	14,88	51,96	51,93	27,97	27,96	5,23	5,23	100,05	100
2	15,01	15,01	52,04	52,04	28,23	28,23	4,72	4,72	100,00	100
3	14,71	14,69	51,72	51,63	29,62	29,57	4,12	4,11	100,17	100
4	14,86	14,88	53,24	53,30	27,05	27,08	4,74	4,75	99,89	100
5	13,02	13,02	48,35	48,35	33,26	33,26	5,37	5,37	100,00	100
Min.	13,02	13,02	48,35	48,35	27,05	27,08	4,12	4,11	99,89	100
Max.	15,01	15,01	53,24	53,30	33,26	33,26	5,37	5,37	100,17	100
Rozsah	1,99	1,99	4,89	4,95	6,21	6,18	1,25	1,26	0,28	0
Priemer	14,50	14,49	51,46	51,45	29,23	29,22	4,84	4,84	100,02	100
Smer. odchýlka	0,83	0,83	1,84	1,85	2,44	2,43	0,49	0,50	0,10	0
Var. koeficient %	5,75	5,74	3,57	3,59	8,33	8,31	10,21	10,25	0,10	0

Analýza jednotlivých frakcií pšenice Csillag a jačmeňa Casanova odhalila zaujímavé rozdiely, pri pšenici je dominujúci podiel zrna v 2. frakcii, kde sa koncentruje viac ako 95% z celkovej hmotnosti vzorky.

V prípade jačmeňa je to podobné, viac ako 50% sa nachádza v 2. frakcii. Tento fenomén môže naznačovať, že zrná pšenice sú vo všeobecnosti rozmerovo homogénnejšie v porovnaní s jačmeňom.

– Analýza vlhkosti zrna

Proces merania vlhkosti zrna pšenice Csillag a jačmeňa Casanova prebiehal s využitím vlhkomera na obilie Pfeuffer HE 50. Meraním pomocou vlhkomera bola zistená vlhkosť pšenice Csillag na úrovni 10,3% a vlhkosť jačmeňa Casanova na úrovni 10,2%.

– Porovnávanie hodnôt s technickými normami

Počas merania pšenice Csillag musí byť splnená súhrnná kritéria určená normami STN 46 1011-1, STN 46 1011-30, STN 46 1100-1, STN 46 1100-2, ako aj pravidlami potravinového kódexu Slovenskej republiky a ďalšími súvisiacimi špecifikáciami uvedenými v týchto normách. Potravinárska pšenica je klasifikovaná do kvalitatívnych tried podľa technických noriem, ktoré rozdeľujú zrno do nasledujúcich kategórií:

a) elitná pšenica je zaradená do kvality triedy E,

b) zlepšujúca pšenica patrí do kvality triedy A,

c) štandardnú kvalitu reprezentuje pšenica triedy B,

d) slabá pečivárska pšenica je klasifikovaná ako kvalita triedy P.

Tabulka 6 Porovnávanie hodnôt s STN 461100-2

	Objemová hmotnosť ($kg.m^{-3}$)	Prímesi (%)	Čisté zrno (%)	Vlhkosť (%)
Namerané hodnoty	836,33	3,96	96,04	10,3
Požiadavky podľa normy STN 461100-2 (Trieda E)	Najmenej: 800	Najviac: 4	-	Najviac: 14

Vzorka pšenice Csillag spĺňa alebo prekračuje priemerné štandardné hodnoty objemovej hmotnosti, prímesi a vlhkosti, ako je stanovené v technických špecifikáciách kvality normy STN 46 1100-2. Tieto kritériá umožňujú zaradenie pšenice do elitnej kvalitatívnej triedy skupiny E.

Pri testovaní jačmeňa Casanova je nutné splniť normy STN 46 1011-1, STN 46 1011- 33, STN 46 1100-1, STN 46 1100-6 a ISO 5527.

Tabulka 7 Porovnávanie hodnôt s STN 461100-6

	Objemová hmotnosť ($kg.m^{-3}$)	Prímesi (%)	Čisté zrno (%)	Vlhkosť (%)
Namerané hodnoty	672,17	1,44	98,56	10,2
Požiadavky podľa normy STN 461100-6 (Trieda A)	Najmenej: 640	Najviac: 3	-	Najviac: 14

Keďže vybraná vzorka jačmeňa spĺňa alebo prekračuje štandardné hodnoty objemovej hmotnosti, množstva prímesí a vlhkosti, ktoré sú stanovené v norme STN 46 1100-6, je možné ju klasifikovať do akostnej triedy A.

CONCLUSION

Cieľom práce bolo zhodnotiť vybranú linku strojov na pozberovú úpravu obilnín vzhľadom na kvalitu produktu. V rámci práce sme podrobne analyzovali čistiaci stroj Schneider Jaquet & Cie SNST 1150, sušičku Mathews Company model 675 BEM-NG/HRS, moričku osív MO 20, dopravníky a sklady.

Z hľadiska kvality produktu, obidve analyzované obilniny pšenica Csillag a jačmeň Casanova boli testované v laboratórnych podmienkach a spĺňali slovenské technické normy. Pšenica bola zaradená do najvyššej triedy E a jačmeň do triedy A. Zistilo sa, že pšenica má výrazne homogénnejšie zrná ako jačmeň, čo sa prejavilo najmä v druhej frakcii, kde pšenica dosiahla viac ako 95% a jačmeň viac ako 50%. Aj napriek väčšej variabilite jačmeňa boli prvá a tretia frakcia stále plne použiteľné**.**

Na základe zistení by bolo z technologického hľadiska prospešné zvážiť implementáciu pokročilejších technológií na zvýšenie uniformity zŕn, najmä pri jačmeni, čo by mohlo prispieť k zlepšeniu kvality konečného produktu. Odporúča sa tiež zaviesť dodatočné monitorovacie a kontrolné postupy pre skladovanie obilnín, aby sa predišlo prípadnej kontaminácii a zabezpečila sa konzistentná kvalita obilnín.

Problematika pozberovej úpravy obilnín z hľadiska strojov, technologického a ekonomického hľadiska je v rámci Slovenskej republiky málo preskúmaná, preto tieto otázky budú predmetom ďalšieho výskumu na Ústave poľnohospodárskej techniky, dopravy a bioenergetiky, Technickej fakulty SPU v Nitre.

REFERENCES

Aerodynamická čistička zrnín ISMIA, 2024. In *Stslevice.sk* [online]. © 2024 [cit.2024-04-15]. Dostupné na: https://stslevice.sk/main.php?actm=7

JCC Čističky VibroCompact, 2024. In *Jk-machinery.sk* [online]. © 2024 [cit.2024- 04-15]. Dostupné na: https://jk-machinery.sk/stroje/jcc-vibrocompact/

MAREČEK, J., 2011. *Posudzovanie kvality obilnín a olejnín z potravinárskeho hľadiska*. In *Naše pole*, roč. 15, č. 11, s. 29. ISSN 1335–2466.

ZIMOLKA, J., 2005. *Pšenice – pestovaní, hodnocení a užití zrna*. Praha: Profi Press. 180 s. ISBN 80-86726-09-6.

Vyhláška č. 2/2014 Z. z. z 19. decembra 2013 o jedlom obilí a mlynských výrobkoch

Normy STN 46 1011-1, STN 46 1011- 33, STN 46 1100-1, STN 46 1100-6 a ISO 5527.

POSPÍŠILOVÁ, D. a kol., 2005. *Ampelografia*. 1. vyd. Bratislava: Výskumná a šľachtiteľská stanica vinárska a vinohradnícka Modra, n.o. 2005. 368 s. ISBN 80-969350-9-7.

COMPUTER MODELLING OF THERMAL STRESS ON GLASS SHEET DURING LASER ENGRAVING

TOMÁŠ ZOUBEK, ROMAN BUMBÁLEK, FRANTIŠEK ŠPALEK, KAREL ŠRAMHAUSER, ZBYNĚK HAVELKA

Faculty of Agriculture and Technology, University of South Bohemia, Department of Technology and Cybernetics, Na Sádkách 1780, 37005 České Budějovice, Czech Republic

Abstract: Computer modelling is often used to understand the nature or behaviour of physical phenomena. In this work, a three-dimensional computer model was created from a glass plate on which twenty dots with a radius of 371.54 μm were burned using a laser engraving process. The distance between the dots was 1.25 mm. A computer simulation of the thermal stress of the laser engraving process was carried out on this model. The input parameters used were the laser travel time between points, the duration of the laser discharge, the laser power, the laser intensity and the laser density over a given area, the heat flux coefficient of the glass sheet and the function controlling the firing of the laser beam at specific points and times. The simulation was carried out for two variants that differed in the order of the fired points. The second variant proved to be more optimal for the geometry and material studied. It resulted in less thermal stress, as lower temperatures were achieved with a defined laser beam, and at the same time there was a greater time delay between processes stressing the same locations.

Keywords: Finite Element Method; COMSOL Multiphysics®; Heat Transfer; Computer Simulation

INTRODUCTION

Laser engraving is used in the glass processing industry mainly for design purposes. Thanks to specialised computer programs, it is possible to take almost any design or image and have it burned onto the surface of glass using laser engraving equipment. As part of the FV30234 project "Research and development of a process for laser printing of small to large format glass surfaces for the needs of the contemporary building industry", it was investigated whether this process could be used for other than purely design purposes. A special grid of dots was designed with a specific pitch and laser power to reflect the required amount of the UV part of the light spectrum to create an optical barrier to flying birds. However, when using the specified pitch of the dots, the material began to exhibit destructive behaviour due to excessive thermal stress. Therefore, one of the sub-problems addressed in the TRIO project FV30234 was to map the thermal stress on the glass surfaces during this specific surface treatment. Given the software and hardware facilities available at the Department of Engineering and Cybernetics at the Faculty of Agriculture and Technology, it was proposed to carry out a study of the thermal stresses described above using computer simulation. The advantages of computer simulations are undoubtedly the possibility of repeating simulations with adjustment of the input values or the possibility of studying the influence of one or more variables on the simulation result.

Methods of computer modelling of physical-technical phenomena contribute greatly to a better understanding of them, which can be of considerable benefit in operational practice. Computer simulations allow the influence of many variables on a mathematically defined model to be studied. In a short time, simulations can provide a wealth of data that would often take years to obtain experimentally. Another advantage is the ability to set custom model conditions under which the simulation can be run. Given the complexity of some of the phenomena being studied, the biggest problem with computer simulations is their questionable correlation with experimentally measured data in the real world. This correlation is influenced by the mere mathematical description of the phenomenon under study, or rather by the accuracy of the mathematical description and the degree of simplification. The next step, where inaccuracies occur, is the numerical solution of the equations describing the phenomenon under study. These solutions often involve further simplifications, which can further

increase the deviations between simulation and reality. Inaccuracies can also arise from the choice of a limited number of variables as input data, simplification of the geometry of the phenomenon under study and inaccurately measured input parameters. When obtaining experimental data for comparison, the accuracy of the measuring instruments used and the method of data acquisition are important. (Abar et al., 2017; Oliveira et al., 2019; Wang and Jiang, 2022; Foo et al., 2023; Sass and Reusken, 2023)

As computing power increases and becomes more widely available, the use of computer simulations is becoming more widespread across disciplines to elucidate the behaviour of selected systems under defined conditions. In health research, for example, a model has recently been developed to simulate pulmonary ventilation flow in advanced COVID-19 disease (Middleton et al., 2022). Redlarski and Jawoski (2013) developed a tool to predict the course of respiratory disease, using data from a large database of previously published results. Another example of the use of computer simulations in healthcare is a model to assess hand tremor in Parkinson's disease (Legaria-Santiago et al., 2022). In the agricultural sector, especially in crop production, one of the most discussed areas of research is the study of compaction of agricultural soils due to the effects of soil management. Research is therefore developing computer models that focus on this issue. Jimenez et al. (2021) use computer simulations to study the effect of mechanised sugar beet harvesting on soil compaction. Escobar et al. (2021) focused on the use of computer models to better understand the interaction between the roller and the partially saturated soil for compaction analysis, and Guimarães Júnnyor et al. (2021) developed a predictive model to compare soil compaction during mechanised harvesting with or without crop rotation on a given plot. Apart from weather forecasting models, the best known applications of computer simulations are computational fluid dynamics (CFD) models and models that simulate the stresses on materials during engineering processing. Models dealing with flow or fluid dynamics include the model used by Kumar et al. (2023) for the design and analysis of a three-way catalytic converter. From an environmental or economic point of view, some technologies and materials are of great interest, which is why many research teams focus on them. Review articles can then be produced to summarise the latest findings on the subject, as in the case of Novia et al. (2023), who present recent advances in modelling bioethanol production processes using CFD tools. Similarly, Tominaga et al. (2023) summarise advances in the use of CFD models, this time in the area of urban aerodynamics and microclimate simulations.

Computer modelling techniques are also used to map heat transfer mechanisms in glass surfaces. This may involve attempting to identify the value of the heat transfer coefficient at the glass/mould frame interface, as done by Cressin et al. (2023). Their work resulted in the development of a methodology to identify the heat transfer coefficient based on a 1D finite difference model. To find a solution to the thermal contact problem between the glass cylinder and the mould, it was necessary to solve thermal equations 1 and 2.

$$C^g(T^g)\rho\frac{\partial T^g(x,t)}{\partial t} = \nabla_x \cdot (k^g(T^g)\nabla_x T^g(x,t)) - \nabla_x \cdot q_{rad}(x,T^g), \quad (1)$$

$$C^m(T^m)\rho\frac{\partial T^m(x,t)}{\partial t} = \nabla_x \cdot (k^m(T^m)\nabla_x T^m(x,t)), \quad (2)$$

where $T^j(x,t)$ is the temperature of the points x at time t, where $j = g$ or m and q_{rad} $(W \cdot m^{-2})$ is the heat flux. The two regions (g and m) are connected by a thermal contact condition $x = 30{,}5\ mm$.

From a different perspective, Béchet et al. (2015) addressed the issue of glass forming. In their work, they developed a 2D model of the forming and tempering processes in glass manufacturing, including radiation heat transfer. The model was to be based on the finite element method, and the calculations were carried out using the ABAQUS® software kernel. Equations 3 and 4 were used to calculate the stresses in the material.

$$\sigma(\bar{r},t) = s(\bar{r},t) + \frac{trace(\sigma(\bar{r},t))}{3}I = s(\bar{r},t) + \frac{\sigma_h(\bar{r},t)}{3}I, \quad (3)$$

$$\varepsilon(\bar{r},t) = e(\bar{r},t) + \frac{trace(\epsilon(\bar{r},t))}{3}I = e(\bar{r},t) + \frac{\epsilon_h(\bar{r},t)}{3}I, \quad (4)$$

where $e(\bar{r},t)$ is the strain tensor and $s(\bar{r},t)$ is the stress tensor, I is unit tensor, $\epsilon_h(\bar{r},t)$ he first invariant of the strain tensor and $\sigma_h(\bar{r},t)$ and is the first invariant of the stress tensor. They then used the generalized Maxwell model for the shear part.

A special case of the cause of thermal stress and heat transfer in glass surfaces is cutting (Nisar et al., 2009), welding (Kahle and Nodop, 2022) or laser beam surface treatment (Lai et al., 2022). The processing of glass using laser discharges can be performed by several types of these devices. In particular, ultrashort pulse lasers (Wu et al., 2022), femtosecond lasers (Witcher et al., 2015) and CO_2 lasers (Mishra et al., 2017) have received much attention. For each type of laser, different pitfalls and possible material defects after their use are described. Cvecek et al. (2014) published a paper presenting experiments based on which it is possible to understand the origin and basic mechanisms of formation and movement of gas bubbles formed in some types of glasses during their processing with an ultrashort pulsed laser. Following this issue, Bulgakova et al. (2015) published a paper entitled " How to optimize ultrashort pulse laser interaction with glass surfaces in cutting regimes?". The focus was on several influences on the final cutting result, including laser wavelength, pulse duration, and laser energy, as well as often neglected influences that affect industrial production, such as debris accumulation, the need to use toxic substances after laser processing, and high sensitivity to relatively small changes in laser parameters, including fluence, tracer velocity, and repetition rate.

In terms of the focus of this work, the most interesting problem addressed is the prediction of heating, heat transfer and thermal stress of glass materials during CO_2 laser processing. The volumetric changes of fused silica (SiO_2) at high temperatures were the focus of Vignes et al. (2013) when they developed a thermomechanical model of laser-induced structural relaxation and deformation. They used equation 5 to calculate the heat transfer.

$$Q(r,z,t,T) = \rho(T) \cdot C_p(T) \cdot \frac{\partial T}{\partial t} - \nabla \cdot (\kappa(T) \cdot \nabla T) \tag{5}$$

where ρ is material density ($g \cdot cm^{-3}$), C_p is the heat capacity at constant pressure (K) and κ is the thermal conductivity ($W \cdot m^{-1} \cdot K^{-1}$).

Tiam and Chiu (2004) presented a heat transfer model to calculate the temperature field in a moving glass rod heated by a CO2 laser. To calculate the heat transfer in the glass for a stable, axisymmetric state, they relied on Eq. 6.

$$\rho C_p v \cdot \nabla T = \nabla \cdot (k\nabla T - q_r - q_{rl}), \tag{6}$$

where ρ is material density ($kg \cdot m^{-3}$), C_p is the specific heat capacity ($J \cdot kg^{-1} \cdot K^{-1}$), is the rod displacement rate ($cm \cdot s^{-1}$), k is the thermal conductivity ($W \cdot m^{-1} \cdot K^{-1}$), q_r is the radiation-induced heat flux (W), q_{rl} is the laser-induced heat flux (W).

Grellier et al (1998) carried out a theoretical and numerical study of the self-regulation of the diameter of optical fibres produced by a CO_2 laser. After completing the theoretical study and interpreting the computer simulation results, they concluded that for small diameters of glass fibres produced by CO_2 laser, its polarisation is important because resonance effects cause oscillations in the equilibrium temperature plots.

When cutting or surface treatment of glass surfaces with a laser, thermal stresses occur, which can cause the material to break during the cutting process. Jiao and Wang (2008) came up with the idea of preheating the material to be cut by using a dual CO_2 laser, where the first unfocused beam will preheat and thus reduce the thermal gradients, and the second already focused beam will cut the glass sheet. They verified their thesis using ANSYS computer modelling software.

Therefore, the aim of this work was to create and numerically implement a computer model of a glass plate thermally stressed during the laser beam engraving process, which will serve for a better understanding of the specifically designed engraving procedure and its adjustment to avoid excessive thermal stress leading to the destruction of the processed material.

MATERIAL and METHODOLOGY

COMSOL Multiphysics® 5.5 software (COMSOL, Inc., USA) was used to create a computer model simulating the thermal stress on the glass plate during the laser engraving process. This tool was used on an HP Z4 G4 workstation with an Intel(R) Core(TM) i9-10940X CPU @ 3.30 GHz 3.31 GHz, 64 GB RAM, Windows 10 Pro, 64-bit operating system, version 22H2, and NVIDIA GeForce RTX 3090 graphics adapter.

To create a thermal stress model of the glass material during the laser engraving process, the initial setup of the COMSOL Multiphysics® 5.5 software was created using the Model Wizard process, in which the three-dimensional dimension of the physical phenomenon to be solved was selected, the physical environment Heat Transfer in Solid was selected, and the entire computer simulation was solved using the Time Depend study. The entire model was created parametrically, which allows for quick change of input values in one place and also the possibility to export them in txt format. The parameters were set in the Global Definitions node, namely the width (25 mm), height (30 mm) and thickness (4 mm) of the glass sheet, the edge of the glass surface not treated by the laser beam (10 mm), the distance between the burned points (1.25 mm), the radius of the burned points (371.54 μm), the time for the laser to move between the burned points (0.5 s) and the time for the laser beam to act on the burned point (0.5 s).

After entering all the necessary parameters from the previous step, it was possible to proceed to the creation of a geometric representation of the studied phenomenon of heat propagation in the glass plate during the laser engraving process. The glass plate was created using the block tool with the dimensions width, height and thickness, while a corner was created with the coordinates. On the created plate it was then necessary to construct 20 cylinders representing the points burned by the laser. The Cylinder tool was used to create the first row of five points, with the Radius parameter set to Radius and the Height parameter set to 0.001 mm, values common to all the points to be burned. The position setting for the starting point of the cylinder construction (the centre of the lower base) is different for each point, or the y and z coordinates are identical and the x axis coordinates change. The specific setup is described by equations 6–8.

$$x = space + (n-1) \cdot spacing, \tag{6}$$

$$y = height - space, \tag{7}$$

$$z = depth - 0.001, \tag{8}$$

where n is the value of the order of the constructed cylinder. After all five cylinders were completed, a second series was created using the Copy tool, where the input (copied) objects are cylinders 1–5 and the displacement vector is $(0, -spacing, 0)$. In the last step of geometry creation, copying was used again, where the input objects were all ten cylinders, the original five and the new five created by the first copy, and the displacement vector was $(0, -2 \cdot spacing, 0)$.

Another part of the model that had to be set up was the functions that control the switching on and off of the laser beam, so that the surface treatment of the glass surface was continuous, with only one point being fired at a time. The functions are set at the node. The Rectangle function, defined by the upper and lower limits, was used to give the best flow for starting, operating and stopping the laser beam. A control function was created for each point to be fired, making a total of twenty. The values of the lower and upper limits are controlled by equations 9 and 10.

$$Lower\ limit = (n-1) \cdot discharge + (n-1) \cdot shift \text{Lowerlimit} = (\text{n-1}) \cdot \text{vyboj} + (\text{n-1}) \cdot \text{posun}, \tag{9}$$

$$Upper\ Limit = n \cdot discharge + (n-1) \cdot shift\ \text{UpperLimit} = \text{n} \cdot \text{vyboj} + (\text{n-1}) \cdot \text{posun}, \tag{10}$$

Once the functions controlling the laser discharge during firing were established, equations describing the intensity and density of the laser beam as a function of position at the firing point, see equations 11–16, had to be defined for each firing point.

$$Dist_{z,y}(n) = ((z - o_{nz}) \cdot e_y + (-y + o_{ny}) \cdot e_z)^2 \tag{11}$$

$$Dist_{z,x}(n) = ((-z + o_{nz}) \cdot e_x + (x + o_{nx}) \cdot e_z)^2 \tag{12}$$

$$Dist_{y,x}(n) = ((y - o_{ny}) \cdot e_x + (-x + o_{nx}) \cdot e_y)^2 \tag{13}$$

$$distance(n) = \frac{Dist_{z,y}(n) + Dist_{z,x}(n) + Dist_{y,x}(n)}{{e_x}^2 + {e_y}^2 + {e_z}^2} \tag{14}$$

$$intensity(n) = 0{,}5 \cdot \frac{e^{\frac{-0.5 \cdot distance(n)}{\sigma^2}}}{\pi \cdot \sigma^2}, \tag{15}$$

$$PowerDensity(n) = P \cdot intensity(n) \tag{16}$$

where x, y, z are the coordinates around the laser beam, o_{nx} is the x-coordinate of the origin of the beam, o_{ny} is the y-coordinate of the origin of the beam, o_{nz} is the z-coordinate of the origin of the beam, e_x is the orientation of the beam in the x-direction, e_y is the orientation of the beam in the y-direction, e_z is the orientation of the beam in the z-direction and σ is the standard deviation with a decision to increase it in case of too coarse elements of the computational mesh.

To monitor the temperature values, specific locations were selected where probes were placed. Coordinates (x, y, z) had to be specified for each probe. A total of 12 probes were placed at the intersection of the diagonals of four adjacent points forming a square. The coordinates of each point were $P_{i,j}$, where i is the row number and j is the column number where the probe is located. The coordinates of the probes can then be defined using equations 17–19.

$$x = space + \left(j - \frac{1}{2}\right) \cdot spacing \tag{17}$$

$$y = height - space - i \cdot spacing \tag{18}$$

$$z = 0.004 \text{ mm} \tag{19}$$

The next step in creating the computer model was to define the materials for the geometry. The entire geometric domain was assigned the material silica glass from the implied materials library.

The correct setting of the physical model and boundary conditions is critical to the functionality of the overall model. A heat source was created for each firing point using the Boundary Heat Sources tool. A separate heat source had to be created for each point as each point was fired at a different time. The heat flux value for each point was defined by Equation 20.

$$Q_b = power\_density(n) \cdot rect(n) \tag{20}$$

where n je pořadí vypalovaného bodu. is the order of the burned point. In the Boundary Heat Source setting, you must specify the units in which the $rect(n)$ variable is substituted into the equation. Without this information, the information will be incomplete for the software and it will not be able to perform the calculation. For the $rect(n)$ parameter, this is a time value because it ensures that the laser beam starts at a specific time, so it will be entered here($t[1/s]$).

Within the physical environment of heat propagation, it is also necessary to define the value of the heat flux. In this setting, the normal ambient temperature of 293.15 K was used and the value of the heat flux coefficient of the glass sheet was set to 5.7 $W \cdot m^{-2} \cdot K^{-1}$, as reported by Tong et al. (2019) in their paper. These values were assigned to all geometric entities that form the virtual representation of the glass sheet used to simulate the laser engraving process. The software uses the equation $q_0 = h \cdot (T_{ext} - T)$, whre h is the heat flux coefficient, T_{ext} is the ambient temperature and the source temperature to calculate the convective heat flux. The second critical part of setting up a computer model to simulate a particular physical phenomenon is the generation of a computational mesh. In this thesis, the finest computational mesh generation was used for the model creation. This was used because of the very small size of the firing points.

At the end of the process, two versions of the computer model were produced, differing in the order in which the points were fired. In the first version, the points were fired from left to right and in rows, whereas in the second version the points were fired one at a time and the rows were omitted. The specific order of the points is shown in Figure 1.

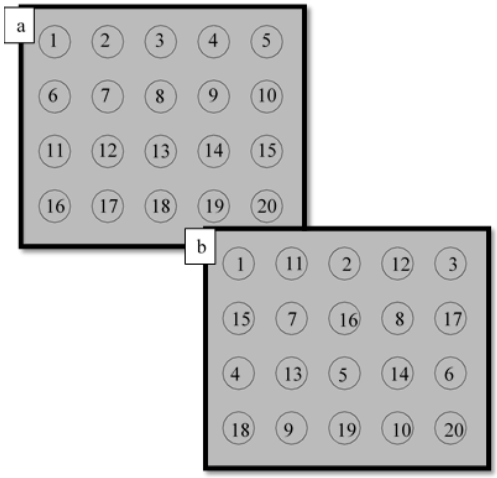

Figure 1 Order of firing points by laser engraving machine in a) variant 1, b) variant 2

Once these versions were completed, a time-dependent study was run, monitoring the burning process of 20 points for 21 seconds. The initial calculation time was set to 0 s, the time-dependent study step was set to 0.1 s and the entire simulation was terminated when the time reached 21 s. In total, the study was calculated for 211 different time points.

RESULTS and DISCUSSION

A computer simulation was performed for both proposed variations of the order of the fired points, using an identical computational grid consisting of 10 139 620 elements with an average quality of 0.5322. The lowest quality element had a value of $4.905 \cdot 10^{-4}$. The lower quality of the computational mesh was due to the large variation in the size of the individual geometry elements, where the overall dimensions of the glass plate were in the order of tens of mm, whereas the average of the fired points had a value of 371.54 μm.

Setting the order of the points had only a minimal effect on the total computation time, with variant 1 taking 22 hours 24 minutes and 4 seconds to compute and variant 2 taking 22 hours 48 minutes and 27 seconds to compute, and the difference of 24 minutes 23 seconds may be due to the different load on the computing setup, which was busy with normal operations in addition to model processing.

Table 1 shows the maximum values of each probe in the computer simulation of the laser engraving of dots in each row. The first row burns points 1–5, the second row burns points 6–10, the third row burns points 11–15 and the fourth and final row burns points 16–20. During the firing of the first row, none of the probes reached the calculated maximum temperature for the entire engraving process. For probes 1–4, the maximum temperatures were calculated for the firing of the second row. The maximum temperatures for probes 5–8 were obtained during the surface treatment that formed the third layer of

dots. For the remaining probes 9–12, the engraving process of the fourth row was the most stressful in terms of recorded temperatures. The minimum temperature differences for probes 4 and 8 were due to the fact that they were boundary probes that only cooled in the following time interval, which was reflected in the highest measured value obtained in that interval. For clarity, the data from Table 1 has also been visualised in the graph in Figure 2.

Table 1 Maximum temperature values [°C] measured by the probes in the computer simulation of firing points in individual rows for variant 1

	1st line	**2nd line**	**3rd line**	**4th line**
Probe 1	796.83	873.76	263.47	185.01
Probe 2	840.93	922.54	292.99	230.18
Probe 3	861.65	936.28	353.35	261.54
Probe 4	838.09	921.23	919.53	284.30
Probe 5	152.29	859.83	914.30	288.15
Probe 6	177.07	908.74	952.16	317.44
Probe 7	189.10	925.71	979.36	387.89
Probe 8	168.36	909.75	951.29	948.94
Probe 9	64.38	192.47	893.64	931.86
Probe 10	74.07	222.76	932.60	963.33
Probe 11	75.03	233.13	963.61	992.00
Probe 12	61.46	205.94	939.44	986.27

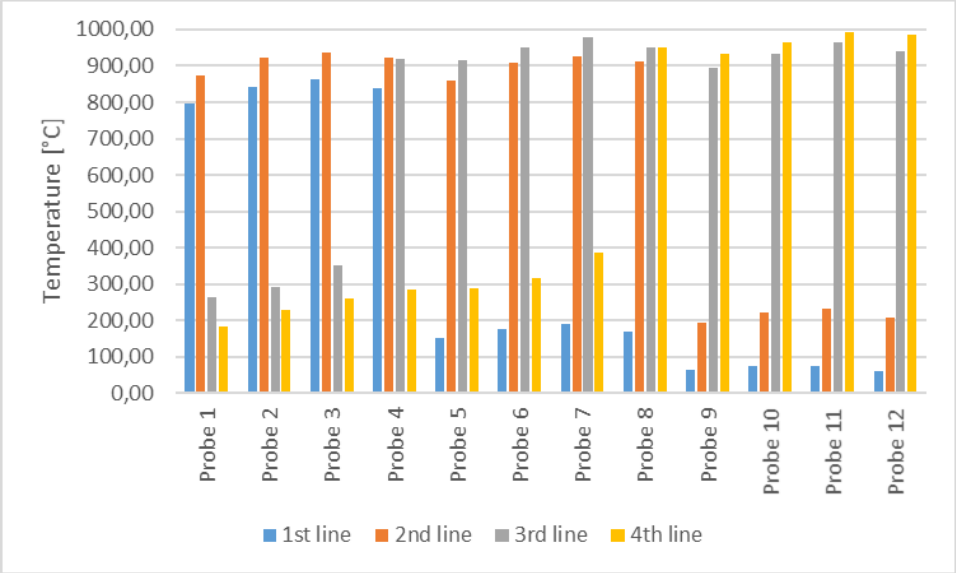

Figure 2 Visualisation of the values measured by the probes in the computer simulation of the firing of points in individual rows in variant 1

In Variant 2, the first, third and fifth dots are burned first in the first and then in the third row, then the second and fourth dots are engraved in the second, fourth, first and third rows, and finally the first, third and fifth dots are formed in the second and fourth rows.The temperature waveform recorded by each probe during the computer simulation of the laser engraving process shows peak temperatures in the range of approximately 100 °C after the initial start-up and heating of the glass sheet throughout its circulation, a time interval of 0–7.5 s. Table 2 shows the maximum temperatures reported by the respective probes during the computer simulation. In contrast to Table 1, the points are not fired in a row but in a series. Points 1, 3, 5, 11 and 13 are included in the first series, points 15, 7, 9, 17 and 19 in the

second series, points 2, 4, 12, 14 and 6 in the third series and finally points 8, 10, 16, 18 and 20 in the fifth series. With the exception of points 8 and 12, the maximum temperature values during all 4 series were within a maximum of 230 °C. At the same time, most of the probes reached their maximum temperature during the entire engraving process only during the fourth run. The only exceptions were probes 3, 7 and 11, which reached their maximum temperature during the third series. However, the difference between the third and fourth runs was marginal. For probe 3 it was 2.27 °C, but this could be due to the fact that the time limit between the third and fourth series was identical to the end of the firing point in the vicinity of the probe and therefore the cooling process was taking place. For probe 7 the difference was 19.58°C and for probe 11 the difference was 37.68°C. For the sake of clarity, the data from Table 2 has also been visualised in the graph in Figure 3.

Table 2 Maximum temperature values [°C] measured by the probes in the computer simulation of firing points in individual rows for variant 2

	1st series	2nd series	3rd series	4th series
Probe 1	663.72	748.52	774.88	825.32
Probe 2	725.43	769.36	799.12	900.30
Probe 3	676.75	835.26	863.63	861.36
Probe 4	721.93	786.86	802.20	872.53
Probe 5	724.58	765.58	816.36	851.05
Probe 6	721.04	796.09	858.87	920.76
Probe 7	677.18	853.88	905.58	886.00
Probe 8	134.24	808.58	839.13	883.57
Probe 9	698.21	782.99	790.41	828.06
Probe 10	696.74	820.28	816.40	876.58
Probe 11	645.99	717.18	876.39	838.71
Probe 12	79.37	769.06	812.92	888.02

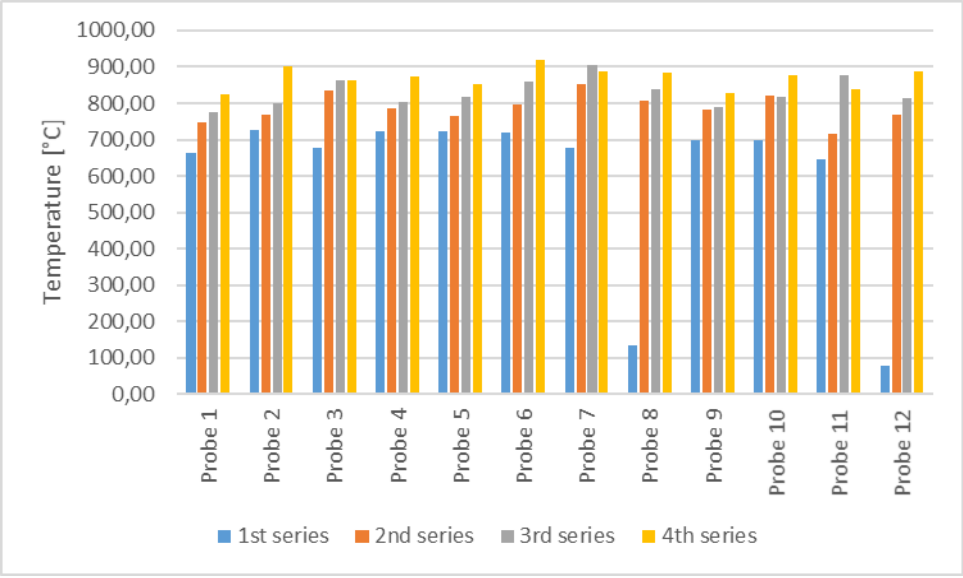

Figure 3 Visualisation of the values measured by the probes in the computer simulation of the firing of points in individual rows in variant 2

In the graphs in Figures 4–6 we can see a comparison of the two proposed variants of the laser engraving procedure on the temperature evolution during the firing of the individual points recorded by the selected probes 1, 6 and 12, which were chosen because they are the initial probe, the probe located practically in the center of the treated area and the final probe. For probe 1, the first firing point is completely identical, but already for the second point there is a noticeable difference in the value of the maximum temperature measured by the probe during engraving in the vicinity. From the graph in Figure 4, the difference in the delay of the next thermal loading between the two variants is also clearly observable. The same observation can also be made from the graphs in Figures 5 and 6, where the variants based on different firing point order are compared from the values obtained by probes 6 and 12. Again, we can observe that higher temperatures are achieved for variant 1 and, conversely, longer time delays between the next thermal stresses for variant 2. Table 3 compares the temperature differences of the maximum measured values. The smallest difference was measured with probe 2, namely 22.24 °C. On the other hand, the largest difference was recorded at probe 11, namely 115.61 °C. The mean temperature difference (69.3825 °C) and the median (70.18 °C) corresponded very well.

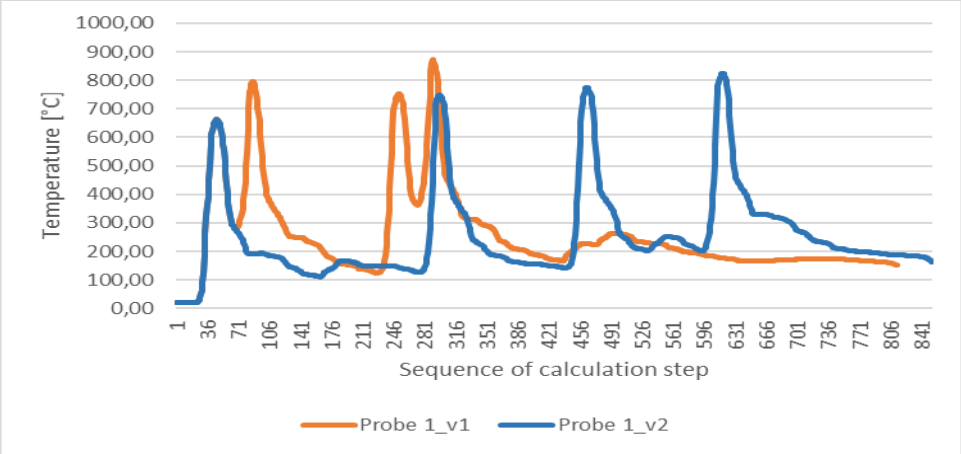

Figure 4 Comparison of the temperature evolution obtained from probe 1 in the computer simulation of the laser engraving process for Variant 1 and Variant 2.

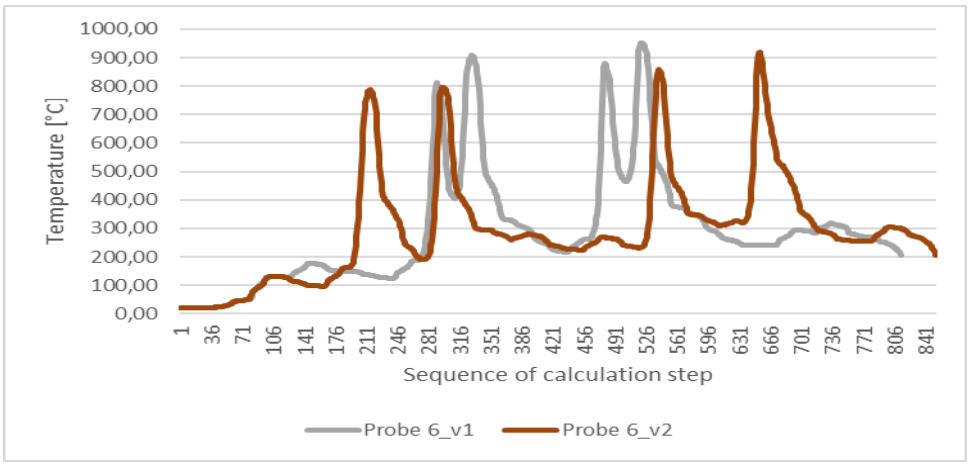

Figure 5 Comparison of the temperature evolution obtained from probe **6** in the computer simulation of the laser engraving process for Variant 1 and Variant 2.

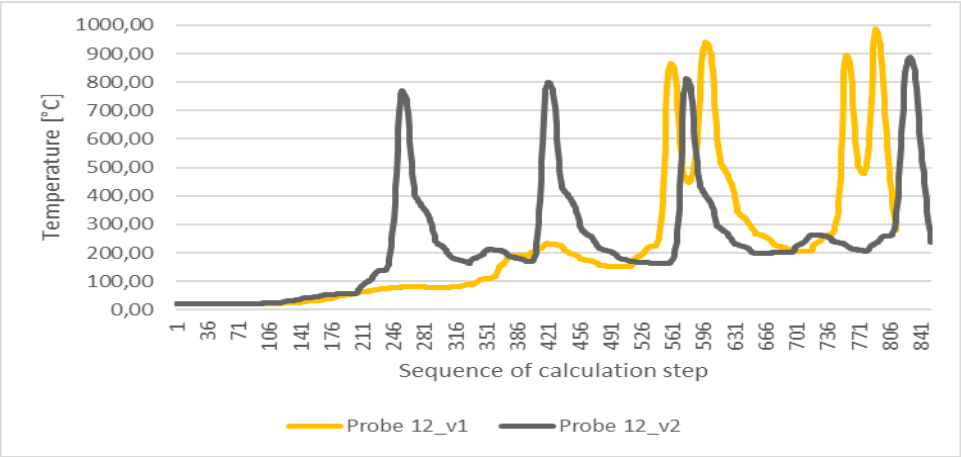

Figure 6 Comparison of the temperature evolution obtained from probe 1**2** in the computer simulation of the laser engraving process for Variant 1 and Variant 2.

Table 3 Comparison of the maximum temperatures obtained from the probes in the computer simulation of the laser engraving process for Variant 1 and Variant 2.

	1st variant	**2nd variant**	**Difference**
Probe 1	873.76	825.32	48.44
Probe 2	922.54	900.30	22.24
Probe 3	936.28	863.63	72.65
Probe 4	921.23	872.53	48.7
Probe 5	914.30	851.05	63.25
Probe 6	952.16	920.76	31.4
Probe 7	979.36	905.58	73.78
Probe 8	951.29	883.57	67.72
Probe 9	931.86	828.06	103.8
Probe 10	963.33	876.58	86.75
Probe 11	992.00	876.39	115.61
Probe 12	986.27	888.02	98.25

A number of observations can be made from the results of the computer simulation of the two different variants and their comparison on the above graph, which can be summarised as follows:

- In Variant 1, higher temperatures are reached during the laser engraving process on all the probes.
- In variant 2, there is a longer time delay before the subsequent re-thermal loading.

Based on the results, it appears that Variant 2, where the individual points are fired out of sequence, is more optimal for the laser engraving process described. In this particular case, the order of the dots was 1, 3, 5, 11, 13, 15, 7, 9, 17, 19, 2, 4, 12, 14, 6, 8, 10, 16 and 20.

CONCLUSION.

The computer simulation of thermal stress during surface treatment of glass material by laser engraving was carried out on a three-dimensional model. Two variants were studied to optimise the firing of individual dots. The first variant was the initial treatment variant, where the firing order of the dots was identical to their chronological order, i.e. dot 1 was fired first, dot 2 second and so on up to dot 20. However, with this type of treatment, destruction of the glass sheet due to excessive thermal stress was not uncommon. For the second variant, the order of the fired points was proposed to be independent of

their chronology, namely the order was 1, 3, 5, 11, 13, 15, 7, 9, 17, 19, 2, 4, 12, 14, 6, 8, 10, 16 and 20. From the results of the computer simulation of the two different variants and their comparison on the above-mentioned graphs, it can be concluded that variant 2 achieved lower temperatures during the surface treatment of the material, on average by 69.3825 °C, and at the same time the time delays between reheating treatments of the same sites were longer. Based on these results, it appears that Variant 2, in which the individual points are fired out of sequence, is more optimal for the laser engraving process described.

Due to the fact that the parameters that are important for the topology of the fired dots, in particular the laser power and the distance between the individual dots, which are necessary for the functionality of the surface treatment, were left out, only the influence of the order of the fired dots was investigated in the work. In order to gain a deeper understanding of the physical phenomenon of laser engraving of the glass surface under investigation, it would have been useful to carry out a study of the influence of laser power or point spacing.

REFERENCES

ABAR, S., THEODOROPOULOS G. K., LEMARINIER, P., O'HARE, G. M. P., 2017. *Agent Based Modelling and Simulation tools*: A review of the state-of-art software. Computer Science Review, 24:13–33, https://doi.org/10.1016/j.cosrev.2017.03.001.

BÉCHET, F., SIEDOW, N., LOCHEGNIES, D., 2015. *Two-dimensional finite element modeling of glass forming and tempering processes, including radiative effects*. Finite Elements in Analysis and Design, 94:16–23, https://doi.org/10.1016/j.finel.2014.09.008.

BULGAKOVA, N. M., ZHUKOV, V. P., COLLINS, A. R., ROSTOHAR, D., DERRIEN, T. J.-Y,, MOCEK, T., 2015. *How to optimize ultrashort pulse laser interaction with glass surfaces in cutting regimes?* Applied Surface Science, 336:364–374, https://doi.org/10.1016/j.apsusc.2014.12.142.

CRESSIN, M., BÉCHET, F., MOREAU, P., LOCHEGNIES, D., NACEUR, H., 2023. *Identification of heat transfer coefficient including radiative effects at the glass/mold interface*. International Journal of Heat and Mass Transfer, 209:1–10, https://doi.org/10.1016/j.ijheatmasstransfer.2023.124145.

CVECEK, K., MIYAMOTO, I., SCHMIDT, M., 2014. *Gas bubble formation in fused silica generated by ultra-short laser pulses.* Optics Express, 22(13):15877–15893, doi: 10.1364/OE.22.015877.

ESCOBAR, A., CAICEDO, B., CABRERA, M., 2021. Interaction between a cylinder and a partially saturated soil for compation analysis. Transportation Geotechnics, 30:1–10, https://doi.org/10.1016/j.trgeo.2021.100600.

FOO, D.C.Y., ELYAS, R., 2023. Introduction to process simulation. In: Foo, D.C.Y. (Ed.), *Chemical Engineering Process Simulation*, secondary published, Radarweg 29, PO Box 211, 1000 AE Amsterdam, Netherlands, pp. 3–28, ISBN 978-0-323-90168-0.

GRELLIER, A. J. C., ZAYER, N. K., PANNELL, C. N., 1998. *Heat transfer modelling in CO laser processing of optical fibres*. Optics Communications, 152:324–328.

GUIMARÃES JÚNNYOR, W. S., DISERENS, E., DE MARIA, I. C., ARAUJO-JUNIOR, C. F., FARHA-TE, C. V. V., DE SOUZA, Z. M., 2019. *Prediction of soil stresses and compaction due to agricultural machines in sugarcane cultivation systems with and without crop rotation*. Science of the Total Environment, 681:424–434, https://doi.org/10.1016/j.scitotenv.2019.05.009.

JIAO, J., WANG, X., 2008. *A numerical simulation of machining glass by dual CO_2-laser beams*. Optics & Laser Technology, 40:297–301, https://doi.org/10.1016/j.optlastec.2007.05.003.

JIMENEZ, K. J., ROLIM, M. M., GOMES, I. F., DE LIMA, R. P., BERRÍO, L. L. A., ORTIZ, P. F. S., 2021. *Numerical analysis applied to the study of soil stress and compaction due to mechanised sugarcane harvest.* Soil & Tillage Research, 206:1–10, https://doi.org/10.1016/j.still.2020.104847.

KAHLE, M., NODOP, D., 2022. *Glass welding with ultra-short laser pulses and long focal lengths – A process model.* In 12th CIRP Conference on Photonic Technologies [LANE 2022], Fürth, Germany, pp. 617–620, https://doi.org/10.1016/j.procir.2022.08.163.

KUMAR, G. S., BADULLA, S., NAGARAJU, J., VENKATESH, P. H. J., NARASIMHULU, G., RAO, V. S., 2023. *Design and analysis of 3-way catalytic converter using CFD.* Materials Today: Proceedings, https://doi.org/10.1016/j.matpr.2023.07.215.

LAI, S., EHRHARDT, M., LORENZ, P., ZAJADACZ, J., HAN, B., LOTNYK, A. ZIMMER, K., 2022. *Ultrashort pulse laser-induced submicron bubbles generation due to the near-surface material modification of soda-lime glass*. Optics & Laser Technology, 146:1–8, https://doi.org/10.1016/j.optlastec.2021.107573.

LEGARIA-SANTIAGO, V. K., SÁNCHEZ-FERNÁNDEZ, L. P., SÁNCHEZ-PÉREZ, L. A., GARZA-RODRÍGUEZ, A., 2022. *Computer models evaluating hand tremors in Parkinson's disease patients. Computers in Biology and Medicine*. 140:1–18, https://doi.org/10.1016/j.compbiomed.2021.105059.

MIDDLETON, S., DIMBATH, E., PANT, A., GOERGE, S. M., MADDIPATI, V., PEACH, M. S., YANG, K., JU, A. W., VAHDATI, A., 2022. *Towards a multiscale computer modeling workflow for simulation of pulmonary ventilation in advanced COVID-19.* Computers in Biology and Medicine, 145:1–11, https://doi.org/10.1016/j.compbiomed.2022.105513

MISHRA, S., SRIDHARA, N., MITRA, A., YOUGANDAR, B., DASH, S. K., AGARWAL, S., DEY, A., 2017. *CO_2 laser cutting of ultra thin (75 µm) glass based rigid optical solar reflector (OSR) for spacecraft application*. Optics and Lasers in Engineering, 90:128–138, https://doi.org/10.1016/j.optlaseng.2016.10.007.

NISAR, S., SHEIKH, M. A., SAFDAR, S., 2009. *Effect of thermal stresses on chip-free diode laser cutting of glass*. Optics & Laser Technology, 41(3):318–327, https://doi.org/10.1016/j.optlastec.2008.05.025.

NOVIA, N., HASANUDIN, H., HERMANSYAH, H., FUDHOLI, A., PAREEK, V. K., 2023. *Recent advances in CFD modeling of bioethanol production processes*. Renewable and Sustainable Energy Reviews, 183:1–15, https://doi.org/10.1016/j.rser.2023.113522.

OLIVEIRA, J. B., JIN, M., LIMA, R. S., KOBZA, J. E., MONTEVECHI, J. A. B., 2019. *The role of simulation and optimization methods in supply chain risk management: Performance and review standpoints*. Simulation Modelling Practice and Theory, 92:17–44, https://doi.org/10.1016/j.simpat.2018.11.007.

REDLARSKI, G., JAWORSKI, J., 2013. *A new approach to modeling of selected human respiratory system diseases, directed to computer simulations.* Computers in Biology and Medicine, 43:1606–1613, https://doi.org/10.1016/j.compbiomed.2013.07.003.

SASS, H., REUSKEN, A., 2023. *An accurate and robust Eulerian finite element met-hod for partial differential equations on evolving surfaces*. Computers and Mathematics with Applications, 146:253–270, https://doi.org/10.1016/j.camwa.2023.06.040.

TIAM, W., CHIU, K. S., 2004. *Temperature prediction for CO2 laser heating of mo-ving glass rods*. Optics & Laser Technology, 36:131–137, https://doi.org/10.1016/S0030-3992(03)00145-2.

TOMINAGA, Y., WANG, L. L., ZHAI, Z. J., STATHOPOULOS, T., 2023. *Accuracy of CFD simulations in urban aerodynamics and microclimate*: Progress and challenges. Buil-ding and Environment, 243: 110723, https://doi.org/10.1016/j.buildenv.2023.110723.

TONG, Y., CHEN, Y., SHAO, W., 2019. *Study on Energy Saving Application Strategy of New ResidentialHouses Envelope Structure in Sanjiangyuan Area Based on DestOrthogonal Simulation*. E3S Web of Conferences 136, 02036, https://doi.org/10.1051/e3sconf/201913602036.

WITCHER, J. J., HERNANDEZ-RUEDA, J., KROL, D. M., 2015. *Fs-Laser Processing of Glass*: Plasma Dynamics and Spectroscopy, International Journal of Applied Glass Science, 6(3):220–228, https://doi.org/10.1111/ijag.12132.

WU, J., REZIKYAN, A., ROSS, M. R., LEZZI, P. J., LUO, J., LIU, A., 2022. *Temperature and thermal stress analysis of ultrashort laser processed glass*. Journal of Non-Crystalline Solids: X, 16:1–6, https://doi.org/0.1016/j.nocx.2022.100124.

VERIFICATION OF THE FUNCTIONALITY OF THE GLASS SURFACE TREATMENT IN TERMS OF PROVIDING A VISIBLE BARRIER TO FREE-CHEWING BIRDS

TOMÁŠ ZOUBEK, ROMAN BUMBÁLEK, MARTIN FILIP, ONDŘEJ TUPÝ, PAVEL OLŠAN

Faculty of Agriculture and Technology, University of South Bohemia, Department of Technology and Cybernetics, Na Sádkách 1780, 37005 České Budějovice, Czech Republic

Abstract: The main objective of this work was to verify the mastery of the design, production technology and manufacture of small, medium and large transparent glass surfaces that reflect light rays in the UV part of the optical spectrum and, on the contrary, transmit rays in the visible part of the optical spectrum to the maximum extent. Such a material would appear to birds as an insurmountable obstacle to be avoided during flight, and the human eye would perceive such a material as transparent with no aesthetically disturbing elements. The functionality of the prototype-coated glass surface bales was verified in a test tunnel with 54 wild bird species at a site close to the test area.

Keywords: laser engraving; test tunnel; UV reflection; design

INTRODUCTION

Today, glass structures are increasingly used in the construction and related industries. However, with this comes the problem of increasing bird mortality. A flying bird does not recognise a transparent obstacle when it hits it, which usually results in fatal injuries. From the point of view of modern architecture and the façade materials market, glass surfaces must be transparent and properly integrated into the environment. And it is the use of light reflection in the UV part of the optical spectrum to deter birds from flying into transparent surfaces without significantly reducing the visibility through the transparent surfaces to the human eye that appears to be a suitable innovative solution to this problem. Nguyen et al. (2017) reported that to improve the reflection of the UV part of the light spectrum, alloying elements or compounds can be added in their appropriate concentrations during the laser printing process of glass surfaces. The gaseous compounds can be added directly to the plasma discharge treating the glass surface. Solid compounds can be used in the form of powders that are baked into the structure and burned onto the glass surface by the plasma discharge. Suitable precursors that positively affect the reflection of the UV part of the light spectrum include TiO_2 by Zhao et al. (2017) and Nagasawa et al. (2018). Zheng et al. (2018) used ZnO for the same purpose. However, $CaZrO_3$ (Subrami et al., 2018) or SiO_2 (Rafiaei et al., 2019) can also be used.

Collision with glass is one of the most common causes of death in wild birds, as birds are unable to perceive it as an obstacle (Klem, 1989; Ogden, 1996). According to Klem (1990) and Veltri and Klem (2005), collisions with glass surfaces are fatal for approximately 50% of birds. It is estimated that 365–988 million birds die annually from collisions with glass surfaces in the USA (Loss et al., 2014), about 25 million birds in Canada (Machtans et al., 2013) and hundreds of thousands of birds in Austria (Rössler and Doppler, 2014). In the Czech Republic, similar estimates are lacking, but the fact that this is also a problem in our area is illustrated by the death of almost 200 birds by hitting a noise barrier near the D47 motorway. This number was counted on one kilometre of this noise barrier wall within six months (Strnad and Bílá, 2015). The highest risk of bird mortality due to collisions with glass is found in large buildings located in regions with low urbanisation (Hager et al., 2017; Ocampo-Peñuela et al., 2016). However, even small glass buildings can affect bird mortality, as shown by Zyśk-Gorczyńska et al. (2020). In their paper, they report that they recorded 155 bird deaths as a result of collisions with glass bus stops in Poland over the course of one year. In total, they monitored 81 glazed bus stops and collisions occurred at 40 of them.

To prevent wild birds from colliding with the glass surfaces, measures have been taken to prevent birds from hitting the glass surfaces. These measures fall into three main groups:

1) Do not use large glazed areas and highly reflective materials.
2) Cover hazardous areas.
3) Place structures in front of and behind the glass surface.

For existing buildings and structures, the most common approach is to modify the glass surfaces so that they are perceived as obstacles by birds. However, most very effective solutions reduce or eliminate transparency or change the appearance of the building. For example, a study by Zyśk-Gorczyńska et al (2020) reported the effect of graffiti and dust on glazed bus stops on reducing the number of bird strikes. However, such a solution is unthinkable for most owners, designers and architects. A comparison of the functionality of surface treatments used to prevent wild birds from colliding with glass surfaces was carried out by Rössler and Doppler (2014). They tested a total of 39 types of surface treatments and categorised them according to their functionality into categories A to D, where category A includes those solutions that resulted in collisions up to 10% of the time during experimental validation, category B includes surface treatments with collision rates between 10 and 19.9%, category C resulted in collisions 20–45% of the time, and all technical solutions with a result of 45% and above are categorised in category D.

Categories A and B only include treatment technologies in the form of visible coatings, which are not acceptable to all building owners, designers and architects. Therefore, methods of treating glass surfaces that reflect the UV spectrum of light are being developed. These solutions are invisible to the human eye or do not cause a disturbing effect. However, the effectiveness in preventing bird collisions with such treated surfaces is not as high as with visible coatings. The disadvantage of stickers or films applied to glass surfaces, apart from their reduced or total lack of transparency, is their temporary nature and the need to replace them.

In terms of the technology used to reflect the UV part of the light spectrum, the result of this study is comparable to the ORNILUX Mikado and Birdpen® products. In the experimental validation, the Ornilux Mikado product was observed in the middle of the tested birds in 37.2% of the cases, which places it in category C. The Birdpen® product is placed in the last category D, as it was observed in the middle of the tested birds in 54.3% of the cases.

MATERIAL and METHODOLOGY

During the experimental verification of the surface treatment, 54 wild birds were captured. The treated glass was tested successively in a test tunnel measuring 7 x 1.2 x 2 m (length x width x height). An ornithological net was placed at a distance of approximately 120 cm in front of the tested panes to prevent direct collision between the bird and the pane. To prevent a collision, birds were caught in the ornithological net. Once caught in the ornithological net, each bird was released by a competent person. This measure ensured that no flying birds were killed during the experiment. The conduct of the experiment and the capture of the birds required for the experiment were supervised by a qualified person holding a bird-trapping licence. During the experimental verification of the functionality of the glass surface treatment using the test tunnel, the treated surfaces, as shown in Figure 1, were alternated with the untreated surfaces. The same Pilkington Optifloat^{TM} Clear 4mm material was used for both treated and untreated glass. The technical properties of this material are given in Table 1.

Table 1 Technical Information of used glass material Pilkington OptifloatTM Clear 4mm (Pilkington, 2024).

Light	Transmittance	0.89
	Reflectance	0.08
Solar Energy	Direct Transmittance	0.83
	Reflectance	0.07
	Absorptance	0.10
	Total Transmittance	0.85
Shading Coefficient	Short Wavelength	0.95
	Long Wavelength	0.03
	Total	0.98
U value	$W \cdot m^{-2} \cdot K^{-1}$	5.80

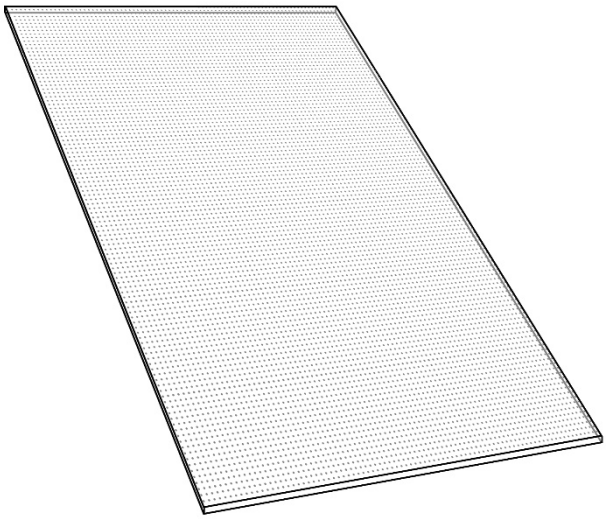

Figure 1 Visualisation of the print form of the surface treated glass (Float clear 4 mm, dot pitch 1.25 mm at 100% laser power).

The test tunnel, see Figure 2, was designed so that there was only one exit for flying birds, which was obstructed by the tested pane and a control untreated pane. A net was placed in front of the panel at a distance of 120 cm. In the experimental test, video recordings and subsequent image processing were used to assess whether the bird chose the treated or untreated glass panel when exiting the tunnel. Immediately after capturing a test individual in the ornithological net, the bird was always released back into the wild. To carry out this experiment, it was necessary to provide a site that had access to electricity and was also close enough to the capture site to avoid excessive psychological stress on the test individuals caused by a long transport to the test site. In the end, the area in front of the Technical Hall of the Faculty of Agriculture and Technology (FAT USB) was used and the capture site was a nearby city park, where the wild birds were transported within about 5 minutes of capture.

For experimental validation in the test tunnel, species commonly found in the vicinity of the FAT USB were captured and used, in particular the field sparrow, blue tit, common robin and black-headed warbler.

Figure 2 Escape routes from the test tunnel, left clear glass without laser treatment (Float type clear 4 mm), right surface treated glass (Float type clear 4 mm, dot pitch 1.25 mm at 100% laser power).

Table 2 Light and solar characteristics of selected treatments and untreated glass surfaces according to ČSN EN 410.

Characteristics	float 4 mm	4 mm float, 1.25 mm dot pitch at 60% laser power	4 mm float, 0.5 mm dot pitch at 60% laser power
Total light transmission	91.7 %	88.6 %	70.8 %
UV reflectance of the treated surface	8.3 %	8.3 %	8.1 %
UV reflectance of the untreated surface	8.0 %	8.1 %	8.1 %

RESULTS and DISCUSSION

The experiment compared the ability of birds to recognise surface-treated glass as an obstacle by having to choose between two paths when escaping from a test tunnel. The first path contained surface treated glass (Float type clear 4 mm, 1.25 mm dot pitch at 100% laser power) and the second path contained untreated glass (Float type clear 4 mm). During the test, solar radiation intensity was recorded using an Ocean Optics STS-UV micro-spectrometer. The readings at the start, during and at the end of the test are shown in Figure 3. It was overcast on both days of the test and the reading was low in the UV part of the light spectrum, which is the basis of the coating's functionality. Over the two days, 54 wild-caught birds were used successively in the experiment. After being captured in a nearby city park, the birds were transported to the test site within approximately 5 minutes. Each bird was placed in a cage at the start of the tunnel for 2 minutes to calm down and get used to the environment, then released from the cage by a remote mechanism and monitored by camera to see which escape route it chose. After testing, each individual was immediately released into the wild. The ability of captured individuals to return to the capture site is demonstrated by the fact that one individual was captured in the same location on both test days. Table 3 shows the escape route chosen by each individual tested.

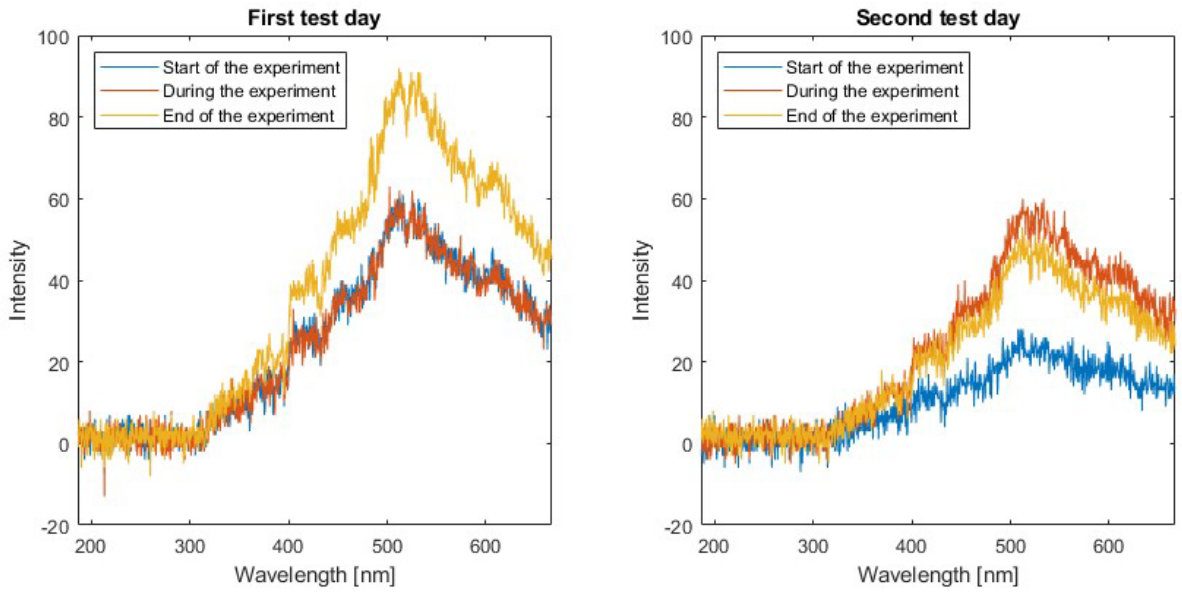

Figure 3 Light intensity measured on both test days.

The video recordings made during the experimental verification of the functionality of the surface treatment of the glass panes using the test tunnel were analysed using automatic image analysis software. The automatic image analysis software is able to detect a change in the video image, store this image and then convert it into a black and white image using edge detection, in which it is easy to see the path chosen by the test subject to escape. A comparison of the original image and the result processed by the automatic image processing software is shown in Figure 4. From the data obtained in this way, only 38.89% of the test subjects considered the coated glass to be an obstacle and tried to escape from the test tunnel by the other route, where the clear glass without laser coating was used.

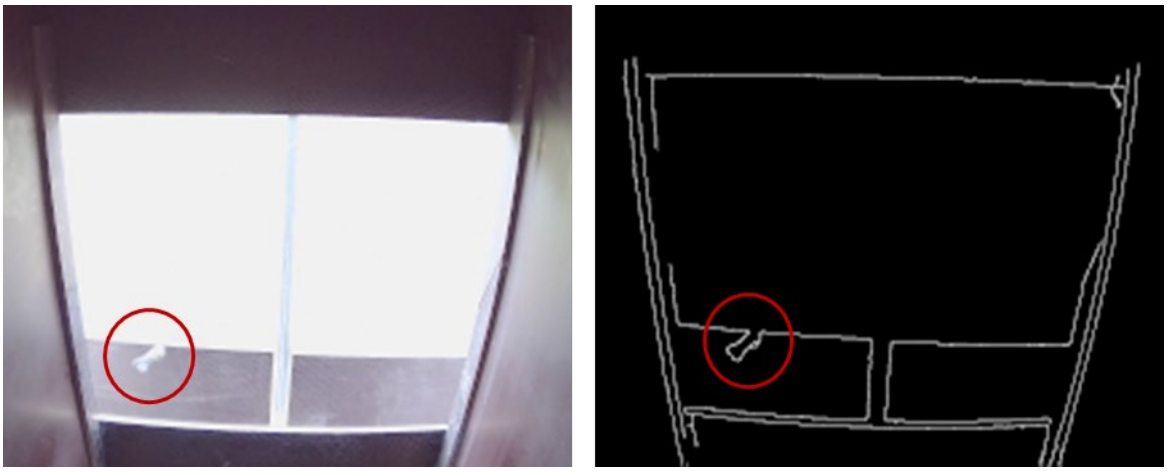

Figure 4 Comparison of the original image and the result processed by the automatic image evaluation software

Table 3 The escape route chosen by each individual bird tested

Identification of the bird tested	Leakage through treated glass	Leakage through untreated glass	Identification of the bird tested	Leakage through treated glass	Leakage through untreated glass
S824170	x		N738908	x	
N738906	x		S824180	x	
S824171	x		TY70257	x	
N738907	x		S999628		x
N905836	x		N908543		x
S824179		x	TP5949	x	
TY35134	x		TP5950		x
TP96203	x		TP5949		x
S999627	x		TP5951	x	
S824174		x	TP5952	x	
S824175	x		TP5953	x	
TZ88734		x	TP5954	x	
TU06795	x		TP5954		x
TV83408	x		TP5953	x	
S824169		x	TP5952	x	
N883186		x	TP5951		x
N738905		x	TP5950		x
N738903	x		N748508	x	
S824168		x	N748509	x	
N908557	x		N748510	x	
N738902	x		N748511		x
N941621		x	S824218		x
N738909	x		S824219		x
S812177	x		SA60449	x	
S824178		x	N748512		x
S824179	x		TP96332	x	
	Leakage through treated glass		**Leakage through untreated glass**		
Summary	**32 (61,11 %)**		**20 (38,89 %)**		

CONCLUSION

In order to verify the functionality of the surface treatment of the glass surfaces with regard to their detection as an obstacle by wild birds, an experimental verification was carried out in a test tunnel. Out of a total of 54 wild birds in the vicinity of the test site, only 38.89% were able to recognise the coated glass as an obstacle. One of the reasons for this low efficiency was the unfavourable weather conditions, in particular the low intensity of sunlight, which is essential for sufficient reflection of the UV part of the light spectrum. At the same time, the experiment in the test tunnel to verify the surface treatment proved to be inappropriately designed. In this experiment, the glasses to be compared were placed close

to the exit of the test tunnel, which shaded most of the glasses tested. The performance of this experimental test failed to demonstrate the functionality of such coated glass in terms of preventing wild bird strikes. Although the laboratory tests over the past three years have been judged positive, the test tunnel verification did not demonstrate sufficient effectiveness of the treated glass.

REFERENCES

HAGER, S.B. et al. 2017. Continent-wide analysis of how urbanization affects bird-window collision mortality in North America. Biological Conservation 212:209–215. https://doi.org/10.1016/j.biocon.2017.06.014.

KLEM, JR., D. 1989. Bird-window collision. Wilson Bulletin 101:606–620.

KLEM, JR., D. 1990. Bird injures, cause of death, and recuperation from collisions with window. Journal of Field Ornithology 61:115–119.

LOSS, S.R., WILL, T., LOSS, S.S., MARRA, P.P. 2014. Bird-building collisions in the United States: estimates of annual mortality and species vulnerability. Ornithology Applications 116(1):8–23. https://doi.org/10.1650/CONDOR-13-090.1

MACHTANS, C. S., WEDELES, C. H. R., BAYNE, E. M. 2013. A first estimate for Canada of the number of birds killed by colliding with building windows. Avian Conservation & Ecology, 8(2):6. https://doi.org/10.5751/ACE-00568-080206.

NAGASAWA, H., XU, J., KANEZASHI, M., TSURU, T. 2018. Atmospheric-pressure plasma-enhanced chemical vapor deposition of UV-shielding TiO2 coatings on transparent plastics. Materials Letters 228:479–481. https://doi.org/10.1016/j.matlet.2018.06.053.

NGUYEN, T.H., DAO, P.H., DUONG, K.L., DUONG, Q.H., VU, Q.T., NGUYEN, A.H., MAC, V.P., LE, T.L. 2017. Effect of R-TiO2and ZnO nanoparticles on the UV-shielding efficiency of water-borne acrylic coating. Progress in Organic Coatings 110:114–121. https://doi.org/10.1016/j.porgcoat.2017.02.017.

OCAMPO-PEÑUELA, N., WINTON, R.S., WU, CH.J., ZAMBELLO, E., WITTIG, T.W., CAGLE, N.L. 2016. Patterns of bird-window collisions inform mitigation on a university campus. PeerJ 4:e1652, https://doi.org/10.7717/peerj.1652.

OGDEN, L. J. E. (1996). Collision course: the hazards of lighted structures and windows to migrating birds. World Wildlife Fund Canada, Toronto, Canada.

PILKINGTON. 2024. Pilkington Optifloat™.

RAFIAEI, S.M., ASHRAFI, F., SAYYADI-SHAHRAKI, A., KARIMZADEH, E. 2019. Enhanced luminescence properties of phosphors coated by silica nanolayers: Study of reflection and emission. Ceramics International 45:1670–1675. https://doi.org/10.1016/j.ceramint.2018.10.044.

RÖSSLER, M., DOPPLER, W. 2014. Vogelanprall an Glasflächen: Geprüfte Muster. Wiener Umveltanwaltschaft.

STRNAD, M., BÍLÁ, H. 2015. Metodika na ochranu krajiny před fragmentací z hlediska ptáků. Ministerstvo životního prostředí.

SUBRAMI, N.K., SHIVANNA, S., NAGARAJ, S.K., SURESHA, B., JAGAJEEVAN, R.B.M., SIDDARAMAIAH, H. 2018. Optoelectronic Behaviours of UV shielding Calcium ZirconateReinforced Polycarbonate Nanocomposite Films: An Optical View. Materials Today: Proceedings 5:16626–16632.

VELTRI, C.J., KLEM, JR.D. 2005. Comparasion of fatal bird injures from collisions with towers and windows. Journal of Field Ornithology 76:127–133. https://doi.org/10.1648/0273-8570-76.2.127.

ZHAO, J., YANG, Y., LI, Y., ZHAO, L., WANG, H., SONG, G., TANG, G. 2017. Microencapsulated phase change materials with TiO2-doped PMMA shell for thermal energy storage and UV-shielding. Solar Energy Materials and Solar Cells 168:62–68. https://doi.org/10.1016/j.solmat.2017.04.014.

ZHENG, Q., HUANG, J., LI, H., CHEN, L. 2018. Preparation of highly visible transparent ZnO/cellophane UV-shielding film by RF magnetron sputtering. Ceramics International 45(3):3729–3734. https://doi.org/10.1016/j.ceramint.2018.11.038.

ZYŚK-GORCZYŃSKA, E., SKÓRA, P., ŻMIHORSKI, M. 2020. Graffiti saves birds: A year-round pattern of bird collisions with glass bus shelters. Landscape and Urban Planning 193:1–7. https://doi.org/10.1016/j.landurbplan.2019.103680.

USE OF DRONES WITH MULTISPECTRAL CAMERAS IN AGRICULTURE

ONDŘEJ TUPÝ

Faculty of Agriculture and Technology, University of South Bohemia, Department of Technology and Cybernetics, Na Sádkách 1780, 37005 České Budějovice, Czech Republic

Abstract: Remote sensing of agricultural areas is a modern technology that offers several innovative solutions for more efficient and sustainable agriculture. The use of drones equipped with multispectral cameras offers a wide range of applications for this specific activity, bringing significant benefits both in terms of work efficiency and environmental protection. Finally, these technologies are also gaining ground in data collection in forestry or in archaeological surveys of selected areas.

Keywords: remote sensing; data collection; optimisation; nature conservation

INTRODUCTION

Both livestock and plant production face increasing challenges, particularly how to feed a growing population on shrinking land with a shortage of labour while being as environmentally friendly as possible. As a result, there is a strong emphasis in the agricultural sector on the use of the latest technologies and agrotechnical practices. Controlled driving, variable rate fertilisation and spraying systems are already commonplace in current technology. At the same time, autonomous robotic platforms are being developed that will be able to perform selected tasks independently or even manage the entire cultivation process of selected crops. For all these systems, it is important to have as much information and data as possible about a given plot of land. Remote sensing of agricultural land can also be used for this purpose, including the use of drones equipped with cameras capable of capturing images in different spectrums of light. In addition to the classic RGB spectrum, which corresponds to the band visible to the human eye, NIR, red-edge, SWIR or thermal infrared are also used. Thermal imaging cameras can visualise the temperature of surfaces in the image. They are useful for detecting thermal anomalies and are also used, for example, to detect game on land to be harvested or mown. With this technology, it is possible to locate the game, see Figure 1, and thus avoid its death during the work process (Cukor et al., 2019). The NIR spectrum can be used to detect vegetation and its health, as healthy vegetation is highly reflective in this band, as shown in Figure 2 (Louw and Chen, 2024). The red-edge spectrum can be used to monitor changes in the chlorophyll content of plants, which can indicate plant stress (Smith et al., 2004). The SWIR band can be used to analyse the moisture content of both soil and vegetation (Krzyszczak et al., 2023).

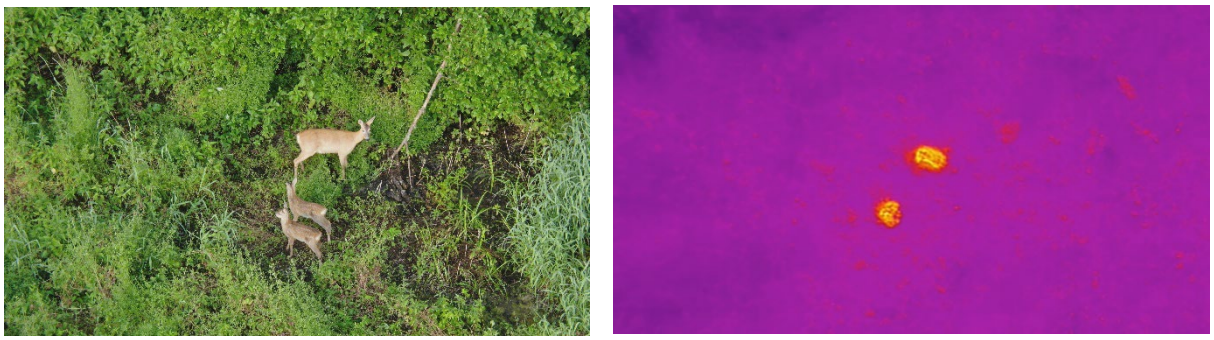

Figure 1 Detect and locate the game using thermal imaging before starting work on a particular piece of land.

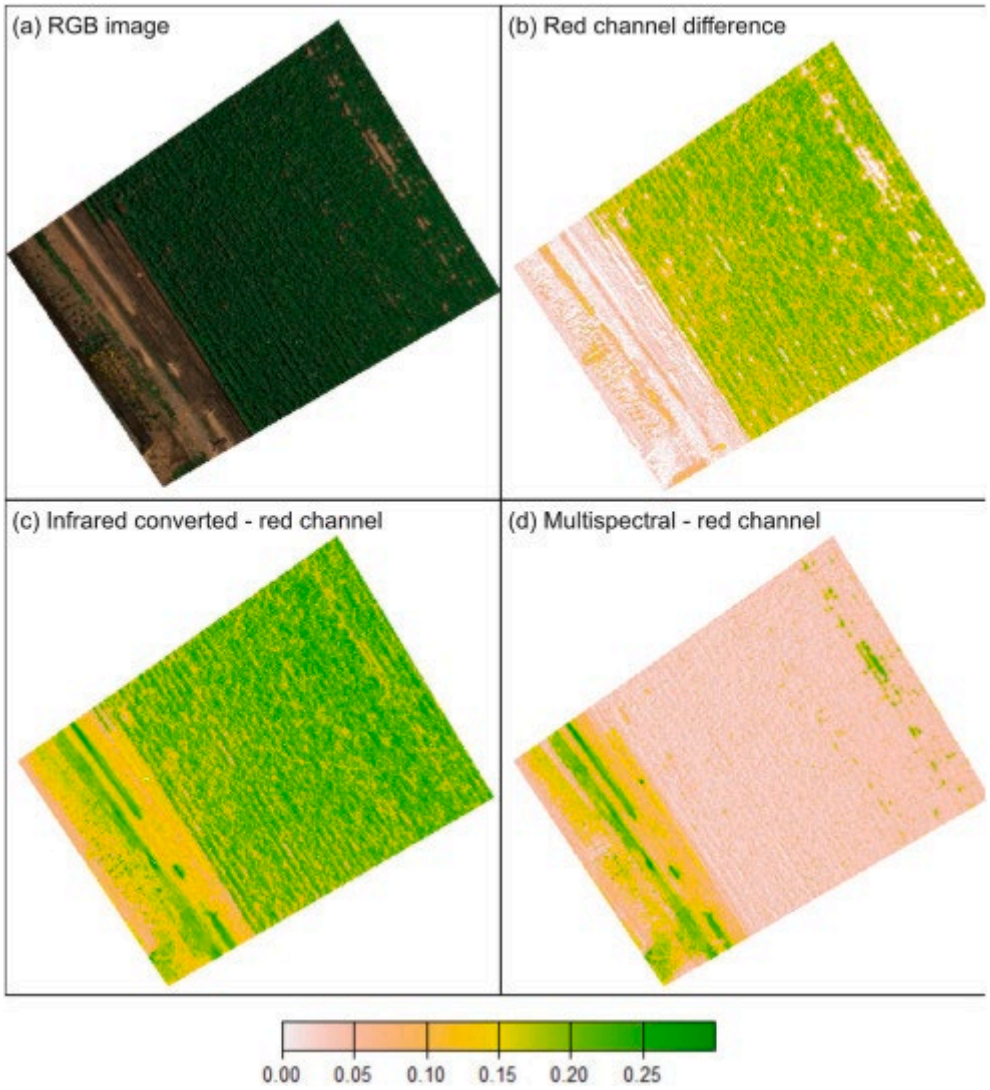

Figure 2 The difference in red reflectance captured by the infrared converted and multispectral camera for a scene over the potato field. Sub-figure (a) shows a true color (RGB) image, (c) and (d), the red-channel's reflectance from the infrared converted and multispectral cameras respectively, and sub-figure (b) the difference between the two sensor's red-channels. (i.e., infrared converted minus multispectral). (Louw and Chen, 2024)

For comprehensive data collection, multispectral cameras can be used to enable efficient monitoring and crop management. This technology provides farmers with accurate and detailed information that can significantly contribute to the optimisation of agricultural processes. Multispectral cameras can detect stress in plants before it is visible to the naked eye (Mandal, 2024). This capability is crucial for the early detection of problems such as water and nutrient deficiencies, pest infestations or diseases (Devi, 2024). By detecting changes in light reflectance in different spectral bands, cameras can identify stress factors, allowing farmers to intervene quickly and minimise potential damage. For example, reduced Normalised Difference Vegetation Index (NDVI) values can indicate plant growth problems, leading to immediate remedial action (Barjaktarovic, 2024). Multispectral imagery can be used to create detailed vegetation maps that can identify different crop types and growth conditions (Deng, 2018). These images can be used to analyse the distribution of crops in a field, track their growth stages and identify potential anomalies. This is useful, for example, for crop planning or evaluating the effectiveness of agronomic practices (Xu, 2021). A vegetation map created from multispectral data can also reveal areas with different soil quality or access to nutrients and water, allowing for targeted and efficient crop management. Analysis of multispectral data is essential for better irrigation scheduling and fertiliser application, which can significantly increase yields and reduce costs. Multispectral imagery can be used to identify which parts of the field need more water or nutrients. This allows you to optimise irrigation systems and fertiliser application, eliminating wasted resources and ensuring that all parts of the field

receive the amount of water and nutrients they need. This targeted water and fertiliser management not only increases efficiency, but also reduces negative environmental impacts, such as contamination of water sources from excess fertiliser (Raewa, 2019).

In crop production, many existing and new technologies are based on the collection, processing and use of data, usually geo-referenced. This includes data on soil conditions, crop stands, crop yields and their variability. The data can be obtained by traditional sampling, but nowadays technologies using remote sensing methods, i.e. using satellite imagery or imagery from a drone or aircraft, are increasingly used (Kakooei, 2017).

APPLICATION OF MULTISPECTRAL CAMERAS IN REMOTE SENSING OF SELECTED LAND AREAS

Large farms often use multispectral imaging to monitor large areas, allowing them to manage their resources efficiently and maximise yields. In the US and Australia, for example, these technologies are widely used in wheat, corn and soybean production. Multispectral cameras are a key tool in precision agriculture, where each part of the field is managed individually based on actual data. This includes the targeted application of pesticides, herbicides and fertilisers, leading to greater efficiency and sustainability. Even small farms can benefit from multispectral imaging as the cost of the technology falls. These farms can monitor the health of their crops and optimise their management with limited resources (Honrado, 2017).

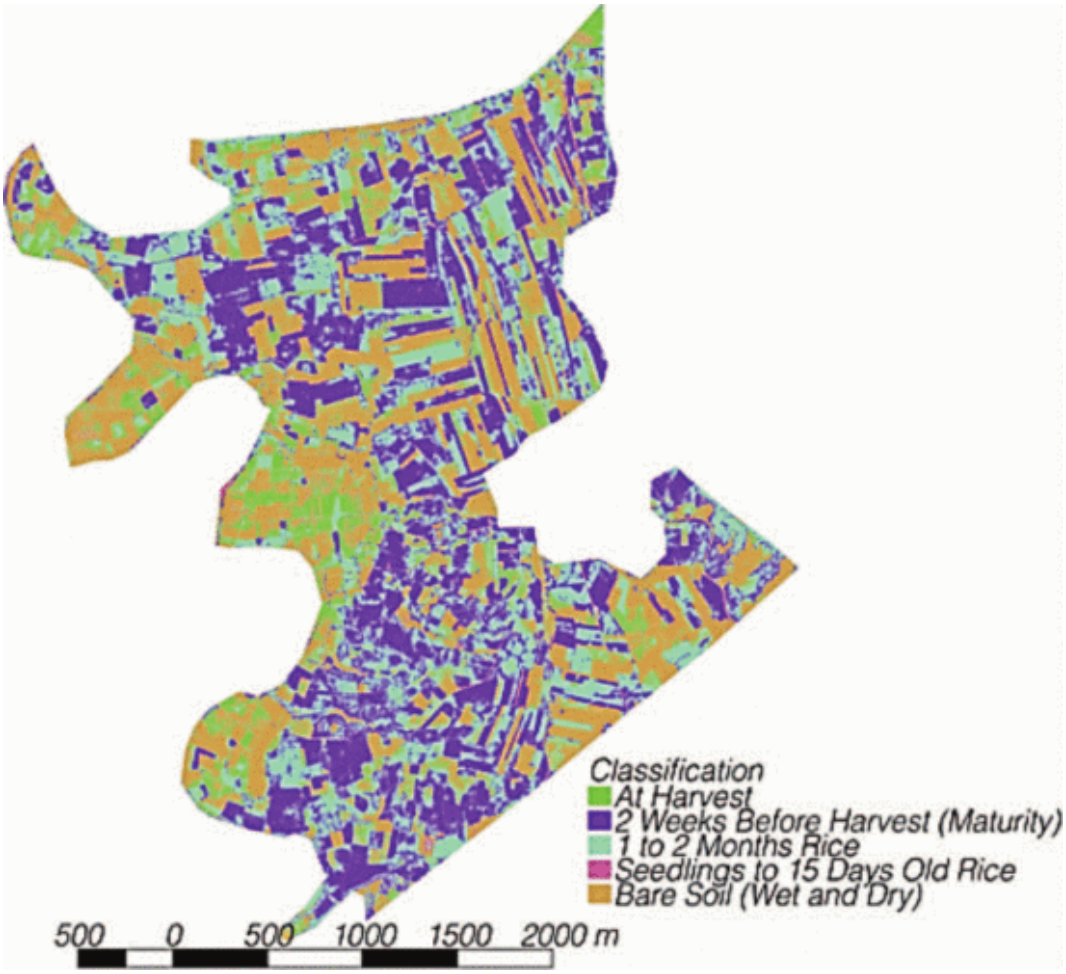

Figure 3 Site A required exclusion of the areas of the town where residences and commercial buildings were located due to the high intensity of NIR reflectance from the roofs. It is divided into 5 categories indicative of the stage in its growth cycle. (Honrado et al., 2017)

Multispectral drone imaging in forestry allows detailed monitoring of forest health. With the ability to scan across multiple spectral bands, cameras can detect changes in vegetation that are not visible to the

naked eye. This includes detecting tree stress caused by lack of water, nutrients or pollution. Multispectral imagery also makes it possible to map growth patterns and monitor forest biodiversity, which is key to maintaining ecosystem health (Marques, 2024). Multispectral cameras can quickly and accurately identify areas affected by pests or diseases. For example, infested trees often have specific spectral characteristics that can be detected using NIR or red-edge bands. As a result, action can be taken quickly and appropriate measures applied to minimise the spread of pests and diseases and protect larger forest stands from devastation. Multispectral cameras on drones are also very useful for environmental monitoring of water bodies. These cameras can analyse water quality, detect the presence of pollutants and monitor algae growth. Imaging in specific bands, such as NIR and SWIR, can detect changes in water chemistry and identify areas with high concentrations of pollutants or algal blooms, which is important for protecting aquatic ecosystems. Multispectral imaging is also key to mapping and monitoring soil erosion. Soil erosion can have devastating effects on agriculture, forestry and infrastructure. With the ability of multispectral cameras to detect changes in surface vegetation and soil structure, experts can monitor erosion-prone areas and plan appropriate erosion control measures. This could include the introduction of vegetation strips, landscaping or changes in land management (Buchelt, 2024).

In the field of archaeology, remote sensing of land using multispectral cameras enables efficient and non-invasive survey and documentation of archaeological sites. This technology provides valuable information that is crucial for the identification, analysis and protection of historical sites and artefacts. Multispectral imagery can reveal underground structures and artefacts that are not visible on the surface. Different materials and soil properties reflect light differently in different spectral bands. Multispectral cameras capture these bands, allowing the identification of anomalies in the ground that may indicate the presence of archaeological features such as old foundations, burials, roads or irrigation systems. This approach is non-invasive and environmentally friendly, minimising damage to sites during surveys. Multispectral cameras allow detailed mapping and documentation of historical and archaeological sites. High-resolution images and the ability to record data in multiple spectral bands provide a wealth of information about the condition and characteristics of sites (Ciccone, 2024). This is crucial for the analysis and interpretation of archaeological finds. Using these images, archaeologists can create accurate maps and models of sites, making it easier to plan and carry out excavations. Multispectral imaging can also be used to track changes in archaeological sites over time. This is important for the protection and conservation of these sites. Regular imaging can help identify hazards such as erosion, vegetation cover, illegal excavation or other activities that could damage the site (Singh, 2024). In this way, archaeologists and conservationists can take timely action to preserve cultural heritage. The technological aspects of multispectral cameras on drones represent an advanced technology that allows sensing in multiple spectral bands simultaneously. This capability provides detailed information about the characteristics and condition of the objects and environment being imaged, which is crucial for applications in agriculture, forestry, archaeology and environmental monitoring (Carvalho, 2024; Collaro, 2024).

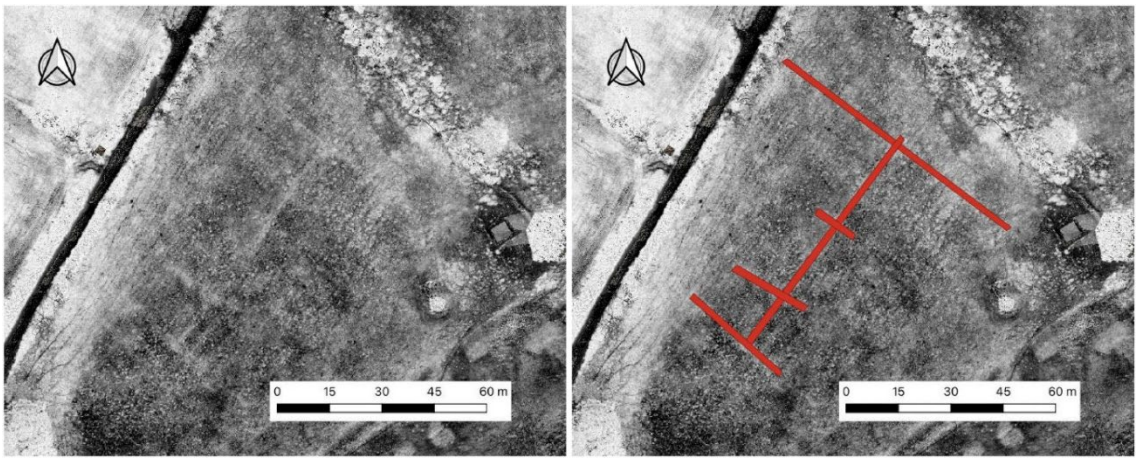

Figure 4 NDVI index and highlighting of the linear anomalies identified in the field west of the Tower (Stracciacappe, May 2021) (Ciccone, 2024).

DISCUSSION

The ability to sense in different spectral bands provides rich and detailed information about the condition and properties of the objects being monitored. With this technology, we can gain important insights that would not be possible with other methods. One of the key advantages of multispectral imaging is that it is non-invasive - it does not damage the objects or the environment under investigation, which is important for long-term monitoring and analysis without adverse effects. Multispectral imaging is an extremely versatile technology that has applications in a wide range of fields. In agriculture, it enables more accurate monitoring of crop growth and health, which can lead to better yields and more efficient use of resources. In environmental protection, it provides valuable data for monitoring changes in ecosystems, monitoring pollution and planning conservation measures. Technological advances in sensors are resulting in higher resolution and sensitivity, leading to significant improvements in the quality and accuracy of the images obtained. Higher resolution allows more detailed analysis of smaller objects and finer structures, while higher sensitivity allows better detection of even subtle changes and signals. These innovations are critical for applications that require accurate and reliable data. The integration of multispectral cameras with other sensor types, such as LiDAR (Light Detection and Ranging) and hyperspectral cameras, opens new possibilities for collecting more complex data. By combining these technologies, much richer and multi-dimensional information can be obtained about the objects and environments being monitored. For example, LiDAR provides detailed 3D terrain and structure models, while hyperspectral cameras provide information on the chemical composition of materials. Advanced algorithms and machine learning are playing an increasing role in the processing and analysis of multispectral data. These technologies enable more efficient and automated image evaluation, increasing the speed and accuracy of analysis. Machine learning can identify patterns and anomalies that would be difficult for a human analyst to detect, improving the usability and applicability of this data in the field. Overall, multispectral sensing is a powerful tool with a wide range of applications. Advances in sensor technology and integration with other technologies, as well as the use of advanced algorithms and machine learning, promise even greater data quality, accuracy and utility in the future.

REFERENCES

BARJAKTAROVIC, M., SANTONI, M. BRUZZONE, L. 2024. *Design and Verification of a Low-Cost Multispectral Camera for Precision Agriculture Application*. IEEE Journal of Selected Topics in Applied Earth Observations and Remote Sensing 17:6945–6957. https://doi.org/10.1109/JSTARS.2024.3377104.

BOKOLONGA, E., HAUHANA, M., ROLLINGS, N., AITCHISON, D., ASSAF, M.H., DAS, S.R., BISWAS, S.N., GROZA, V., PETRIU, E.M. 2016. *A compact multispectral image capture unit for deployment on drones*. In: 2016 IEEE International Instrumentation and Measurement Technology Conference Proceedings. IEEE. https://doi.org/10.1109/I2MTC.2016.7520445.

BUCHELT, A. ADROWITZER, A., KIESEBERG, P., GOLLOB, CH., NOTHDURFT, A., ERESHEIM, S., TSCHIATSCHEK, S., STAMPFER, K., HOLZINGER, A. 2024. *Exploring artificial intelligence for applications of drones in forest ecology and management*. Forest Ecology and Management 551: 121530. https://doi.org/10.1016/j.foreco.2023.121530.

CARVALHO, D. 2024. *A critical theory of the drone in archaeology: on space, epistemology, and automation*. Drone Systems and Applications 12:1–7. https://doi.org/10.1139/dsa-2023-0142.

CICCONE, G. 2024. *Investigating archaeological remains at Stracciacappe, Rome: comparing traditional sources with UAV-based multispectral, thermal and microtopographic analysis*. Drone Systems and Applications 12. https://doi.org/10.1139/dsa-2023-0114.

COLLARO, C., HERKOMMER, M. 2025. Research, application, and innovation of LiDAR technology in spatial archeology. In: *Encyclopedia of Information Science and Technology, Sixth Edition*. IGI Global:1–33. https://doi.org/10.4018/978-1-6684-7366-5.ch054.

CUKOR, J., BARTOŠKA, J., ROHLA, J., SOVA, J., MACH8LEK, A. 2019. Use of aerial thermography to reduce mortality of roe deer fawns before harvest. PEERJ 7: e6923. https://doi.org/10.7717/peerj.6923.

DENG, L. MAO, Z., LI, X., HU, Z., DUAN, F., YAN, Y. 2018. *UAV-based multispectral remote sensing for precision agriculture: A comparison between different cameras*. ISPRS journal of photogrammetry and remote sensing 146:124–136. https://doi.org/10.1016/j.isprsjprs.2018.09.008.

HONRADO, J.L.E., SOLPICO, D.B., FAVILA, C.M., TONGSON, E., TANGONAN, G.L. LIBATIQUE, N.J.C. 2017. *UAV imaging with low-cost multispectral imaging system for precision agriculture applications*. In: 2017 IEEE Global Humanitarian Technology Conference (GHTC). https://doi.org/10.1109/GHTC.2017.8239328.

KAKOOEI, M., BALEGHI, Y. 2017. *Fusion of satellite, aircraft, and UAV data for automatic disaster damage assessment*. International journal of remote sensing 38(8–10):2511-2534. https://doi.org/10.1080/01431161.2017.1294780.

KRZYSZCZAK, J. BARANOWSKI, P., PASTUSZKA, J., WESOLOWSKA, M., CYMERMAN, J., SLAWINSKI, C., SIEDLISKA, A. 2023. *Assessment of soil water retention characteristics based on VNIR/SWIR hyperspectral imaging of soil surface*. Soil and Tillage Research 233:105789. https://doi.org/10.1016/j.still.2023.105789.

LOUW, A.S. CHEN, X. 2024. *Assessing the accuracy of an infrared-converted drone camera with Orange-Cyan-NIR filter for vegetation and environmental monitoring*. Remote Sensing Applications: Society and Environment 35:101229. https://doi.org/10.1016/j.rsase.2024.101229.

MARQUES, T., CARREIRA, S., MIRAGAIA, R., RAMOS, J., PEREIRA, A. 2024. *Applying deep learning to real-time UAV-based forest monitoring: Leveraging multi-sensor imagery for improved results*. Expert Systems with Applications 245:123107. https://doi.org/10.1016/j.eswa.2023.123107.

RAEVA, P.L., ŠEDINA, J., DLESK, A. 2019. *Monitoring of crop fields using multispectral and thermal imagery from UAV*. European Journal of Remote Sensing 52:192–201. https://doi.org/10.1080/22797254.2018.1527661.

SINGH, R.K., SINGH, S., KUMAR, M., SINGH, Y., KUMAR, P. 2024. *Drone Technology in Perspective of Data Capturing*. Technological Approaches for Climate Smart Agriculture. https://doi.org/10.1007/978-3-031-52708-1_18.

SMITH, K.L., STEVEN, M.D., COLLS, J.J. 2004. Use of hyperspectral derivative ratios in the red-edge region to identify plant stress responses to gas leaks. Remote Sensing of Environment 92(2):207–217. https://doi.org/10.1016/j.rse.2004.06.002.

XU, R., LI, CH., BERNARDES, S. 2021. *Development and testing of a UAV-based multi-sensor system for plant phenotyping and precision agriculture*. Remote Sensing 13(17):3517. https://doi.org/10.3390/rs13173517.

PREDICTION OF TRACTOR REPAIR AND MAINTENANCE COSTS

ANTONÍN DOLAN, MARTIN FILIP

Faculty of Agriculture and Technology, University of South Bohemia, Department of Technology and Cybernetics, Na Sádkách 1780, 37005 České Budějovice, Czech Republic

Abstract: For all businesses, the main indicator of success is their economic balance sheet. Agricultural enterprises are no exception in this respect. The desire to reduce costs and increase income is therefore quite logical and this topic is therefore also very topical and interesting for many research teams. This has led to the development of various scientific studies on the need to reduce costs in the acquisition, operation and maintenance of agricultural machinery.

Keywords: agricultural machinery, tractor, prediction of repair and maintenance costs

INTRODUCTION

The first step in the acquisition of agricultural equipment, which is often an investment in the order of units to tens of millions of crowns, is to determine the specific use of the machine and select its required parameters. Once it is clear what the company's intentions for the machine are and which parameters it requires, scientific studies comparing selected machines according to specific parameters can help with the selection of a particular machine. Examples of such studies are Wollner et al. (2015) comparing CASE 8120 and NEW HOLLAND CX 8080 combine harvesters, and Grisso et al. (2012) using data measured at the Nebraska Tractor Test Laboratory (NTTL) in their work on comparing selected parameters in tractors. Todorovic et al. (2012) looked at the acquisition of agricultural equipment from a different perspective. In their work, they investigated the economically justifiable investment in purchasing a combine harvester on a family farm.

Once agricultural equipment is purchased, the cost of maintenance and repairs begins to add to the purchase price. A number of researchers are therefore looking at the potential savings in the operation of agricultural equipment. Kosiba et al. (2012) studied the characteristics of the hydraulic circuit in a John Deere 8100 tractor using different oils. Other works that allow savings are the model for optimal organization of crossings in agriculture by Mileusnić et al. (2012) and the visual program for the optimal speed and gear ratio for the most economical driving in terms of fuel consumption for tractors with 32 kW engine developed by Kumar and Pandey (2015).

In economic planning on farms, the problem is mainly the randomness of the costs of repairing agricultural machinery and for this reason it is interesting to map their accidents. Gligorević et al. (2012) focused on the Belgrade area, where they mapped 185 cases of farm equipment accidents over a period of five years. However, repair costs are not only due to accidents, but also to the gradual ageing of the equipment caused by its use. Sailer et al. (2008) looked specifically at the effect of farm machinery use on its market price, repair costs and annual use.

As the maintenance and repair costs of farm machinery increase, so do efforts to develop a model that predicts them based on their use or the area farmed. Either the models use regression analysis tools on data already collected, such as in the works of Dahab et al. (2016), Khodabakhshian et al. (2011), Lipse et al. (2012), Lorencowicz et al. (2015) and Niari et al. (2012), or a model using neural networks for prediction has already emerged, as presented by Rohani et al. (2011). This paper also uses a regression-based model to predict maintenance and repair costs and compares five different regression models according to their level of reliability based on cumulative maintenance and repair costs since commissioning.

MATERIAL and METHODOLOGY

In the following part of this thesis, data collected from eight agricultural entities on the maintenance and repair costs of John Deere tractors are evaluated. More specifically, six Series 7 machines of type 7810 and four Series 8 machines of type 8120. All machines had an identical year of manufacture. Series 7 and 8 are similar in terms of parameters, so we have taken the liberty of evaluating their maintenance and repair costs together in this paper. As can be seen from Table 1, where the owners of the specific machines are also listed, the maximum difference in their purchase prices was 850 thousand CZK. CZK. The difference was not only in the purchase prices of the individual tractors, but also in the engine power of the 7810 and 8120 machines. The engine power of the 7810 machines is 130.5 kW and that of the 8120 machines is 149.1 kW.

Table 1 Cost of tractor purchases

	Type of tractor	Owner of the tractor	Purchase price without VAT [CZK]	Engine power [kW]
Tractor 1	7810	CIZ-AGRO	3 000 025	130.5
Tractor 2	7810	ZD Černovice	2 500 000	130.5
Tractor 3	7810	Rozvoj Kosova Hora	2 350 000	130.5
Tractor 4	7810	Agrodružstvo Načehradec	2 600 000	130.5
Tractor 5	7810	Agrodružstvo Vyšetice	2 630 830	130.5
Tractor 6	7810	Agrodružstvo Záhoří	2 640 930	130.5
Tractor 7	8120	Žilovská zemědělská a.s.	3 100 000	149.1
Tractor 8	8120	Žilovská zemědělská a.s.	2 700 000	149.1
Tractor 9	8120	Žilovská zemědělská a.s.	3 100 000	149.1
Tractor 10	8120	Karlík Vladislav ml.	3 200 000	149.1

Data on the cost of repairing individual tractors was collected by the repair shops used by the farmers to repair and maintain their machines over a four-year period beginning when the machines were put into operation, with annual usage of individual machines ranging from 1 500 to 2 000 MTh · yr^{-1}. A summary of the maintenance and repair costs of specific machines for each year is recorded in Figure 1.

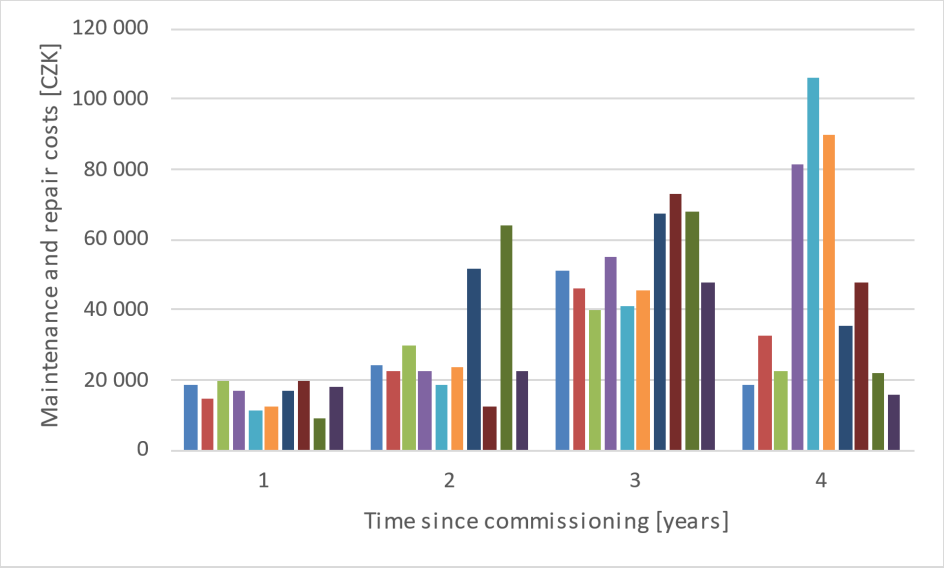

Figure1 A summary of maintenance and repair costs for specific machines for each year

Using regression analysis, linear, exponential, logarithmic, polynomial and power models of the trend in tractor repair costs as a function of time since introduction into service were developed.

Table 2 Percentage of tractor repair and maintenance costs from purchase price

	Type of tractor	Accumulated costs [% of purchase price]			
		1st year	2nd years	3rd years	4th years
Tractor 1	7810	0.63	1.44	3.15	3.78
Tractor 2	7810	0.59	1.48	3.33	4.63
Tractor 3	7810	0.85	2.12	3.81	4.77
Tractor 4	7810	0.64	1.52	3.64	6.76
Tractor 5	7810	0.43	1.14	2.71	6.75
Tractor 6	7810	0.47	1.37	3.09	6.50
Tractor 7	8120	0.55	2.22	4.41	5.55
Tractor 8	8120	0.73	1.20	3.92	5.69
Tractor 9	8120	0.29	2.35	4.54	5.25
Tractor 10	8120	0.57	1.27	2.77	3.26

Two statistics are important for the usability of the models. Namely, the correlation coefficient r, the formula of which is equation 1 and which tells us about the degree of dependence of data Y, in our case the cost of maintenance and repair of machines, on data X, or the time since commissioning.

$$r_{xy} = \frac{\frac{1}{n}\sum_{i=1}^{n}(x_i - \bar{x})(y_i - \bar{y})}{s_x \cdot s_y} \tag{1}$$

where x and y are the mean values of the data sets and s_x and s_y are the standard deviations quantifying the dispersion of the data around its mean value.

The second important characteristic value of the models in this paper is the coefficient of determination, sometimes referred to as the reliability value of the model. The coefficient of determination obtained from equation 2 lies in the interval $0;1$ and the closer it is to the value 1 the more accurate the regression model is to the initial data.

$$R^2 = 1 - \frac{s_{yx}^2}{s_y^2}, \tag{2}$$

where $s_{yx}^2 = \sum_{i=1}^{n}(y_i - \hat{y}_i)^2$ and $s_y^2 = \sum_{i=1}^{n}(y_i - \bar{y}_i)^2$ when $\hat{y}_i$ is the functional value of the regression function corresponding to the i-th x-component.

The computer programs STATISTICA Base CZ, MS Office and MATLAB R2015a were used to process, evaluate and graphically display the obtained data and regression models.

RESULTS and DISCUSSION

To assess which of the regression models more closely approximates the obtained data, it is sufficient to compare their coefficients of determination, which, together with the specific equations of our models, are presented in Table 3. The plots of each regression model together with the obtained data are ordered in ascending order of the value of the coefficient of determination in Figures 2–6.

Table 3 Equation of models

Models	General equation	Coefficient of determination
Linear	$1.6084 \cdot x - 1.2668$	0.9858
Exponential	$0.3173 + e^{0.7446x}$	0.9655
Logarithmic	$3.3098 \cdot \ln(x) + 0.1246$	0.9051
Polynomial	$0.1809 \cdot x^2 + 0.7042 \cdot x - 0.3626$	0.9958
Powerful	$0.5613 + x^{1,6247}$	0.9969

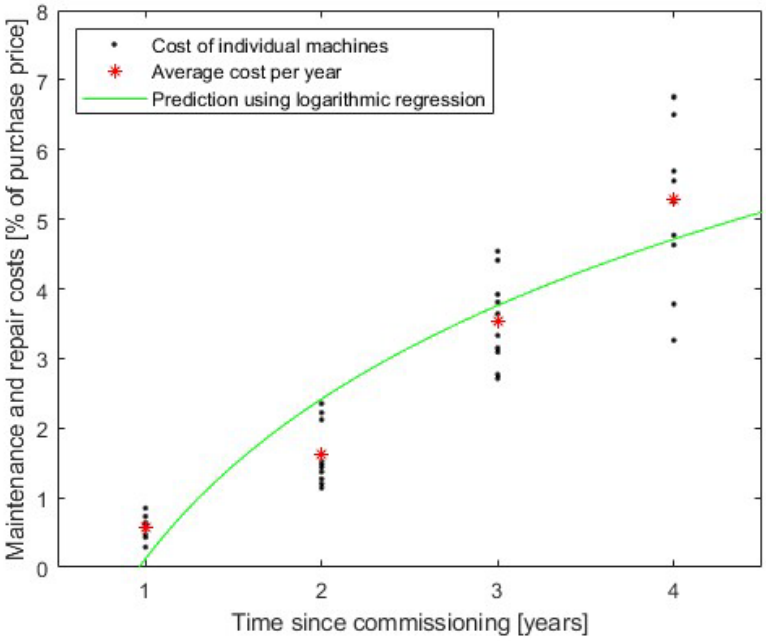

Figure 2 Predicting tractor repair and maintenance costs using logarithmic regression

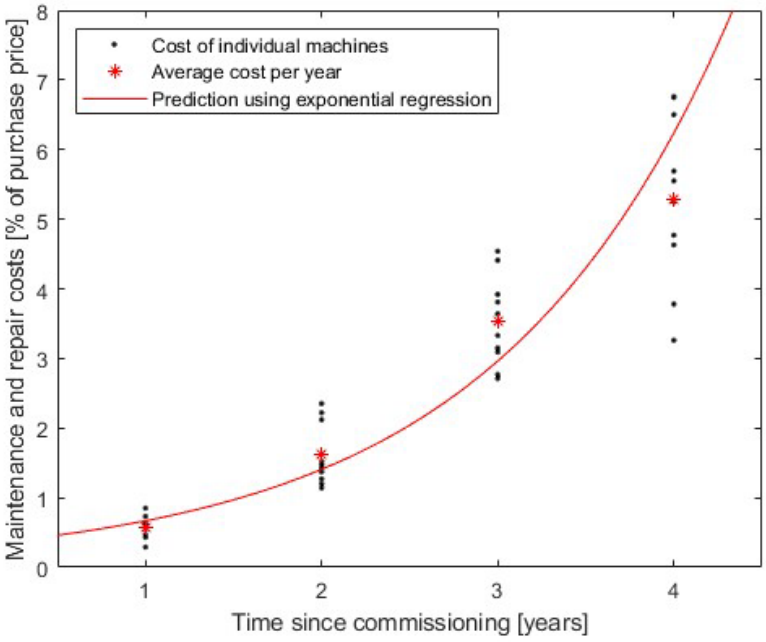

Figure 3 Predicting tractor repair and maintenance costs using exponential regression

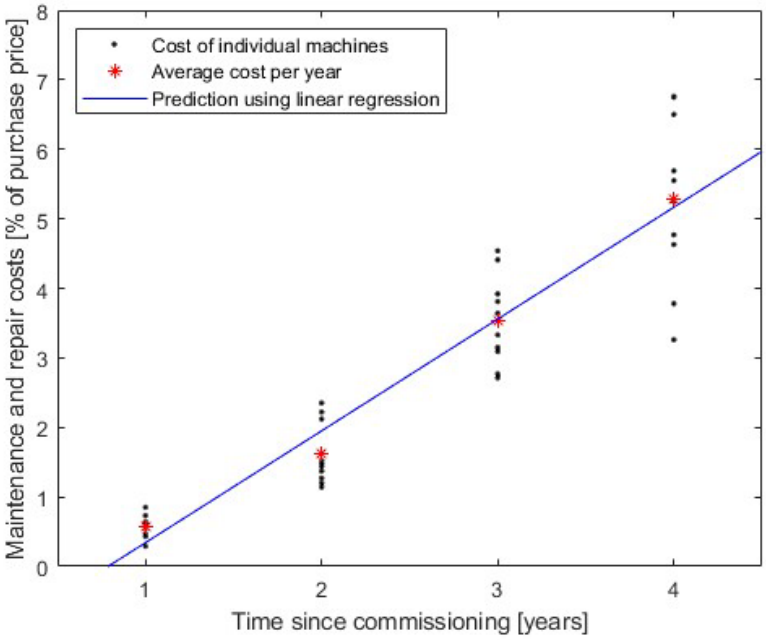

Figure 4 Predicting tractor repair and maintenance costs using linear regression

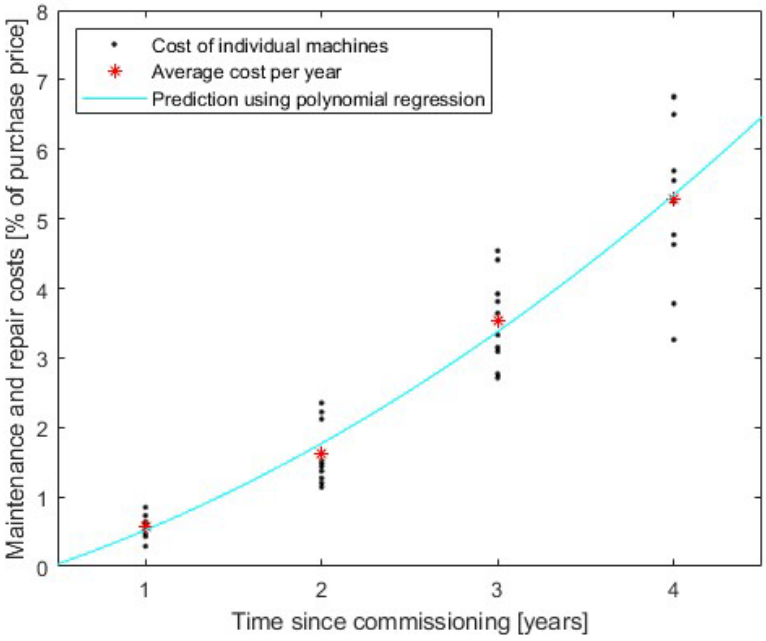

Figure 5 Predicting tractor repair and maintenance costs using polynomial regression

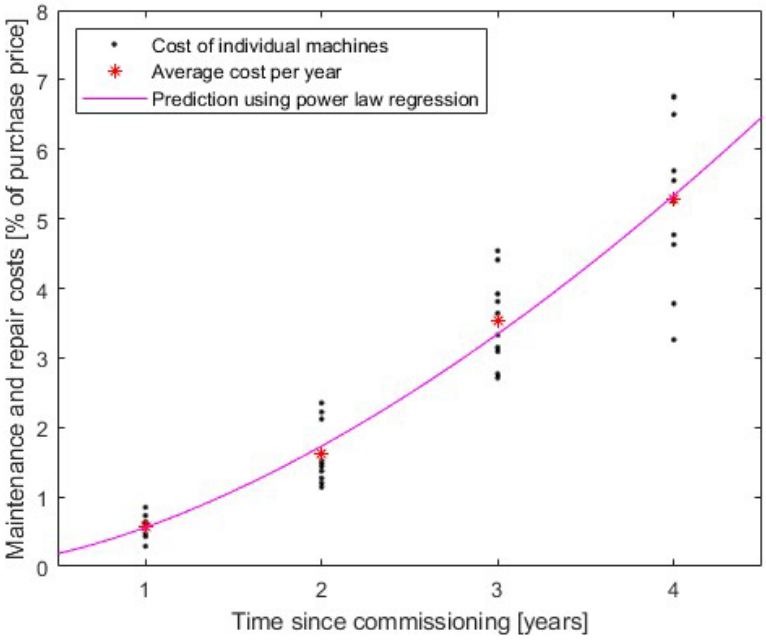

Figure 6 Predicting tractor repair and maintenance costs using power law regression

CONCLUSION

The cost of maintenance and repair of agricultural equipment is one of the factors that fundamentally affects the bottom line of all agricultural companies. For effective management, it is necessary to monitor this factor over the long term to form the basis for sound management decisions. The determination of the equations for estimating the cost of maintenance and repair is affected by the considerable degree of randomness of the input values. It is not possible to include factors in the resulting equations that have a major impact on the overall result. The quality of the operator, the difficulty of the work tasks, the difficulty of the terrain and climate, the distance of service and the regularity of maintenance are factors that are effectively impossible to include in the calculations yet can have a major impact on the accuracy of the estimate.

The results indicate that the most reliable regression is the power regression with a general equation ($Y = 15.966 + x^{0.791}$) and a coefficient of determination of 0.9181. The average cost of maintenance and repairs for the first 4 years of operation of the tractors under study, with a probability of 91.81%, is 129 461 CZK and corresponds to a value of 4.65% of the average purchase value of the machine.

Sailer (2008) studied the effect of the time of use of agricultural machinery and tractors on the degree of realization of operating parameters. The result was a statistical evaluation of the functional dependence of the decline in residual market value, the growth in repair costs and the evolution of the annual use of machines. The result for the 258 agricultural machines and 51 tractors under study can be used in the calculation of maintenance and repair cost estimates. He established a linear regression equation for estimating the annual cost of tractors $y = 1.4718 \cdot x$ with a determination value $R^2 = 0.995$. The maintenance and repair cost derived from this regression is expressed as a percentage of the purchase price of the new machine and reaches 14.718% in 4 years of machine operation. This is significantly higher than the calculation from this paper. This may be due to the lower amount of input data used to determine the regression.

Dahalab tracked average repair and maintenance costs with increasing age on 3 tractor brands in Sudan. His results show relatively higher repair costs from 10 years of age of the machine. By statistical processing of the data, he determined a power regression: $Y = 1.883\ x^{1.101}$, with a determination value of $R^2 = 0.989$. The value of the maintenance and repair costs for the first 4 years in this case corresponds to 8.66%.

Lips and Burose observed agricultural machinery in Switzerland and derived the maintenance and repair costs as a function of the expected lifetime of the machine. They evaluated 4 sections of agricultural machinery: tractors, ploughs, mowers and self-picker trailers. They monitored 1 083 machines, of which 655 were tractors. The intensity of use is low with an average of 272 moto-hours per year. Lips and Burse estimated the life of the tractors at 37 years or 10 000 moto-hours. The repair and maintenance costs of the machines range between 0.012–0.036 of the catalogue price of the machine. For tractors, they estimated a maintenance and repair factor of 0.022/10 000 moto-hours. Increasing the intensity of use reduces the value of the factor and therefore the total cost of maintenance and repair.

Lorencowicz writes in his article that the coefficients for calculating tractor maintenance and repair costs are not universal and vary from country to country.

REFERENCES

BRACANOVIĆ, Z., PETROVIĆ, V., GROZDANIĆ, B., JANKOVIĆ, S., 2014. Energy Saving of Agricultural Tractors when Using Different Types of Bulbs. Agricultural Engineering, XXXXIX (3):73–83.

DAHAB, M. H., MOHAMED, A. O., KHEIRY, A. N. O., 2016. Repair and Maintenance Costs Estimation as Affected by Hours and Age of Agricultural Tractor in New Halfa Area – Sudan. International Journal fo Agricultural Innovations and Research, 4(5):824–829.

GLIGOREVIĆ, K., OLJAČA, M. V., PAJIĆ, M., DIMITROVSKI, Z., DRAŽIĆ, M., 2012. Accidents with Tractor Drivers in Public Transport in Belgrade. Agricultural Engineering, XXXVII (2):71–79.

GRISSO, R. D., VAUGHAN, D. H., PERUMPRAL, J. V., ROBERSON, G. T., PITMAN, R., HOY, R. M., 2012. Using Tractor Test Data for Selecting Farm Tractors. Agriculture Engineering, XXXVII (1):1–9.

KHODABAKHSHIAN, R., SHAKERI, M., 2011. Prediction of Repair and Maintenance Costs of Farm Tractors by Using of Preventive Maintenance. International Journal of Agriculture Sciences, 3(1):39–44.

KOSIBA, J., TKÁČ, Z., HUGO, L., BUREŠ, L., TULÍK, J., CHRASTINA, J., 2012. Characteristics of hydraulic circuit of tractor John Deere 8100. Contemporary agricultural engineering, 38(3):201–210.

KUMAR, N., PANDEY, K. P., 2015. A visual program for predicting optimum gear and throttle position for best fuel economy for 32 kW tractor. *Computers and Electronics in Agriculture*, 119:217–227.

LIPS, M., BUROSE, F., 2012. Repair and Maintenance Costs for Agricultural Machines. *International Journal of Agricultural Management*, 1 (3): 40-46.

LORENCOWITZ, E., UZIAK, J., 2015. Repair cost of tractor and agricultural machines in family farm. In: Farm Machinery and Processes Management in Sustainable Agriculture, 2015. Gembloux, Centre wallon de Recherches agronomiques: 152–157.

MILEUSNIĆ, Z., MIODRAGOVIĆ, R., MIŠKOVIĆ, D., DIMITRIJEVIĆ, A., 2012. Basic Model for Optimal Transport Organisation in Agriculture. *Agricultural Engineering*, XXXVII (3):91–105.

NIARI, S. M., RANJBAR, I., RASHIDI, M., 2012. Prediction of Repair and Maintenance Costs of John Deere 4955 Tractors in Ardabil Province, Iran. *World Applied Sciences Journal*, 19(10):1412–1416.

POPOVIĆ, S., UGIRNOVIĆ, M., TOMAŠEVIĆ, S., 2015. Manage-Management of Agricultural Company through Monitoring of Total Cost of Maintenance Tractor. *Agricultural Engineering*, XL (2):101–106.

PRANAV, P. K., PHUKAN, Y., SAHA, B., 2016. Computer Program for Cost Estimation of Agricultural Machines. *Agricultural Engineering*, XLI (1):1–10.

ROHANI, A., ABBASPOUR-FARD, M. H., ABDOLAHPOUR, S., 2011. Prediction of tractor repair and maintenance costs using Artificial Neural Network. *Expert System with Applications*, 38:8999–9007.

SAILER, J., KAVKA, M., KAVKA, P., KAVKA, P., 2008. Influence of using time of selected agricultural machines and tractors on residual market price, repair costs and annual utilisation. *Research in Agricultural Engineering*, 54(4):199–207.

TODOROVIĆ, S., IVANOVIĆ, S., MARKOVIĆ, T., 2012. Economically Justified Amount of Investment in Purchase of Harvester at Family Farms. *Agricultural Engineering*, XXXVII (2):81–90.

WOLLNER, A., BARTOŠ, P., CELJAK, I., DOLAN, A., PETROVIĆ, A., 2015. Rating of Harvester Threshers Case 8120 and New Holland CX 8080. *Agriculture Engineering*, XL (1):19–30

Jihočeské univerzita v Českých Budějovicích
Fakulta zemědělská a technologická

ISBN 978-80-7694-077-2

www.fzt.jcu.cz